

ORNL
MASTER COPY

MAY 29 1990
ORNL/TM-11557

ornl

OAK RIDGE
NATIONAL
LABORATORY

MARTIN MARIETTA

**Two-Dimensional
Position-Sensitive Detectors for
Small-Angle Neutron Scattering**

**S. A. McElhaney
and
R. I. Vandermolen**



Advanced Neutron Source

OPERATED BY
MARTIN MARIETTA ENERGY SYSTEMS, INC.
FOR THE UNITED STATES
DEPARTMENT OF ENERGY

This report has been reproduced directly from the best available copy.

Available to DOE and DOE contractors from the Office of Scientific and Technical Information, P.O. Box 62, Oak Ridge, TN 37831; prices available from (615) 576-8401, FTS 626-8401.

Available to the public from the National Technical Information Service, U.S. Department of Commerce, 5285 Port Royal Rd., Springfield, VA 22161.

NTIS price codes—Printed Copy: A06 Microfiche A01

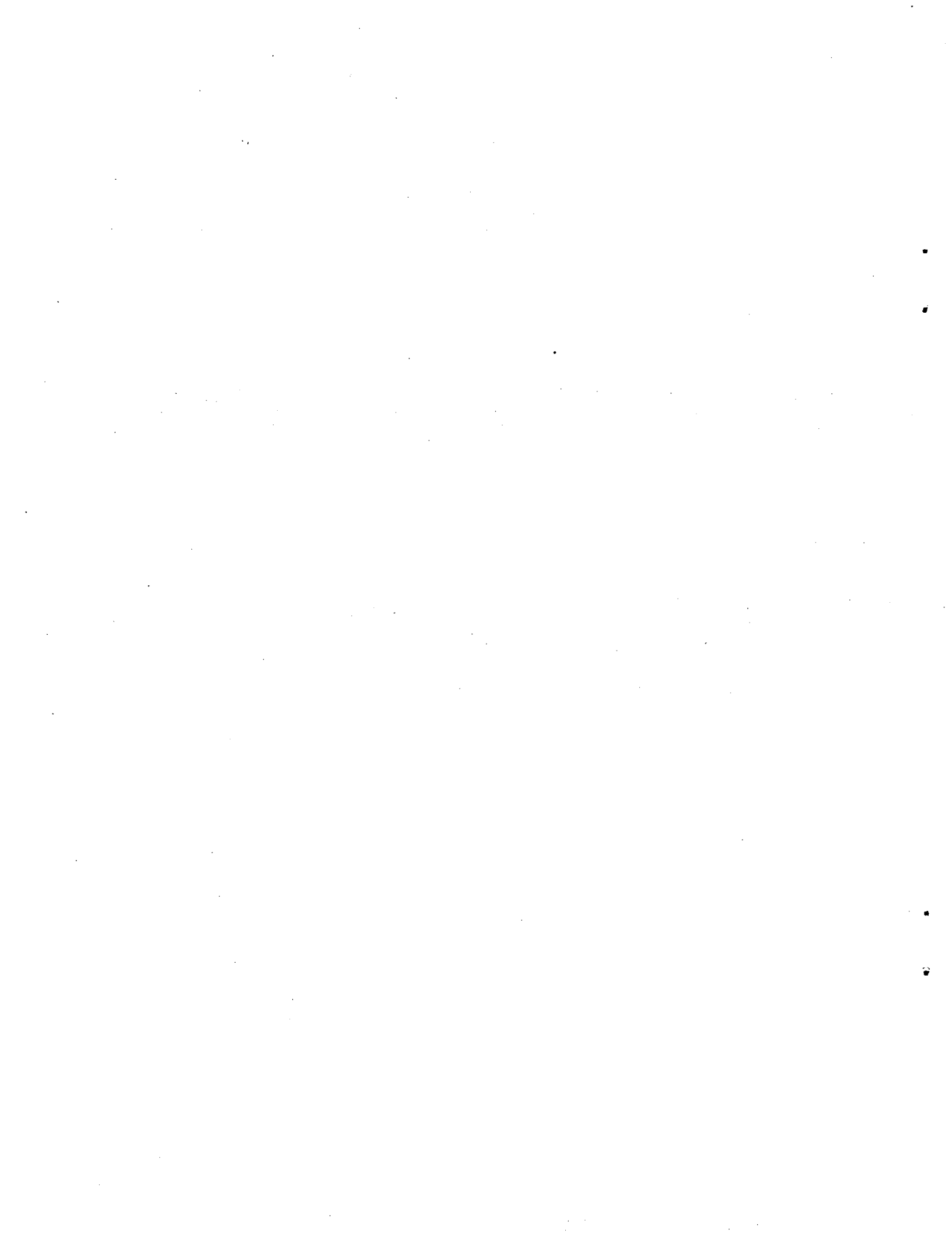
This report was prepared as an account of work sponsored by an agency of the United States Government. Neither the United States Government nor any agency thereof, nor any of their employees, makes any warranty, express or implied, or assumes any legal liability or responsibility for the accuracy, completeness, or usefulness of any information, apparatus, product, or process disclosed, or represents that its use would not infringe privately owned rights. Reference herein to any specific commercial product, process, or service by trade name, trademark, manufacturer, or otherwise, does not necessarily constitute or imply its endorsement, recommendation, or favoring by the United States Government or any agency thereof. The views and opinions of authors expressed herein do not necessarily state or reflect those of the United States Government or any agency thereof.

**Two-Dimensional Position-Sensitive Detectors
for Small-Angle Neutron Scattering**

S. A. McElhaney
R. I. Vandermolen

Date Published: May 1990

Prepared by the
Oak Ridge National Laboratory
Oak Ridge, Tennessee 37831
operated by
Martin Marietta Energy Systems, Inc.
for the
U.S. DEPARTMENT OF ENERGY
under Contract No. DE-AC05-84OR21400



I. CONTENTS

I.	CONTENTS.....	i
II.	LIST OF FIGURES.....	iii
III.	INTRODUCTION.....	1
IV.	GASEOUS ELECTRONIC DETECTORS.....	1
A.	^3He DETECTORS.....	1
1.	Individual Resistive Wire Multidetector.....	2
2.	Medium Pressure ^3He PSPC.....	4
a.	ORDELA (ORNL) Detector.....	4
b.	Riso Detector.....	4
c.	BNL Detector.....	7
3.	High Pressure ^3He Multielectrode Detector.....	9
B.	BF_3 DETECTORS.....	11
1.	LETI Detector.....	11
2.	Jeu de Jacquet Detector.....	13
C.	CURRENT DEVELOPMENTS.....	13
V.	SCINTILLATION DETECTORS.....	16
A.	GLASS/CRYSTAL SCINTILLATORS.....	16
1.	ANL ^6Li -Glass "Anger" Camera.....	16
2.	RAL ^6Li -Glass "Anger" Camera.....	17
3.	KFA ^6Li -Glass "Anger" Camera.....	20
4.	KFA $^6\text{Li}(\text{Eu})$ "Anger" Camera.....	21
5.	KFA ^6Li -Glass Scintillator with Position-Sensitive PMT.....	21
6.	RAL Fiber-Optic Encoded Detector.....	24
B.	PHOTOIONIZATION DETECTORS.....	24
C.	PLASTIC SCINTILLATORS.....	26
D.	MCP DETECTORS.....	28
E.	CURRENT DEVELOPMENTS.....	28
VI.	SEMICONDUCTOR DETECTORS.....	31
A.	MICROSTRIP PLATE.....	31
B.	CURRENT DEVELOPMENTS.....	31
VII.	NEUTRON IMAGING SYSTEMS.....	33
A.	MRC CAMERA.....	33
B.	"FLY'S EYE" CAMERA.....	33
C.	CHARGE COUPLING DEVICE.....	36
D.	CURRENT DEVELOPMENTS.....	36
VIII.	FOIL DETECTORS.....	37
A.	PROPORTIONAL COUNTER WITH Gd FOIL.....	37
B.	AVALANCHE CHAMBER WITH Gd FOIL.....	39

C.	LOW-PRESSURE MULTISTEP CHAMBER.....	39
IX.	PHOTOGRAPHIC DETECTORS.....	43
X.	DATA COLLECTION TECHNIQUES.....	44
A.	RESISTIVE ENCODING.....	44
1.	Charge Division Encoding.....	44
2.	Time-Difference Decoding.....	47
B.	INDIVIDUAL COUNTER ARRAYS.....	47
1.	Individual Resistive Wire Encoding.....	47
2.	Fiber-Optic Encoding.....	50
C.	MULTIELECTRODE ENCODING.....	54
1.	Position Determination Through Coincidence.....	54
2.	Center-of-Gravity.....	54
3.	Centroid Finding by Convolution.....	54
4.	Delay Line Encoding.....	57
5.	Center-of-Cluster.....	61
D.	ANGER CAMERAS.....	61
1.	Unified Anger Camera.....	61
2.	Multifield Anger Camera.....	61
E.	NEUTRON IMAGING SYSTEMS.....	63
1.	TV Camera Tube.....	63
2.	CCD.....	63
XI.	COMPUTER CONSIDERATIONS.....	64
XII.	CONCLUSIONS.....	66
XIII.	ACKNOWLEDGEMENTS.....	67
XIV.	REFERENCES.....	69
XV.	ABBREVIATIONS.....	75
XVI.	APPENDIX.....	77

II. LIST OF FIGURES

Fig. 1 - Schematic diagram of one of the ^3He PSPC used in the MURR detector array.....	3
Fig. 2 - Diagram of the ORDELA (ORNL) detector.....	5
Fig. 3 - Exploded view of the Riso detector.....	6
Fig. 4 - Electrode configuration for the a) $18 \times 18 \text{ cm}^2$	8
b) $50 \times 50 \text{ cm}^2$ BNL detector.....	8
Fig. 5 - Electrode diagram of the high pressure ^3He multidetector.....	10
Fig. 6 - Schematic diagram of the BF_3 LETI detector.....	12
Fig. 7 - Electrode diagram of the Jeu de Jacquet "backgammon" detector.....	14
Fig. 8a - General design for a neutron "Anger" camera.....	18
Fig. 8b - Weighted-resistor encoding scheme for the ANL camera.....	18
Fig. 9 - The seven tube multifield encoding scheme for the RAL camera.....	19
Fig. 10 - Example of the selection of nine PMTs in a KFA camera.....	22
Fig. 11 - Diagram of the KFA ^6Li scintillator with position-sensitive PMT.....	23
Fig. 12 - Principle of the fiber-optic encoding scheme pioneered by Davidson and Wroe.....	25
Fig. 13 - Schematic diagram of a plastic scintillator detector.....	27
Fig. 14 - Diagram of the MCP detector.....	29
Fig. 15 - Electrode configuration and dimensions for the MS plate detector.....	32
Fig. 16 - Schematic diagram of the neutron imaging camera developed by Arndt.....	34
Fig. 17 - Layout of the "Fly's Eye" system developed by Davidson.....	35
Fig. 18 - Proportional counter with Gd foil developed at CERN.....	38
Fig. 19 - Electrode diagram of the avalanche chamber with Gd foil. A is a mylar window; B, C, and D are the standard MWPC; E and F are the preamplification electrodes; G is a Gd foil mounted on an aluminum ring, H; I is an incident neutron, converting to an electron that ionizes along the track, J.....	40
Fig. 20 - General view of a low-pressure multistep chamber.....	41

Fig. 21 - Basic charge-division decoder.....	45
Fig. 22 - Charge-division encoding applied to a multiwire cathode.....	46
Fig. 23 - Decoding circuitry for the NIST detector.....	48
Fig. 24 - MURR-SANS detector, single channel.....	49
Fig. 25 - Encoding scheme for RAL PSD.....	51
Fig. 26 - Electronics for the RAL fiber-optic encoded PSD.....	52
Fig. 27 - RAL fiber-optic encoded PSD, later version.....	53
Fig. 28 - Coincidence method using multicathode area detector.....	55
Fig. 29 - Center-of-gravity method.....	56
Fig. 30 - Centroid finding by convolution.....	58
Fig. 31 - Centroid finding by convolution.....	59
Fig. 32 - Delay line decoding.....	60
Fig. 33 - Center-of-cluster method.....	62

III. INTRODUCTION

In this paper, various detectors available for SANS* are discussed, along with some current developments being actively pursued. A section has been included to outline the various methodologies of position encoding/decoding¹ with discussions on trends and limitations. Computer software/hardware vary greatly from institute and experiment and only a general discussion is given to this area².

IV. GASEOUS ELECTRONIC DETECTORS

This section deals with detectors using gaseous mediums, usually ³He or BF₃, for neutron conversion and electronic readout methods for localization. Gaseous mediums which use other means of readout (such as PMTs for photoionization) or combinations of gases with other converters (foils or thin films) will be discussed in later sections.

Gaseous detectors have been proven over the years to be reliable and efficient for SANS. They are extremely stable over long acquisition times and relatively insensitive to γ and detector background. These characteristics make the gaseous detector well suited to low count rate applications. Gaseous detectors also have relatively high count rate capability (10^5 c/s), which has recently been extended even higher (see current developments in this section). The overall efficiency of gaseous detectors is excellent in comparison to other detection mediums, approaching 100% for cold neutrons.

The technology involved in designing a gaseous MWPC, however, is extremely delicate. Skilled techniques are required in replacing damaged electrodes and purifying gases. Special two-chamber architectures (described later in this section), designed to accommodate pressurized gases, contribute to parallax errors and uncertainties in TOF, already present due to "thick" detection mediums. Even though the resolution of gas detectors has been greatly improved, there are intrinsic resolution limitations resulting from the ranges of charged particles created by neutron absorptions.

A. ³He DETECTORS

The ³He detector is the most popular gaseous electronic detector for SANS. The popularity is due mainly to high neutron absorption cross-sections. Depending on the pressurization of ³He gas, it can be applicable to either long or short wavelength neutrons with excellent absorption efficiencies. However, high pressures can also be a hindrance, requiring special maintenance and construction. At lower pressures, or when detecting cold neutrons, special additive gases are mixed with ³He to reduce the charged particle ranges. This additive gas may increase the γ -sensitivity. Recent advances in gas mixtures, however, have almost eliminated this problem (see ORDELA detector in this section).

* Acronyms are defined in Section XV.

1. Individual Resistive Wire Multidetector

This detector, developed by Berliner *et al* at MURR^{3,4}, is a 50 x 64 cm² array of one-dimensional ³He-filled proportional counters. Each of the 43 individual counters (Fig. 1) is 12.7 mm in diameter with a 610 mm sensitive length. The fill gas comprises 6 atm of ³He and 4 atm of Ar (with 5% CO₂). The counter anode is a 15 μm diameter nickel-chrome wire, with 3900 Ω resistance. Individual counters are placed 19 mm apart in the array, which has a negligible effect on the solid angle subtended by each counter.

The x-positional encoding for this multidetector is accomplished by charge division (encoding methods are outlined in section X). Each detector element has two charge-sensitive, low-input impedance preamplifiers with its own single circuit board electronics module.

Spatial resolution: 0.5 x 1.27 cm², although resolutions of approximately 0.25 cm have been reported by Alberi⁵.

Efficiency: 84% at 4.75 Å.

Uniformity of detector: Good; inoperative detectors can be replaced.

Continuity of efficiency: There may be changes in the sensitive gas length from one detector to another and "dead regions" are formed by walls and/or spacing between individual counters.

Stability of detector: Good.

Count rate: A 10⁵ cps maximum rate was reported by Agamalyan *et al* at LNPI⁶ using a 41 counter array based on the MURR design. The count rate is limited by the duration of shaped pulses (4 μs for the LNPI detector) and properties of the fill gas.

Background: There is low γ-sensitivity for the MURR detector, particularly if pure ³He is used as the fill gas in individual counters. The application of individual electronic on each counter minimizes the amount of cross-talk between channels.

TOF capability: A MURR detector is currently used on KENS at KEK in Japan⁷.

Maintenance: Individual counters can be easily replaced if they become inoperable. Also, by using commercially available counters, purification and precision machining is avoided by the user.

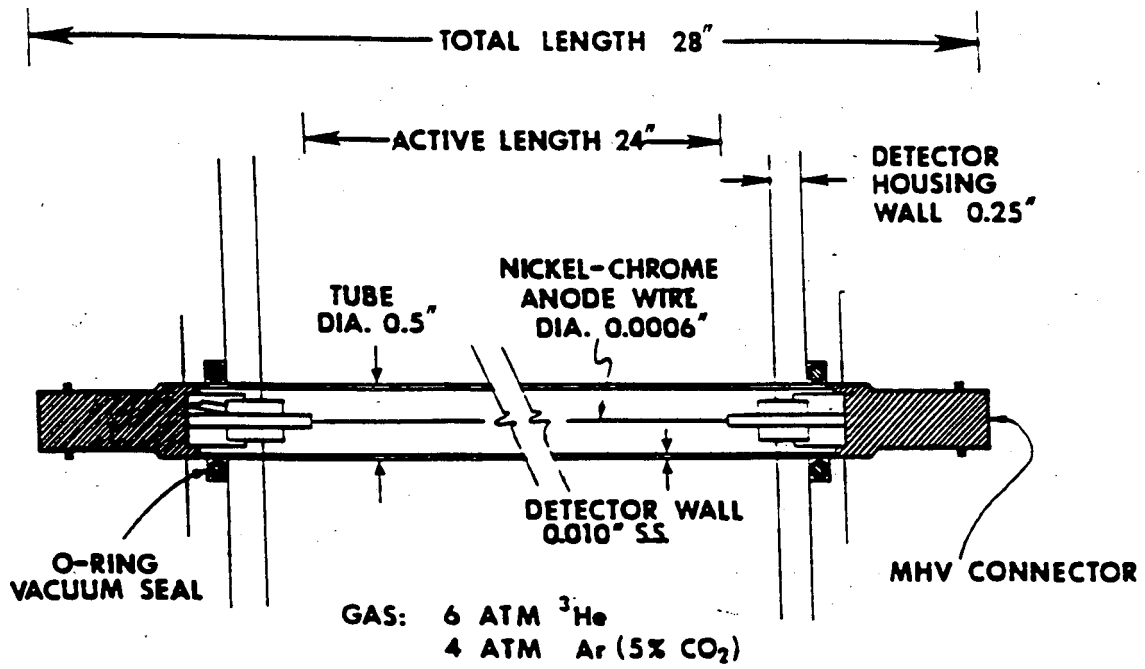


Figure 1

Schematic diagram of one of the ^3He PSC used in the MURR detector array.

2. Medium Pressure ^3He PSPC

a. ORDELA (ORNL) Detector

The ORDELA⁸ detector is a commercially manufactured PSPC originally developed at ORNL^{9,11}. It has a $65 \times 65 \text{ cm}^2 \times 2.5 \text{ cm}$ active volume filled with 65% ^3He and 35% CF_4 at 3 atm pressure. The specially developed gas mixture¹⁰ has a high neutron detection efficiency, good spatial resolution, low γ -sensitivity, and improved count rate capabilities. In order to maintain a uniformly thick gas-detection medium, a ^4He buffer gas is used to support the 0.8 cm thick, flat entrance window. This buffer gas (transparent to 4.75 \AA neutrons) is also maintained at 3 atm inside a 1 cm thick aluminum dome (Fig. 2). This is referred to as a two-chamber architecture.

A resistance-capacitance position encoding method, using time-difference decoding, was developed for localizing neutron events¹¹. The two cathode wire grids are fabricated by a continuous wire construction acting as two independent, orthogonal RC lines, using $125 \mu\text{m}$ diameter stainless steel wire of $0.6 \Omega/\text{cm}$. Each wire turn is 70 cm long and spaced 0.5 cm between adjacent turns. The separation between anode and cathode planes is 0.5 cm.

Spatial resolution: $1 \times 1 \text{ cm}^2$.

Efficiency: 80% at 5 \AA .

Uniformity of detector: $\pm 2\%$ integral, $\pm 15\%$ differential.

Continuity of efficiency: Good.

Stability of detector: The ORNL detector used at NIST reports a stability better than 0.5 mm per day¹².

Count rate: A 2×10^4 n/s count rate is possible with 10% coincidence loss. The maximum count rate capability is 10^5 n/s.

Background: There is a low γ -sensitivity with this gas mixture. NIST reports ~ 5 cps total background across the entire detector.

TOF capability: A thick entrance window and detection medium creates uncertainties in determining the flight path length. A smaller, $18.9 \times 18.9 \text{ cm}^2$, ORDELA detector is currently being used at the IPNS and a $40 \times 40 \text{ cm}^2$ ORDELA detector has recently been purchased¹³.

Maintenance: The maintenance for MWPCs is very involved. The detector is fragile, difficult to repair if electrodes are damaged, and gas purification is necessary.

b. Riso Detector

The Riso detector^{14,15} was inspired by the ORNL PSPC. The Riso has a

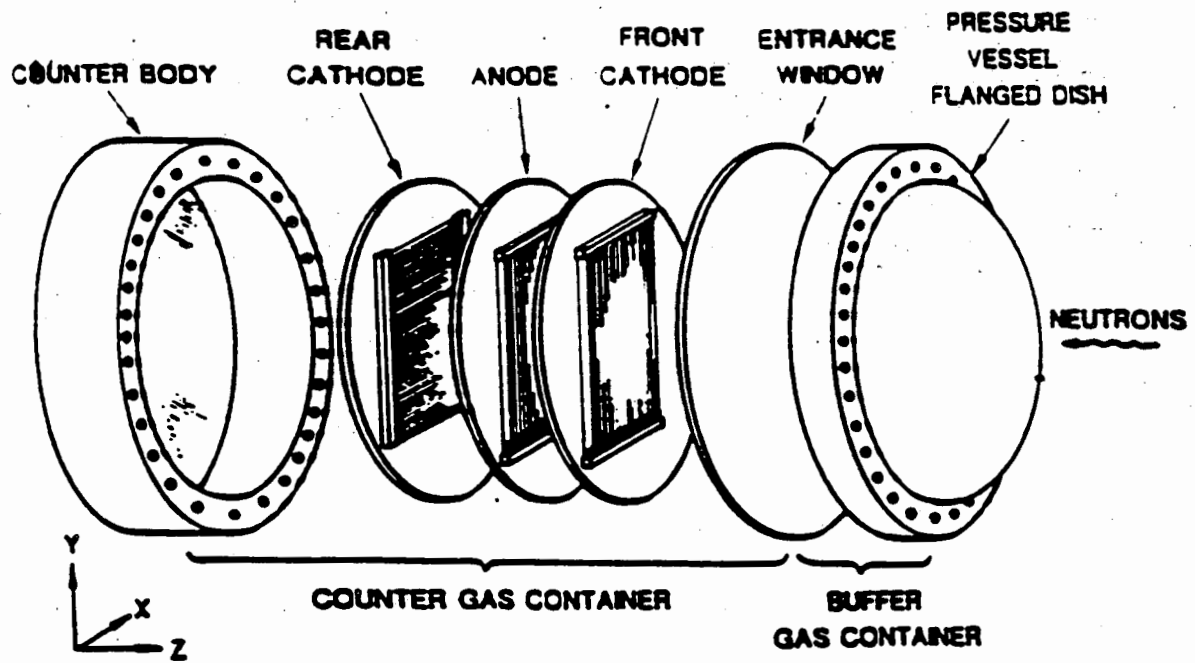


Figure 2
 Diagram of the ORDELA (ORNL) detector.

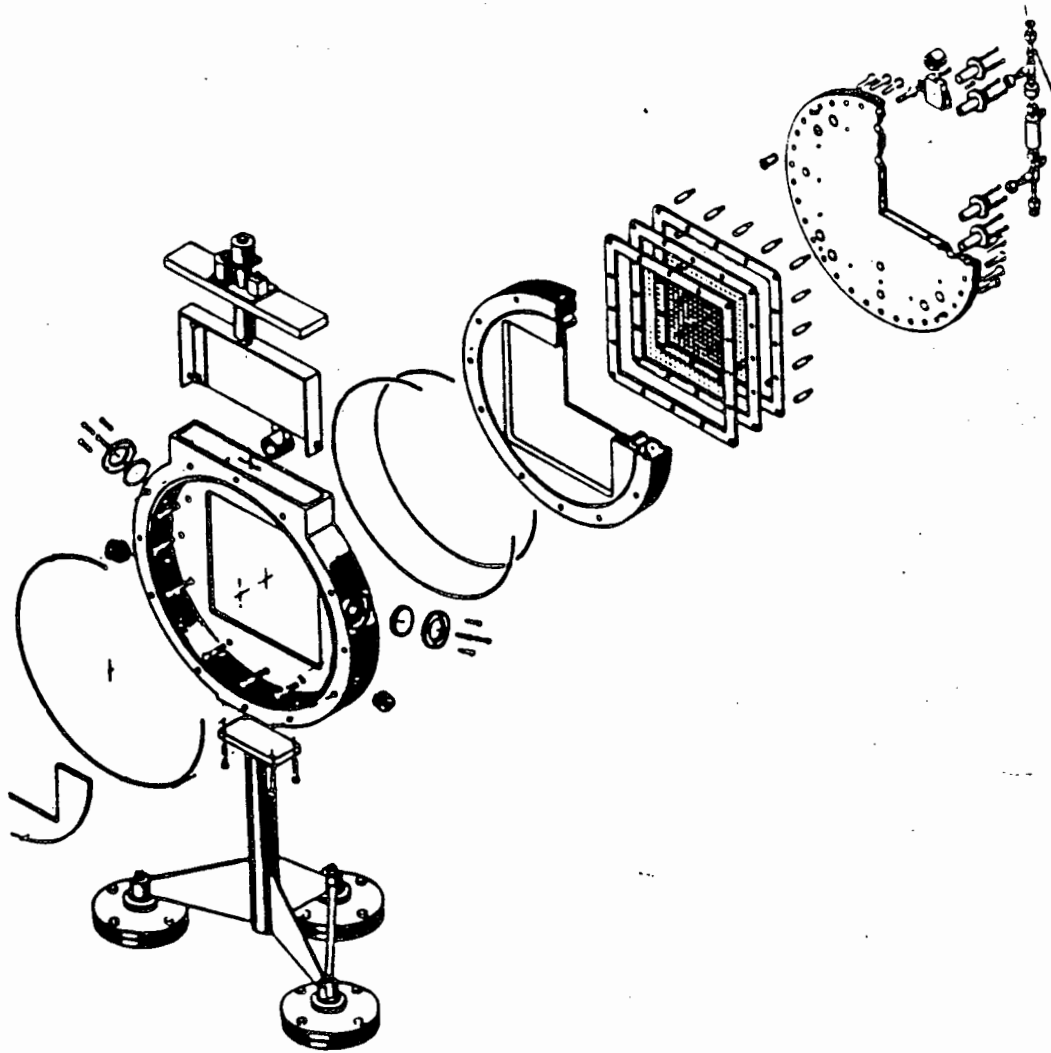


Figure 3

Exploded view of the Riso detector.

58 x 58 cm² x 4.5 cm sensitive volume with a gas filling of 1 atm ³He and 1.35 atm Ar (with 10% methane). The size of the active volume was chosen to avoid problems with curvature in a single entrance window design (Fig. 3).

The central anode plane has 99 stainless steel wires measuring 20 μm in diameter, with the two outermost wires having 40 μm and 60 μm diameters. The wires are spaced 6 mm apart on the grid and interconnected by 68 Ω standard resistors. The cathode planes are similar to the anode, except all wires are 50 μm diameter phosphorbronze and interconnected with 47 Ω resistors. The double delay line method for position encoding, determining differences in rise-times for pulses arriving at two charge-sensitive preamplifiers, was used for the Riso detector.

Spatial resolution: 6.5 x 7.5 mm². A spatial resolution of 8 mm was reported by NERF¹⁶.

Efficiency: 76% at 4 Å, 97% at 10 Å.

Uniformity of detector: ± 5%.

Continuity of efficiency: There are discontinuities near the edges of the detector due to an increase in grid capacitance.

Stability of detector: Small changes in efficiency were observed over a period of several months. The positional response was unaltered over a period of six months.

Count rate: 10⁵ cps. Reliable count rates of ≤ 10⁴ were reported by JAERI¹⁷ and NERF¹⁶.

Background: There is < 0.1 cps under normal operating conditions.

TOF capability: A thick detection medium creates uncertainties in determining the flight path length. However, the accuracy is better than for the ORNL detector which uses a flanged dish (dome) in front of the entrance window. A 59 cm diameter Riso detector is currently being used at LANL¹⁸.

Maintenance: Similar to ORNL detector.

c. BNL Detector

This detector, designed at BNL^{19,20}, is a 50 x 50 cm² x 1.2 cm PSPC. It uses an unique gas-fill mixture of 4.1 atm ³He and 1.6 atm C₃H₈. The counting gas is contained within a flat, uniform thickness using the two-chamber architecture described earlier for the ORNL detector. The BNL spherical dome is filled with ⁴He and maintained at the same pressure as the ³He counting gas. An 8 mm thick intermediate aluminum window separates the flat, active volume from the inactive spherical volume (3 mm thick).

Three electrode planes are equally spaced within the active volume of the BNL detector (Fig. 4). The anode grid consists of 129 interconnected, horizontal gold-plated tungsten wires of 25 μm diameter. This grid is then sandwiched between the two cathode planes,

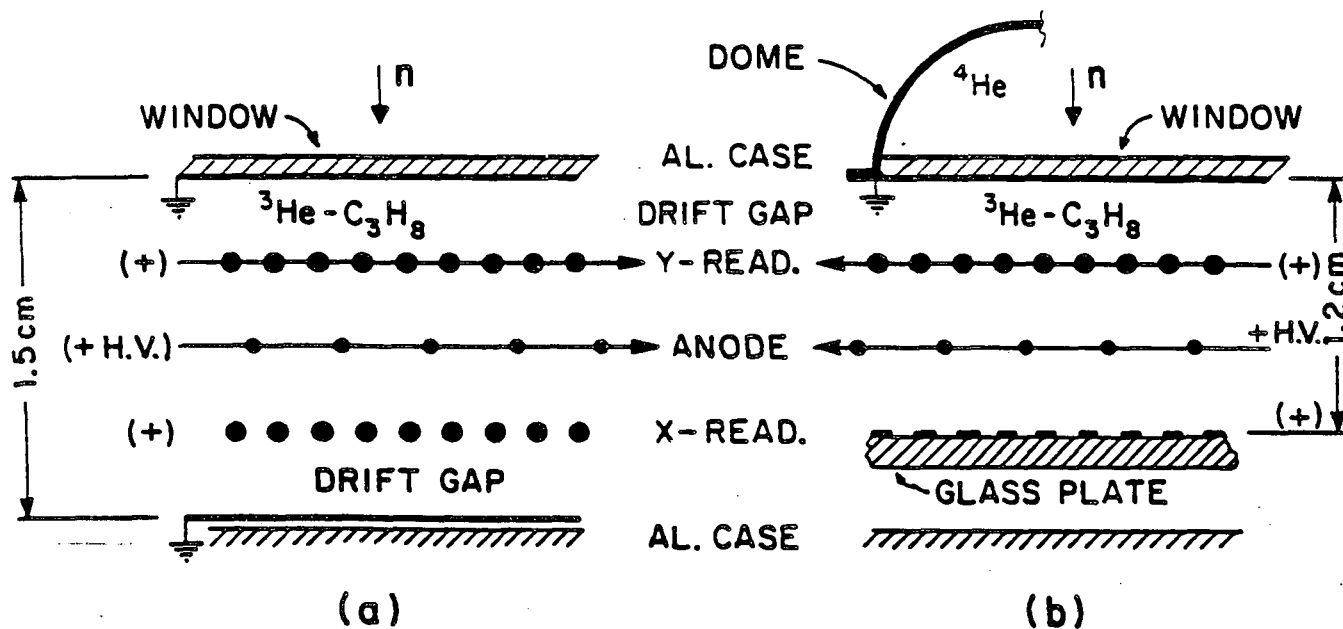


Figure 4

Electrode configuration for the a) $18 \times 18 \text{ cm}^2$ and b) $50 \times 50 \text{ cm}^2$ BNL detector.

4 mm from each. The front cathode (y-position readout) is 257 resistively-connected, horizontal wires intercalated with the anode wires. The back cathode (x-position readout) consists of 161 vertical copper strips, interconnected by resistors, evaporated onto a thick glass plate. A specially designed centroid finding method using convolution, utilizing 33 charge-sensitive preamplifiers at 5-strip spacings, was developed by Radeka and Boie for the positional readout of this detector²¹.

A detector developed by RRI is based on the BNL design but uses a wire-to-wire encoding method for localization²².

Spatial resolution: $2 \times 2 \text{ mm}^2$. Other versions of this detector, developed at BNL, have resulted in spatial resolutions of $\sim 1 \text{ mm}$.

Efficiency: 75% at 5 Å.

Uniformity of detector: $\pm 0.1\%$ integral, $\pm 2\text{-}3\%$ differential. In the smaller, $18 \times 18 \text{ cm}^2$ detector, areas of higher counting probability differed by as much as 15% from areas of lower counting probability²³. A matrix of correction factors was constructed to correct uneven sensitivity.

Continuity of efficiency: Good.

Stability of detector: Good.

Count rate: Typical count rate is 10^4 n/s . A maximum reliable count rate is 10^5 n/s .

Background: There is low γ -sensitivity.

TOF capability: A thick entrance window and detection medium creates uncertainties in determining the flight path length.

Maintenance: Similar to ORNL detector.

3. High Pressure ^3He Multielectrode Detector

Jacobe *et al* at ILL developed a multidetector which uses pure ^3He at pressures of 15-20 atm²⁴. Additional gases are added for cold neutron detection. The general electrode configuration is shown in Fig. 5. This detector consists of three or four parallel electrode planes with x-coordinates taken from the anode wires and y-coordinates from the cathode strips. This is a typical drift detector with a complete separation between the localization and detection gap.

The entrance cathode is a printed circuit of 16 copper electrodes, 4 mm wide and 1 mm in separation. The cathode is 0.4 mm thick and located 3 mm from the anode grid, which is composed of 25 μm diameter stainless steel wires spaced 2.54 mm apart. The back cathode grid is positioned 3 mm behind the anode. It is made of 100 μm diameter wires spaced 1.27 mm in separation and held at the same potential as the entrance cathode. The pulses created on this grid are not used for localization but can be used for counting rates. A drift region of 20-30 mm is placed between the cathode grid and the rear cathode, which

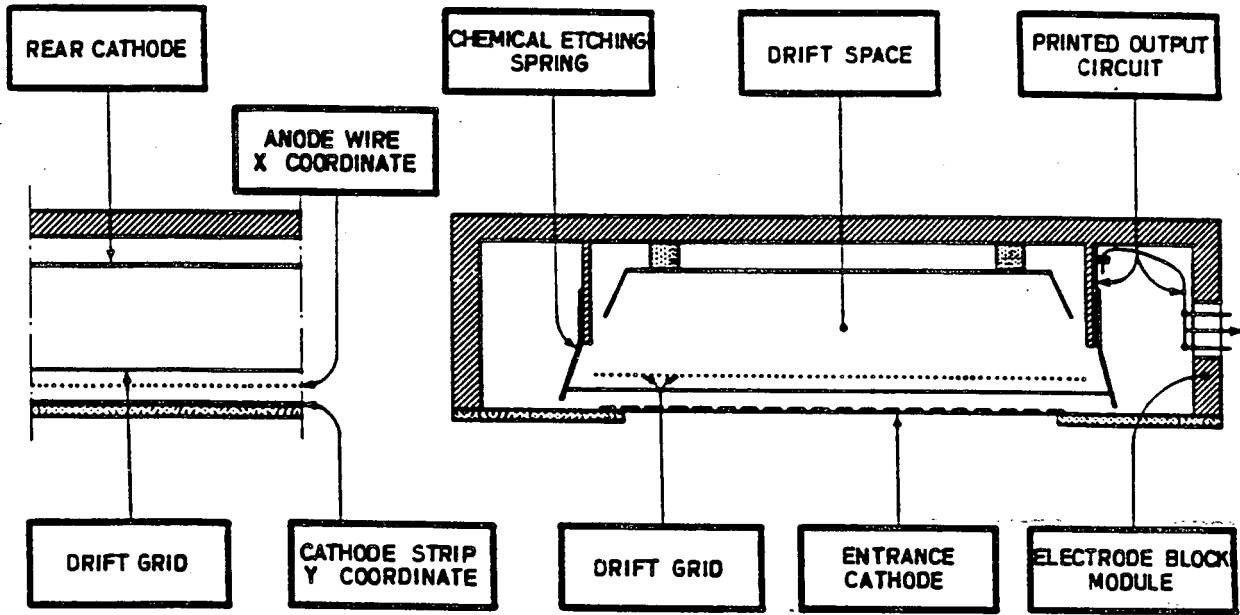


Figure 5

Electrode diagram of the high pressure ^3He multidetector.

is also a printed circuit. This distance is limited by parallax, but could be increased in a curved detector. Each channel of the multidetector has a separate amplifier.

Spatial resolution: 3.05 x 6.5 mm².

Efficiency: 90% at 0.4 Å possible.

Uniformity of detector: ± 5%.

Continuity of efficiency: Good.

Stability of detector: A test run over a three day period showed ± 0.05% variation in cell counting.

Count rate: Typical count rates are probably 10⁴ n/s.

Background: The multidetector, and versions similar to it, have low γ -sensitivity. There is very little cross talk in this detector since each electrode has its own amplifier and performs independently.

TOF capability: A thick entrance window (10 mm) and detection medium creates uncertainties in determining the flight path length.

Maintenance: Similar to ORNL detector.

B. BF₃ DETECTORS

The BF₃ gaseous electronic detector, even though slightly less efficient for neutron absorption than ³He, produces ~ 3 times more ion-pairs and has a better signal-to-noise ratio. These features are a result of a larger energy release (Q-value) in neutron absorption by ¹⁰B, thereby creating a larger pulse for detection. The overall efficiency for BF₃ is better suited to long wavelength (cold) neutrons because of recombination effects in the gas at pressures greater than 3 atm. High counting rates can also cause compositional problems in this gas. BF₃ tends to dissociate at extended high count rate periods. The dissociation, which leads to formation of electronegative fluorine, reduces the performance and lifetime of the detector. One of the most troublesome aspect of BF₃ is the difficulty in working with a corrosive gas.

1. LETI Detector

The BF₃ detectors have been developed primarily by Allemand *et al* at LETI Laboratory (CEA-CENG)²⁵. The effective volume for this "chequer board" type detector is 64 x 64 cm² x 1 cm with a fill gas of enriched BF₃ at atmospheric pressure. The two-chamber architecture, described for ORNL and BNL ³He detectors, incorporates 1 atm CO₂ buffer gas, transparent to 6 Å neutrons. The buffer gas is kept separate from the counting medium by an 1 mm thick aluminum entrance window (Fig. 6).

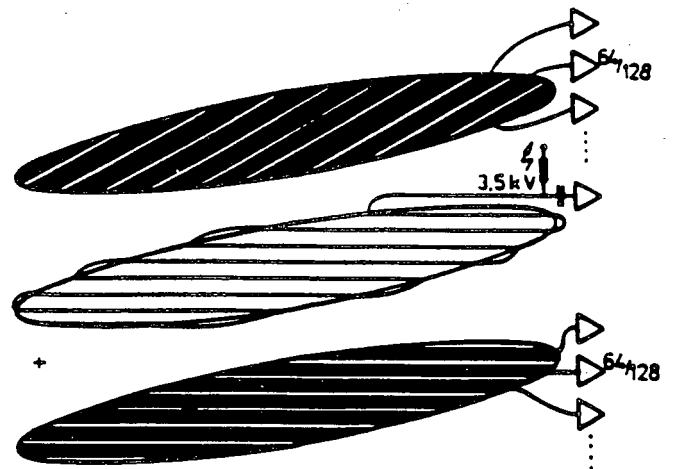
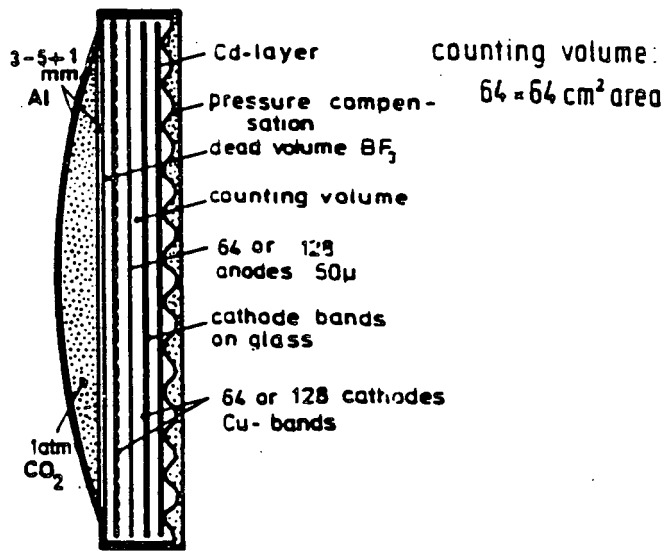


Figure 6

Schematic diagram of the BF_3 LETI detector.

An anode wire grid is placed at mid-plane in the detection volume. The anode wires are the same step-width as the two-orthogonally oriented cathodes (10 mm and 5 mm, respectively). The readout signal is taken off the two cathodes and identified by coincidence measurements. Addresses are created by observing the coincidence of pulses at the vertical and horizontal electrodes.

Spatial resolution: $0.5 \times 0.5 \text{ cm}^2$. A spatial resolution of 0.25 cm was reported for a multidetector design of this detector²⁶.

Efficiency: 60% at 6 Å.

Uniformity of detector: Good.

Continuity of efficiency: Good.

Stability of detector: Good.

Count rate: Typical count rates are 10^4 n/s with 10% dead time. Maximum count rate capabilities $\sim 10^5$ n/s.

Background: A normal background count is 1 c/h cm^2 , randomly distributed over the entire detector²⁷.

TOF capability: Similar to ORNL detector. A $64 \times 64 \text{ cm}^2$ LETI detector is currently being used at the ISIS at RAL²⁸.

Maintenance: The maintenance for MWPCs is very involved. The detector is fragile, difficult to repair if electrodes are damaged, and gas purification is necessary.

2. Jeu de Jacquet Detector

The "backgammon" detector was developed at LETI by Allemand and Thomas²⁹. It differs from the "chequer board" detector by means of readout. This readout method is based on a continuous change in the signal. The crossed cathodes (Fig. 7) produce a signal height at each end of the strip which depends on one coordinate of the detection origin.

C. CURRENT DEVELOPMENTS

There have been many developments over past years in gaseous detector designs. Most of this attention resulted from the fact that even though the gaseous electronic detectors required skilled maintenance, they could be constructed in ordinary facilities with conventional materials. Some advances, which may someday be adapted to neutron position-sensitive detectors, include the parallel plate avalanche chamber which uses a parallel gap amplification consisting of meshes inside of wires^{30,31,32}, the double-grid avalanche chamber³³, and several radial drift devices which address the problem of parallax³⁴. Several other avalanche chambers are discussed in Section VIII of this paper.

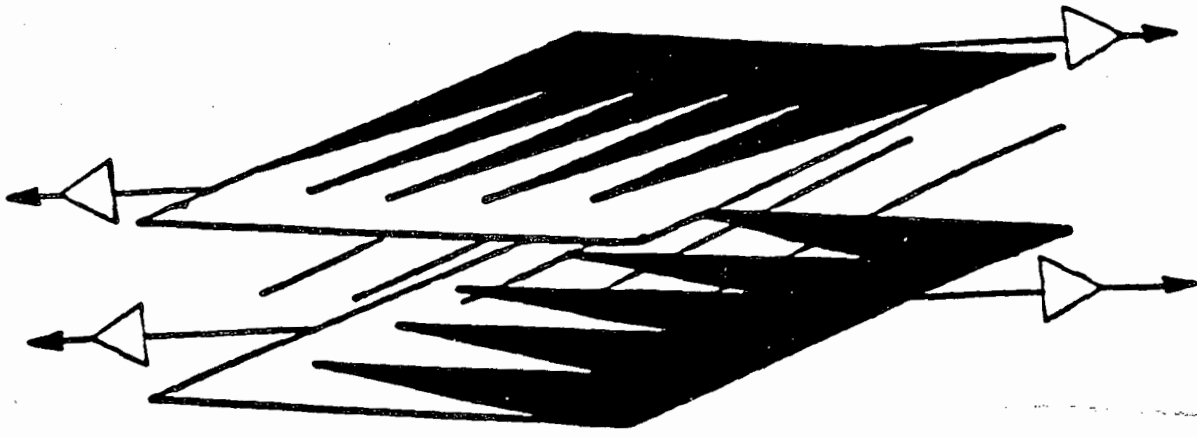


Figure 7

Electrode diagram of the Jeu de Jacquet "backgammon" detector.

Under a DOE-SBIR Phase I contract, Kopp, at ORDELA, has developed a new counting and encoding method³⁵. This system improved the count rate capability to 10^7 n/s (10^5 n/s/pixel) and increased detector endurance 100 fold, compared to transmission line encoding. Phase II of this program will focus on a new generation of PSDs for high-intensity neutron scattering experiments.

A development is reportedly being made at ILL to construct a 100×100 cm² detector using a ³He fill gas³⁶. One limitation to this detector may be the count rate capabilities.

V. SCINTILLATION DETECTORS

The scintillation detectors developed for neutron scattering evolved with the advent of pulsed neutron sources. These sources provided a need for detectors which could handle high instantaneous count rates and broad spectra of neutrons into the epithermal energy region. Scintillation detectors, which provide high efficiencies for both long and short wavelength neutrons at minimal thicknesses and without high pressures, were the obvious choice.

There are several advantages to scintillation detectors, depending on the needs of the user. The positional resolution, though currently similar to gaseous electronic detectors, could possibly be made much smaller with advancements in encoding techniques. Also, since intrinsic dead time for scintillators is small (~ 60 ns for ^6Li -glass), these detectors are suitable to very high count rates. The problems associated with scattering and parallax errors are virtually eliminated due to thin, light-tight window possible for scintillators. This, along with short decay constants, makes scintillators ideal for TOF measurements. The various shapes and sizes capable with scintillator detectors makes very versatile detectors possible.

The major problem associated with scintillation detectors is the high γ -sensitivity. Even though this may be overcome at pulsed sources where the γ -flash is approximately $100 \mu\text{s}$ ahead of thermal neutrons, it is still a concern for reactor sources. One solution is to use pulse-shape discrimination, which would probably reduce count rates and result in longer acquisition times. Fortunately, there are several ongoing efforts (see current developments in this section) to produce scintillators less sensitive to γ 's. A more subtle problem with scintillations involves use of PMTs. Magnetic fields in and around the detector can cause deflections of electrons in the PMTs, resulting in gain changes. Ever increasing technology in the PMT industry should help minimize this problem.

A. GLASS/CRYSTAL SCINTILLATORS

The glasses and crystals used in scintillation detectors have very high efficiencies. However, as already mentioned, there is a major concern with γ -sensitivity. Also, due to limitations in manufacturing, it is often necessary to use an array of scintillators for large area detectors. This can lead to "dead regions" at scintillator junctions

For ^6Li -glass, there is the added problem of increased background intrinsic to the detector. These glasses are often activated with cerium which may cause noise due to the presence of radioactive isotopes.

1. ANL ^6Li -glass "Anger" Camera

The detector developed by Strauss *et al* at ANL for the IPNS is comprised of an array of PMTs coupled to a thin ^6Li -glass scintillator³⁷. This detector was modeled after the Anger camera³⁸ developed for medical research. The most recent version of this detector³⁹ uses a $30 \times 30 \text{ cm}^2 \times 0.1 - 0.2 \text{ cm}$ thickness of ^6Li -glass, doped with a cerium activator. A thin air gap ($< 0.1 \text{ mm}$) couples the scintillator to a light disperser of boron loaded glass. The

boron glass is then optically coupled to a layer of plexiglass. A 7 x 7 array of square PMTs (each 51 x 51 mm²) is coupled directly to the back of the plexiglass. The disperser is a light guide which spreads the scintillations before they reach the PMTs (Fig. 8a).

The localization of neutron events is obtained by determining the centroid of the light cone reaching the PMTs. Each PMT has a resistor-weighted output (Fig. 8b) dependent on its x- and y-coordinates on the array. The output of an event is then divided by the unweighted sum of all PMTs.

Spatial resolution: 2-3 mm.

Efficiency: 60% at 0.5 Å.

Uniformity of detector: Good.

Continuity of efficiency: The continuity may depend on the quality of the glass.

Stability of detector: Sources of trouble may be caused by gain changes in the PMTs, resulting from changes in temperature or "walk".

Count rate: Scintillators offer the possibility of very high count rates. The decay time for ⁶Li-glass is ~ 60 ns.

Background: Glass scintillators have a high γ -sensitivity. However, with proper electronics, most of the γ -interactions can be rejected.

TOF capability: The entrance window and detection medium contribute little uncertainty to the flight path length.

Maintenance: This is a compact device requiring minimal machining and no fragile components.

2. RAL ⁶Li-glass "Anger" Camera

A ⁶Li-glass "Anger" camera, developed at RAL, is due to be installed soon at ISIS⁴⁰. This camera is based on the same design as the aforementioned ANL camera (Fig. 8a). Like the ANL camera, the RAL camera uses a 30 x 30 cm² x 2 mm active area ⁶Li-glass scintillator, divided into 128 x 128 pixels. There is a 0.1 mm thick air gap between the glass scintillator and disperser (40 mm thick). Unlike the ANL camera, the RAL design uses 45 hexagonal PMTs.

The high fluxes expected at ISIS required a different encoding scheme than that used by the ANL camera. The multifield approach for position encoding, developed by Seeger, was adopted for the RAL camera⁴¹. This method is based on the response of a central PMT and 6 surrounding PMTs in the hexagonal (Fig. 9). The centroid of the neutron event is determined by the distribution of light to the 7 PMTs.

Spatial resolution: 2-3 mm.

Efficiency: 63% at 0.5 Å.

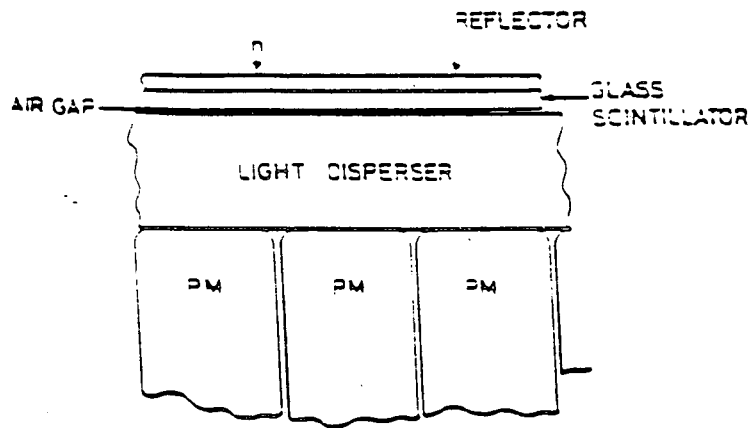


Figure 8a

General design for a neutron "Anger" camera.

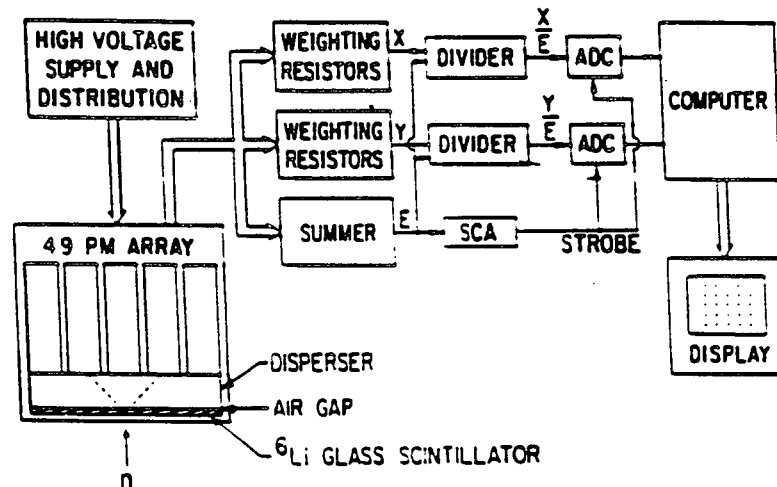


Figure 8b

Weighted-resistor encoding scheme for the ANL camera.

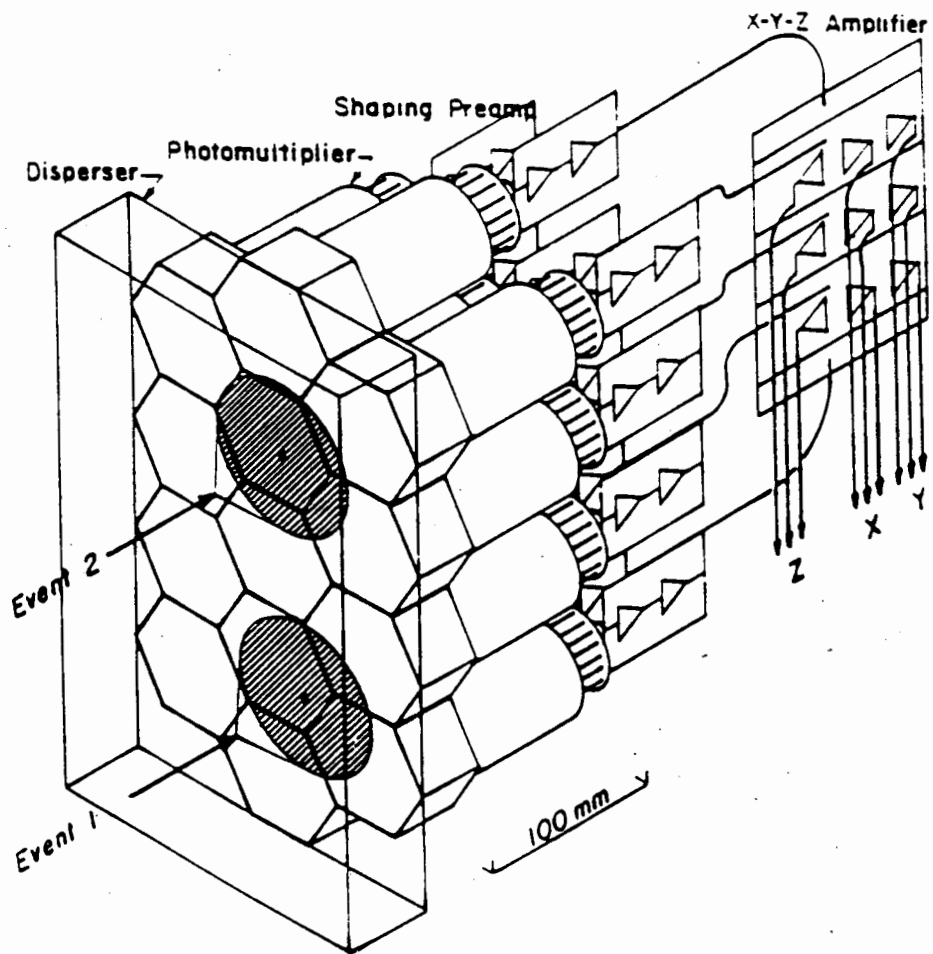


Figure 9

The seven tube multifield encoding scheme for the RAL camera.

Uniformity of detector: Good to a few percent.

Continuity of efficiency: The continuity may depend on the quality of the glass.

Stability of detector: Sources of trouble may be caused by gain changes in the PMTs, resulting from changes in temperature or "walk".

Count rate: Count rates of $> 10^6$ should be attainable. The decay time for ^6Li -glass is ~ 60 ns.

Background: Glass scintillators have a high γ -sensitivity. However, with proper electronics, most of the γ -interactions can be rejected. There is some intrinsic background (~ 1 count/min/cm²) due to radioactive isotopes in a Ce-activated glass. The problem with cross talk between spatial channels was found to be less than 1% for this type detector⁴².

TOF capability: The entrance window and detection medium contribute little uncertainty to the flight path length.

Maintenance: This is a compact, robust detector requiring minimal machining and no fragile components.

3. KFA ^6Li -glass "Anger" Camera

A ^6Li -glass "Anger" Camera has been installed at KFA and is in a test phase⁴³. The detector has an active area 60×60 cm² and is 0.1 cm in thickness. An 8×8 array of photomultipliers is coupled to the back of the scintillator for the encoding. This is a gain stabilized detector with a look-up table for linearization.

Spatial resolution: 7 mm.

Efficiency: 95% at 7 Å.

Uniformity of detector: Good.

Continuity of efficiency: The continuity may depend on the quality of the glass.

Stability of detector: There is long-term stability due to the gain stabilization.

Count rate: 5×10^5 cps.

Background: Glass scintillators have a high γ -sensitivity. There is an extremely high γ -discrimination required for low signal SANS experiments.

TOF capability: The entrance window and detection medium contribute little uncertainty to the flight path length.

Maintenance: This is an easily serviced detector requiring minimal machining and no fragile components.

3. KFA ${}^6\text{Li}(\text{Eu})$ "Anger" Camera

The camera developed at KFA by Jansen *et al* replaces the ${}^6\text{Li}$ -glass scintillator for the ANL and RAL cameras with a ${}^6\text{Li}(\text{Eu})$ crystal scintillator⁴⁴. The ${}^6\text{Li}(\text{Eu})$ crystal was favored over the ${}^6\text{Li}$ -glass scintillator because it was found to have 12 times the light output⁴⁵. In early reports, KFA was using circular PMTs with an encoding scheme similar to that described for the RAL camera. The centroid is located by looking at the response of a central and 8 surrounding PMTs (Fig. 10).

The 2-dimensional version of this camera has an active area of $55 \times 45 \text{ mm}^2$ with a reported spatial resolution of 1 mm and insensitive to γ s $< 3.5 \text{ MeV}$ ⁴⁶.

4. KFA ${}^6\text{Li}$ -glass Scintillator with Position-Sensitive PMTs

This $55 \times 45 \text{ mm}^2$ detector, also developed by Kurz *et al* at KFA⁴⁷, couples a thin ${}^6\text{Li}$ -glass or ${}^6\text{Li}(\text{Eu})$ crystal scintillator to a recently marketed⁴⁸ position-sensitive PMT (Fig. 11). The 1 mm thick ${}^6\text{Li}$ -glass scintillator is optically coupled to the front surface of the PMTs instead of using the air gap method used on previously mentioned cameras (experimental data showed this arrangement to yield a better spatial resolution). A ${}^6\text{Li}(\text{Eu})$ crystal scintillator will be tested with this PMT as soon as the crystal is available.

The readout method for the PMT uses charge-sensitive preamplifiers connected to the x- and y-resistor chains shown in Fig. 11.

A similar development was undertaken at ILL by Baruchel *et al*⁴⁹. They used a ZnS-LiF scintillator, $0.25 \mu\text{m}$ thick, coupled to a multi-PMT developed at Laboratoire d'Annecy-Le-Vieux de Physique des Particules.

Spatial resolution: 1 mm. A resolution of 0.5 mm is expected with the ${}^6\text{Li}(\text{Eu})$ crystal. The ILL development reported a $200 \mu\text{m}$ resolution over an $8 \times 8 \text{ mm}^2$ sensitive area.

Efficiency: 15% at 1.8 \AA reported by ILL.

Uniformity of detector: Maximum deviation from linear response was $\pm 1.5 \text{ mm}$.

Continuity of efficiency: The continuity may depend on the quality of the crystal or glass.

Stability of detector: Not reported.

Count rate: The experiments run at KFA required a flux $< 10^4 \text{ n/s cm}^2$.

Background: Glass and crystal scintillators have high γ -sensitivities. Hamamatsu⁴⁸, in their early developments, reported a 65% cross-talk to the adjacent anodes of the PMT.

TOF capability: No information was available.

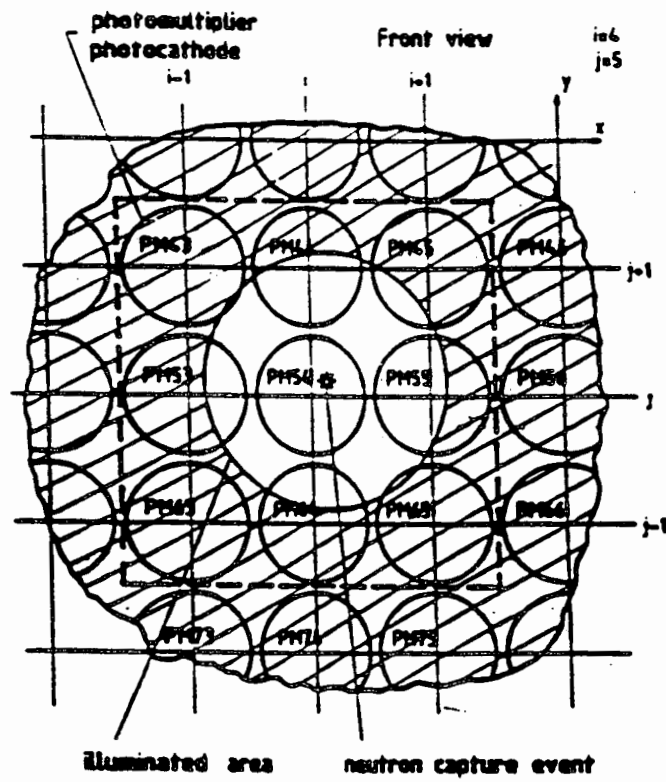


Figure 10

Example of the selection of nine PMTs in a KFA camera.

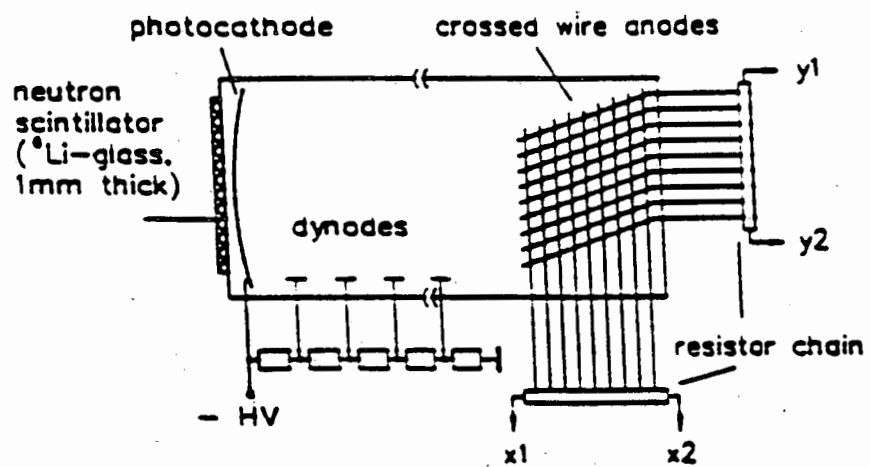


Figure 11

Diagram of the KFA ^6Li scintillator with position-sensitive PMT.

Maintenance: This is a compact, relatively robust detector requiring minimal machining and no fragile components.

5. RAL Fiber-Optic Encoded Detector

A fiber-optic encoding scheme was pioneered by Davidson and Wroe^{50,51} of RAL in developing a scintillation detector with a reduced amount of PMTs (Fig. 12). For a 2-dimensional detector, the scintillator is comprised of 10 mm x 10 mm slices of ⁶Li-glass. Three bundles of fibers are then coupled to the back of each slice for encoding into PMTs. The light produced by a neutron event, in the scintillator, is divided among the three bundles and distributed to a unique combination of PMTs. A triple coincidence between signals from the entire array of PMTs is then decoded electronically to determine the localization of neutron events.

Spatial resolution: 10 mm.

Efficiency: 70% for 2 mm thick scintillator at 1 Å. The overall efficiency depends on the amount of light loss within the fiber-optic elements, which is usually significant.

Uniformity of detector: Good.

Continuity of efficiency: There is a discontinuity of 0.1 mm between the slices of scintillators which act as "dead regions".

Stability of detector: A three day measurement showed a relative stability of $\pm 0.2\%$ ⁵².

Count rate: 10⁶ cps maximum.

Background: Davidson and Wroe reported a detection efficiency of 0.5% for γ -rays of 1.2-1.3 MeV. The intrinsic background was 2-3 cpm per element.

TOF capability: Very good. The 1-2 mm thickness of scintillator adds very little uncertainty to the flight path length.

Maintenance: The small slices of scintillator can easily be replaced if damaged, as with the fibers and PMTs.

B. PHOTOIONIZATION DETECTORS

The photoionization detectors combine the characteristics of a gaseous detector and a scintillator. They have a high efficiency, low background and γ -sensitivity, and good spatial resolution. However, because they involve a gaseous medium, they require special housing for high pressures, extensive maintenance and purification, and are not as easy to use for TOF experiments.

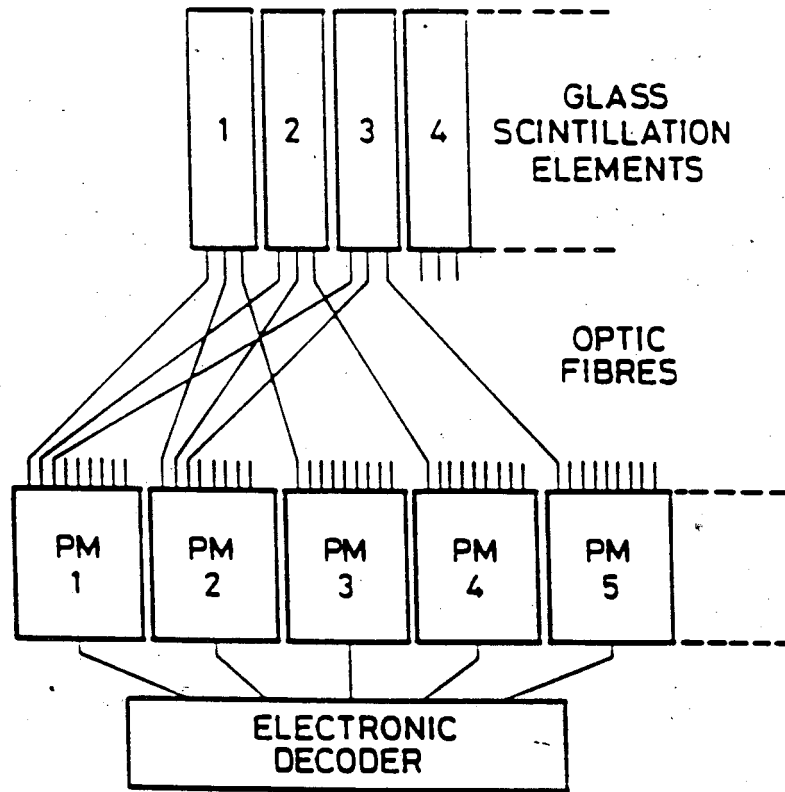


Figure 12

Principle of the fiber-optic encoding scheme pioneered by Davidson and Wroe.

The idea of using a gaseous medium for a neutron scintillation detector was investigated by Nguyen Ngoc *et al* with a prototype ^3He -Xe detector⁵³. This prototype detector contained a 100 mm drift field region and a 6 mm region for light production. The fill gas comprised 4 atm Xe and 0.3 atm ^3He . A set of 50 mm diameter PMTs was optically coupled to the rear of the detector.

Spatial resolution: 1.8 mm.

Efficiency: 95% for 2.5 Å.

Uniformity of detector: Good.

Continuity of efficiency: Not reported.

Stability of detector: Not reported.

Count rate: Good.

Background: Low γ -sensitivity.

TOF capability: This capability should be similar to the ORNL and other MWPC detectors.

Maintenance: This detector is similar to gaseous electronic detectors in maintenance with the requirement of purification and special housing.

C. PLASTIC SCINTILLATORS

The Kelvin Laboratory in Scotland has recently developed a large area plastic neutron detector⁵⁴. This detector is 100 x 100 cm² x 10 cm with light collection by 4 PMTs located at the corners of the square (Fig. 13).

Spatial resolution: 2 cm at center, 6 cm at corners for 17 MeV muon test particles. Test are still being conducted on the neutron detector.

Efficiency: 14% light collection.

Uniformity of detector: The use of contour maps and algorithms are required for each PMT since this is a corner collection technique.

Continuity of efficiency: Not reported.

Stability of detector: The gain of the PMT increases by 2% as the count rate is increased up to 10⁴ cps. The gain increases more rapidly beyond this point and fall rapidly at 10⁶ cps.

Count rate: Should be high, the decay time for plastics is usually < 10 ns.

Background: Plastics have a high γ -sensitivity. Special electronics would be required to discriminate against the γ 's.

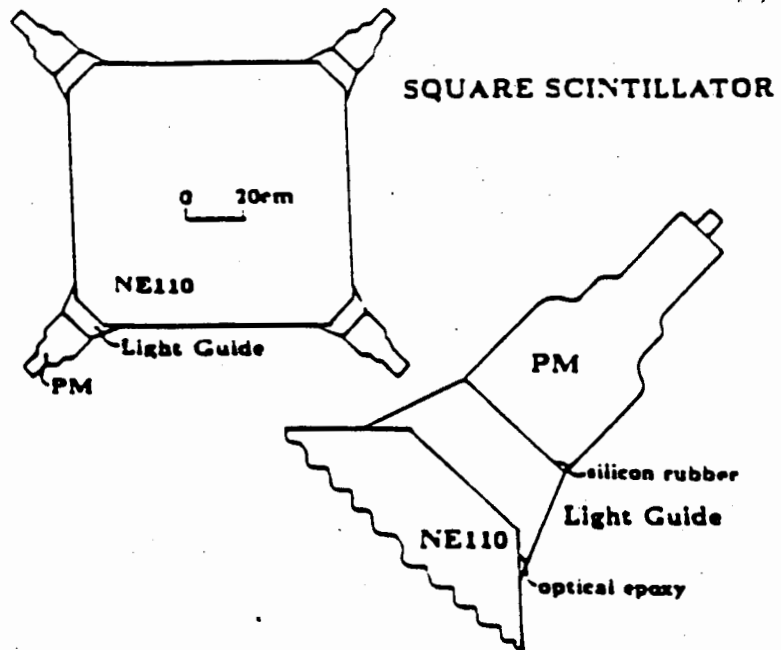


Figure 13

Schematic diagram of a plastic scintillator detector.

TOF capability: The thin entrance window and detection medium contributes very little uncertainty to flight path length.

Maintenance: This is a compact, robust detector requiring minimal machining and no fragile components.

D. MCP DETECTORS

A position-sensitive neutron detector was developed at NIST by Schrack⁵⁵ using a microchannel plate. A 0.5 mm thick enriched ⁶Li-glass scintillator was optically coupled to a fiber-optic faceplate of the MCP (Fig. 14). The faceplate serves as a light guide directing the light to the photocathode at the rear of the faceplate. Created electrons are then multiplied in the MCP electron multiplier and produce a shower at the resistive anode. A readout is taken from each corner of the resistive anode. The centroid of the current distribution on the anode is used to localize incident neutron events.

Spatial resolution: 0.75 mm. Optical scattering in the scintillator and faceplate contribute to spread in resolution. Gao *et al*⁵⁶ have developed a particle and photon MCP detector with a spatial resolution of 15 μm .

Efficiency: 60% at 1.8 \AA .

Uniformity of detector: Good.

Continuity of efficiency: Good.

Stability of detector: The detector has been used several hundreds of hours and shows no sign of changed sensitivity or resolution.

Count rate: Not reported.

Background: The scintillator and MCP are both γ -sensitive.

TOF capability: A thin entrance window and detection medium contributes little uncertainty in flight path length.

Maintenance: Relatively simple to replace inoperable parts.

E. CURRENT DEVELOPMENTS

Several developments are being actively pursued at RAL in the area of scintillation detectors. For the most part, detectors at ISIS have employed ⁶Li-glass because of the speed and efficiency for neutron detection. However, interest has since returned to a ⁶Li-loaded ZnS scintillator to reduce γ sensitivity⁵⁷. Currently, the detector efficiency is > 95% for 1 \AA neutrons.

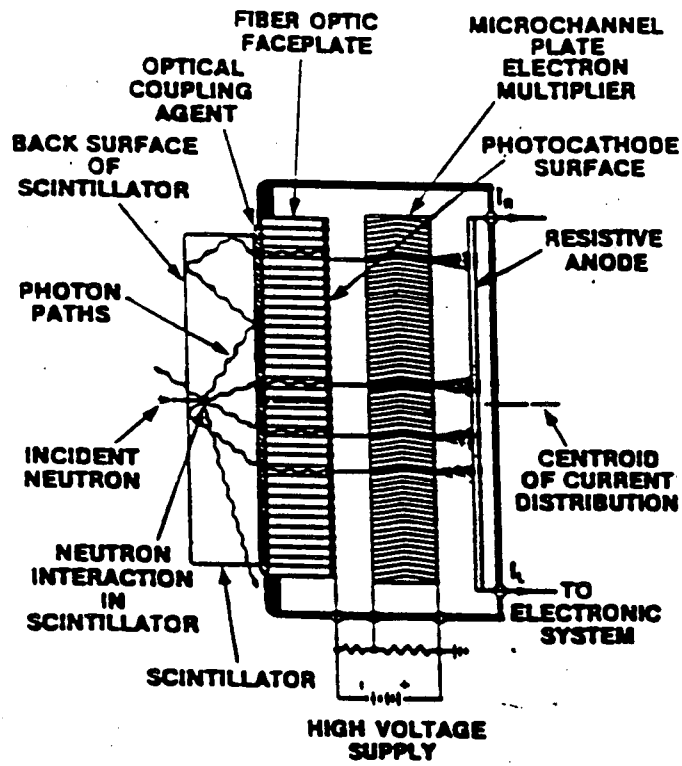


Figure 14

Diagram of the MCP detector.

Also at RAL, Davidson has developed a 1-dimensional scintillation detector which combines the fiber-optic encoding system he helped pioneer with direct coupling of the PMTs to the scintillator⁵⁸. This combination yielded a 1 mm positional resolution, 10^{-4} cpm/cm² γ -sensitivity, and 0.08 cpm/cm² natural background. At the moment, the design is limited to 1-dimensional detectors.

Kurz *et al* at KFA are continuing to develop ⁶LiI as a scintillation detector with reduced γ -sensitivity. They are also investigating the possibility of using ⁶LiH or ⁶LiD.⁵⁹

Other areas of recent development, which may lead to possible applications in neutron detection, include scintillator optical-fiber images^{60,61}, research on light guides⁶², and work in electroluminescence^{63,64}.

VI. SEMICONDUCTOR DETECTORS

The use of semiconductors as neutron PSDs is still in its early development stages. They have shown great promise with their excellent spatial resolution capabilities and short decay times. This makes the semiconductor a good candidate for high count rate environments.

The major difficulties associated with semiconductors are high γ -sensitivity, susceptibility to radiation damage, and high costs. However, increased research in this field should reduce the cost and produce devices which are more radiation hardened.

A. MICROSTRIP PLATE

This new type of detector, developed at ILL by Oed⁶⁵, replaces the multiwire configuration generally used for electron multiplication in gases with a microstrip plate. The MS-plate consists of a positively charged thin conductor strip between adjacent negatively charged strips. As the electrons drift toward the positive conductor strip, they experience an avalanche amplification.

The general electrode configuration of a MS-plate detector is given in Fig. 15. The anode of the detector corresponds to the MS-plate and the cathode, to which the negative high voltage is applied, is a thin polypropylene entrance window. The distance between the window and the anode plate is 70 mm. The detector has a gas fill of 0.2 atm ³He, 0.6 atm hexafluoroethane, and 1.2 atm ⁴He. A limiting count rate was determined to be $>10^6$ counts/cm² across the detector surface. The positional resolution has not been fully tested, but, since the spacing between the strips can be much smaller than the smallest wire spacing in a MWPC, it seems possible to reach correspondingly higher positional resolution.

A position-sensitive neutron detector with a total surface of 64 x 64 cm² is presently being tested at ILL.

B. CURRENT DEVELOPMENTS

The area of semiconductor PSDs for neutron detection is still limited. However, with developments such as charged-coupled devices⁶⁶ and amorphous silicon PSDs⁶⁷ the potential for future designs is promising.

An effort is currently underway by Downing at NIST to develop a CID detector for neutrons with a resolution in the 10 μ m range⁶⁸.

Another development is being pursued by Walter and Dabbs⁶⁹ of Intraspec, Inc. under SBIR. The current detector uses a 5 mm square ⁶Li converter semiconductor subarray. Each element has a separate amplifier and scaler/readout register located on a few slices of silicon. Preliminary tests, under Phase I, have shown good efficiency and count rate capabilities.

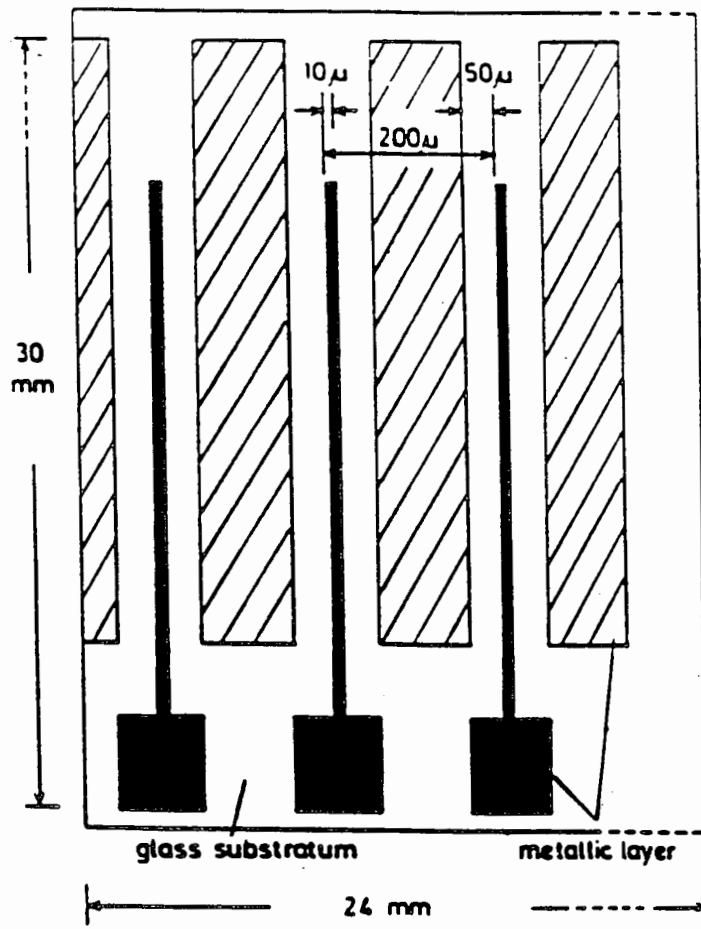


Figure 15

Electrode configuration and dimensions for the MS plate detector.

VII. NEUTRON IMAGING SYSTEMS

The field of neutron imaging has presented the possibility of investigating materials close to real-time. These detectors have low γ -sensitivity, good spatial resolution, and appear to be stable and reliable. Unfortunately, they provide a low efficiency due to the reduced light intensity from the screen and losses in the optical system.

A. MRC CAMERA

The neutron TV camera developed by Arndt at MRC^{70,71} is shown in Fig. 16. This detector has a 400 x 400 mm² ⁶LiF-ZnS scintillation screen divided into a 300 x 300 pixel image. The neutrons are detected by this converter screen and produce light which is projected onto a image-orthicon TV camera tube. Readout is performed by scanning the tube (625 lines at 50 Hz).

Spatial resolution: 1.3 mm.

Efficiency: Effective absorption coefficient for the scintillator screen is 74% at 9 Å.

Uniformity of detector: Good.

Continuity of efficiency: Good.

Stability of detector: Good.

Count rate: Not reported.

Background: Reported to have no undue γ -sensitivity.

TOF capability: Not possible.

Maintenance: The parts of the detector can be replaced if they become inoperable.

B. "FLY'S EYE" CAMERA

In the "Fly's Eye" camera developed by Davidson at ORNL, light is collected from the ⁶LiF-ZnS scintillation screen, intensified, and fiber-optically coupled to a TV camera⁷². There are no lenses in this system. The screen is 15 cm in diameter with a 17,500 cm² active area (Fig. 17). The scanning rate is 30 frames/s.

Spatial resolution: 0.13 mm horizontal and 1.0 mm vertical.

Efficiency: 15% at 1.7 Å for 0.25 mm phosphor thickness.

Uniformity of detector: Good.

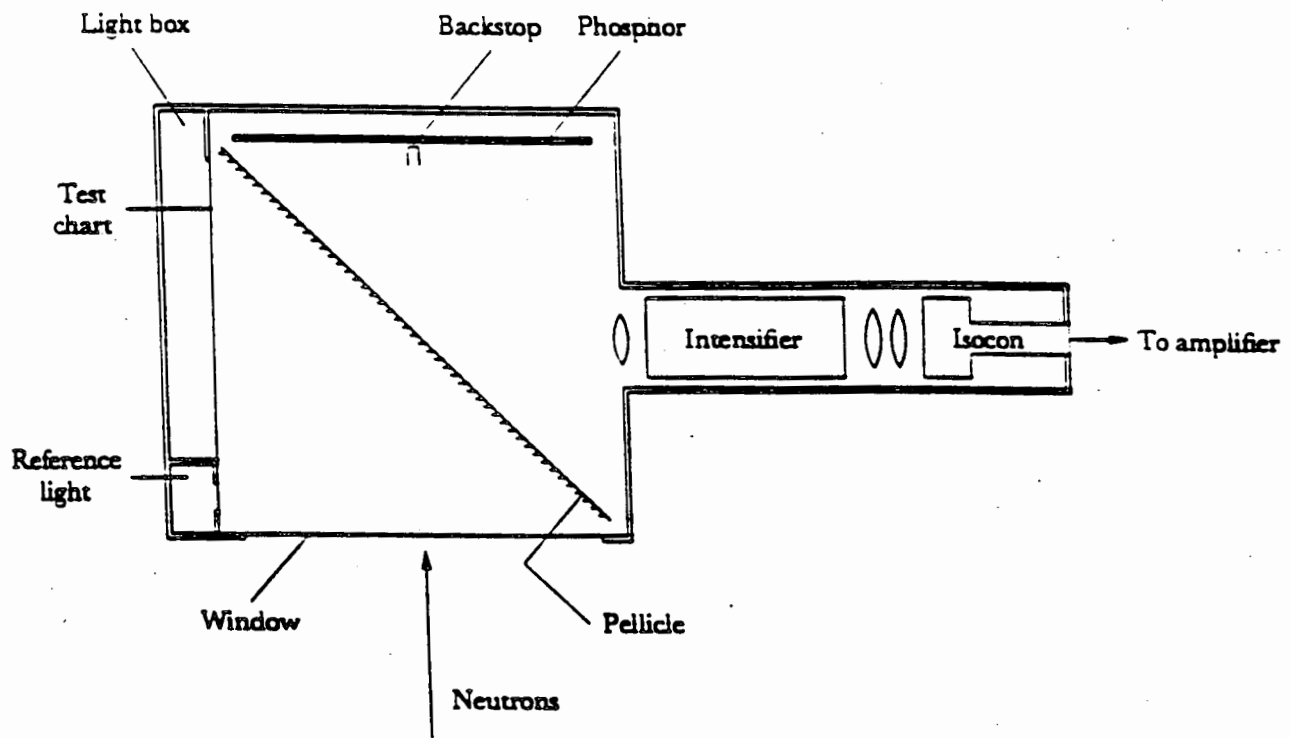


Figure 16

Schematic diagram of the neutron imaging camera developed by Arndt.

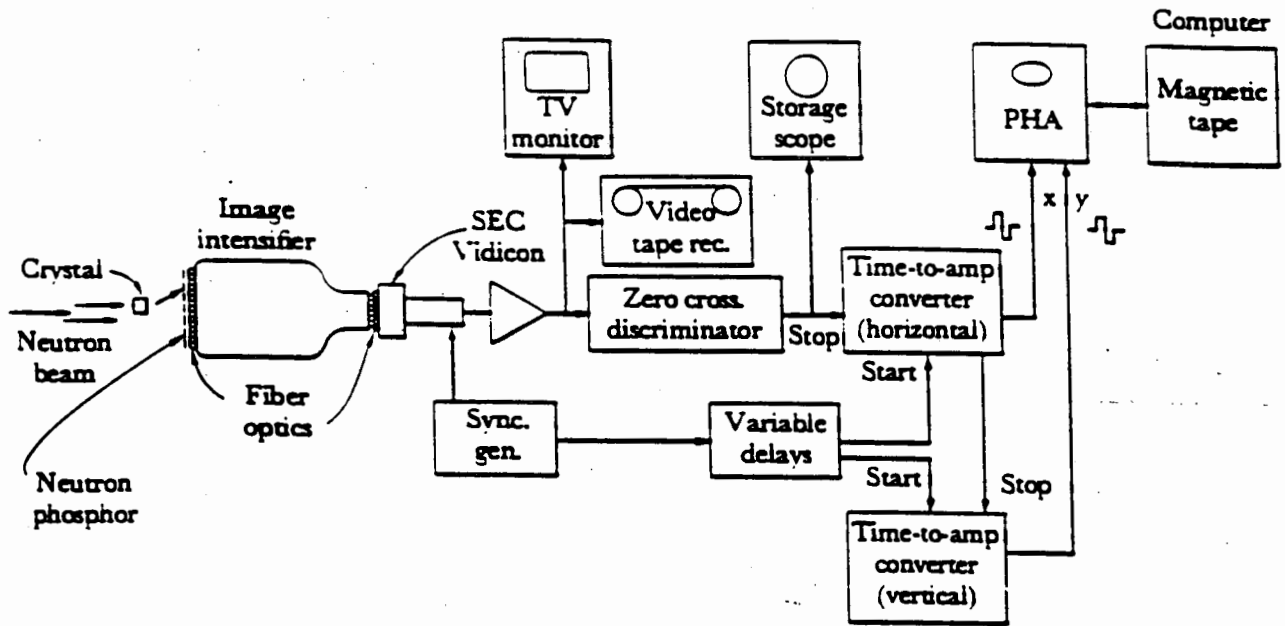


Figure 17

Layout of the "Fly's Eye" system developed by Davidson.

Continuity of efficiency: There is a 20% variation in response due to optics and electro-optics (beam-landing errors). This can be compensated for to within a few percent.

Stability of detector: Good.

Count rate: 10^5 cps for the whole detector.

Background: Relatively insensitive to γ s.

TOF capability: Not possible.

Maintenance: The parts of the detector can be replaced if they become inoperable.

C. CHARGE COUPLING DEVICE

An imaging technique was developed at LNPI by Chernyshov *et al*⁷³ using a scintillator with a charge coupling device. The scintillator, a 1 mm thick $^6\text{Li}(\text{Ce})$ glass, is optically coupled to the entrance face of a image converter tube (ICT). The weak flashes produced are amplified (total gain $\sim 10^6$) and recorded by the charge coupling device. This device has a frame frequency of 25 Hz and a line frequency of 15.625 kHz.

Spatial resolution: 0.4 mm.

Efficiency: 83% effective absorption of neutron on scintillator at 1.8 Å.

Uniformity of detector: Good.

Continuity of efficiency: Not reported.

Stability of detector: Not reported.

Count rate: 10^5 cps per cm^2 flux was recorded.

Background: The scintillator and charge coupled device are γ -sensitive. The authors suggested cooling the device or using special hardware/software for computer processing.

TOF capability: Not possible.

Maintenance: The parts of the detector can be replaced if they become inoperable.

D. CURRENT DEVELOPMENTS

Davidson, ORNL, is currently working on a new system which is a PC based image processor and recorder⁷⁴. This system has not been tested, but the expected spatial resolution is around 1 mm.

VIII. FOIL DETECTORS

The foil detector is not a very efficient means of neutron detection. When the thickness of the foil is optimized, range of produced alphas in ${}^6\text{Li}$ or ${}^{10}\text{B}$ matches foil thickness, the efficiency is $< 10\%$ for thermal neutrons. The use of Gd foils is very promising (absorption cross-section of 74000 barns at 1 Å), but is only 30% efficient.

The special geometry involved with foil (thin layers) make these detectors better suited to long wavelength neutrons. However, by changing the type of converter foil in the detector (${}^{\text{nat}}\text{Gd}$ for high thermal cross-section or ${}^{157}\text{Gd}$ for higher epithermal cross-sections), long and short wavelength measurements are possible.

A. PROPORTIONAL COUNTER WITH Gd FOIL

A proportional counter which utilizes Gd foil for neutron conversion was developed by Jeavons *et al.*, at CERN⁷⁵. There are three major parts to this detector (Fig. 18): the converter, the high-density drift chamber, and the proportional counter. The converter is a 25 μm foil made of natural Gd and high sensitivity to thermal neutrons. The drift chamber is a stacked pattern of alternating conducting (aluminum) and insulating (epoxy-resin) sheets, each 0.1 mm thick. The sheets have holes drilled in them of 0.85 mm diameter. The proportional counter is a standard design. The anode consisted of 20 μm diameter wires spaced 1.5 mm apart. The cathodes, located 3 mm away from the anode, used 100 μm diameter wires of 1 mm spacing. The fill gas was pure isobutane at atmospheric pressure.

Localization of the neutron events was readout by the center-of-gravity method⁷⁶.

Spatial resolution: 1 x 1 mm².

Efficiency: 22% at 1.8 Å.

Uniformity of detector: Good.

Continuity of efficiency: Problems arise in the areas where the drift chamber is not drilled.

Stability of detector: Good.

Count rate: Not reported; probably the same as for other PSPCs.

Background: This detector had a relatively high response to γ 's in the drift chamber. Different gas mixtures are required to make the region transparent to γ radiation. A detector background level of 1 cps per cm² was reported.

TOF capability: Probably the same as with other PSPCs, depending on window and detection medium thicknesses.

Maintenance: Similar to the ORNL and other MWPC detectors.

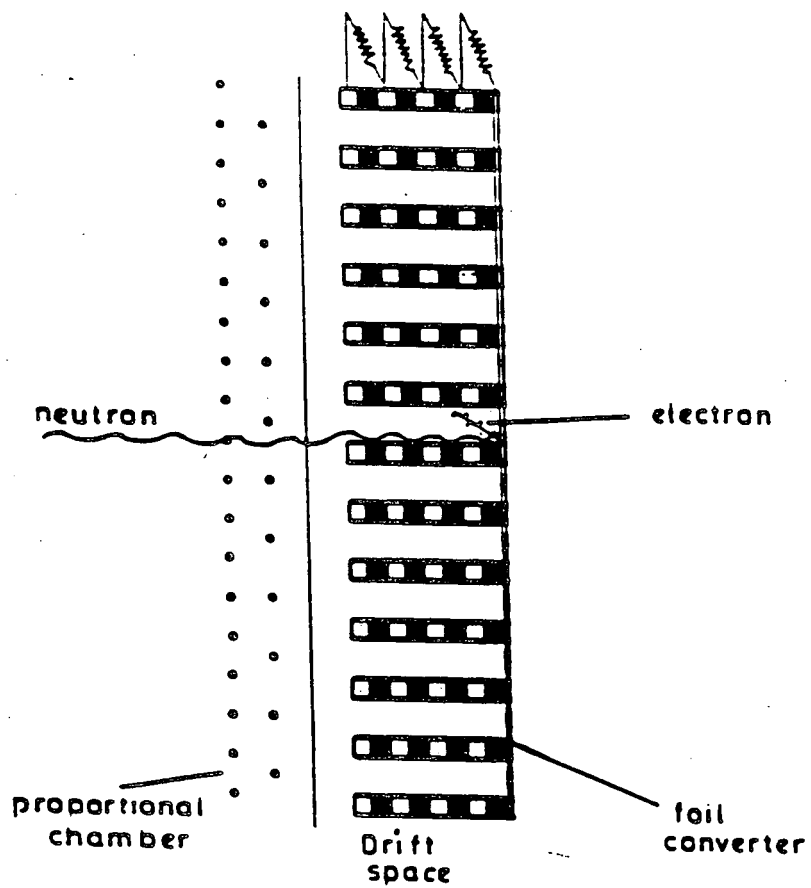


Figure 18

Proportional counter with Gd foil developed at CERN.

B. AVALANCHE CHAMBER WITH Gd FOIL

A multistep avalanche chamber was used by Melchart *et al*⁷⁷, CERN, to develop a position-sensitive neutron detector using a Gd foil converter. The detector, shown in Fig. 19, is comprised of a 10 μm thick natural Gd foil, two wire meshes which serve as the avalanche or preamplification section, and a standard proportional counter. The avalanche region consists of electrodes E and F. Electrode F is a stainless steel wire mesh using 30 μm diameter wires at 500 μm spacing. The second preamplification electrode, E, uses 10 μm diameter Ni wires, 100 μm apart. The Gd foil is pressed against the outer electrode and produces a 3 mm spacing between electrodes E and F.

The MWPC has an anode plane, C, made of 10 μm diameter gold-plated tungsten wires spaced 1.27 mm. The two orthogonal cathode planes, B and D, use Cu-Be wires, 100 μm in diameter and 1.27 mm apart. The separation between the anode and cathode planes is 5 mm. The two-dimensional readout was performed by the center-of-gravity technique.

Spatial resolution: 700 μm .

Efficiency: 25% at 2.4 \AA .

Uniformity of detector: Good.

Continuity of efficiency: Good.

Stability of detector: Good.

Count rate: Not reported; probably the same as for other PSPCs.

Background: Should have a low γ response, but tests have not been completed.

TOF capability: Probably the same as with other PSPCs, depending on window and detection medium thicknesses.

Maintenance: Should be similar to the ORNL and other MWPCs.

C. LOW-PRESSURE MULTISTEP CHAMBER

A LPMSC was developed by Anisimov *et al*^{78,79} at JINR using a thin boron converter. The LPMSC, shown in Fig. 20, is composed of a MWPC with a 4 mm anode to cathode distance, a 3 mm preamplification gap (PT), and a transfer gap 5 mm wide (TC). The 23 x 18 cm^2 neutron converter was made by depositing a 6 μm layer of 86% ^{10}B enriched boron onto a 2 mm thick aluminum sheet. The chamber was filled with 0.007 atm of isobutane.

The coordinates of the event are readout from the cathodes by means of a delay line with a delay of 2 ns/mm and an impedance of 400 Ω .

Spatial resolution: 700 μm .

Efficiency: No less than 3% at 1.8 \AA . Higher concentrations of ^{10}B increased the efficiency to 5%.

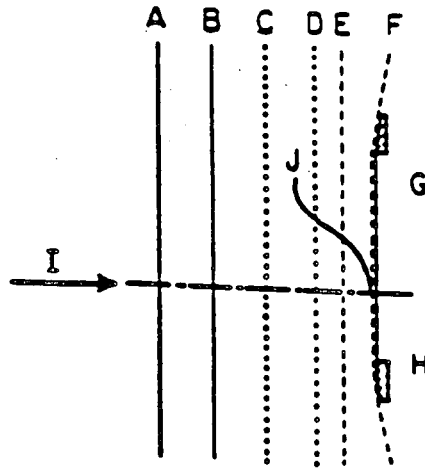


Figure 19

Electrode diagram of the avalanche chamber with Gd foil. A is a mylar window; B, C, and D are the standard MWPC; E and F are the preamplification electrodes; G is a Gd foil mounted on an aluminum ring, H; I is an incident neutron, converting to an electron that ionizes along the track, J.

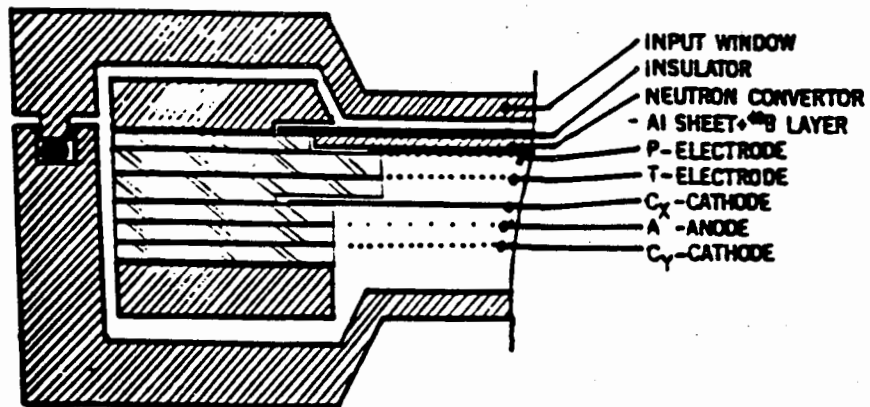


Figure 20

General view of a low-pressure multistep chamber.

Uniformity of detector: < 0.4% integral.

Continuity of efficiency: This was the determining factor for the size of the detector. Larger sensitive areas were limited by technological limitations for preparing a homogeneous layer of converter.

Stability of detector: Not reported.

Count rate: 2×10^5 cps maximum.

Background: A detection efficiency of $10^{-6}\%$ was reported for 60 keV γ s. The detector background did not exceed 0.02 events/cm².

TOF capability: Probably the same as with other PSPCs, depending on window and detection medium thicknesses.

Maintenance: Should be similar to the ORNL and other MWPCs.

IX. PHOTOGRAPHIC DETECTORS

Photographic film is the longest-established and cheapest PSD available. It also possesses the highest spatial resolution available, 20-30 μm with Gd foil. The detectors are robust, unaffected by magnetic fields, capable of withstanding high count rates, and give very low parallax errors. Most importantly, there are no electronics involved and little, if any, maintenance is required.

The major disadvantage to photographic detectors is the difficulty in obtaining quantitative results. Results are often dependent on the careful exposures and development processes.

X. DATA COLLECTION TECHNIQUES

The count rate capability of neutron PSDs is often influenced by, if not principally dependent upon, readout and position-decoding electronics. Although there are a myriad of detector types and materials in use, the associated electronics and encoding/decoding techniques fall into a much smaller number of broadly-defined methodologies. These methods of decoding are often only partially dependent upon detector types and, in fact, a single decoding method may be applicable to more than one style of detector. A good example is the delay line encoding method, which is used with both multiwire gas detectors and etched microstrip detectors. Another generalized method is the "group/element" encoding method, which is used with scintillation arrays and multiwire gas detectors. For this reason, a discussion of the electronics for neutron detection cannot proceed on a "detector class" basis but must instead treat electronic decoding methods as separate building blocks that can be used with any class of detector that has the prerequisite signal outputs. Although many decoding methods were specifically designed for a particular detector/encoding type, and are thus treated as such by presenting them within the context of their parent detectors, enough of the encoding/decoding methods are general enough that the "detector class" approach could not be used.

A. RESISTIVE ENCODING

Gas PSDs with resistive encoding include a number of detector topologies, the simplest of which is the 1-D PSPC. All of these detectors operate by utilizing the charge produced by the capture of a neutron in the fill gas of the detector. Charge division encoding and time-difference decoding are often employed to ascertain the position of the capture along the axis of the detector.

1. Charge Division Encoding

Charge division encoding is the standard method for determining the position of a neutron capture in gas PSDs. As an illustrative example, in a 1-D PSPC (Fig. 21) the position of the capture can be determined by the relationship:

$$Q_b/(Q_a + Q_b) = (x\rho + Z)/(l\rho + 2Z)$$

where Q_a and Q_b are the charges collected at each end of the detector wire, l is the length of the detector wire, x is the distance between the capture point and the A end of the wire, ρ is the wire resistivity, and Z is the input impedance of either of the preamps. By utilizing this relationship, the magnitudes of Q_a and Q_b , after suitable amplification and conditioning, can be compared to yield the value of x .

One of the applications of charge-division encoding is in the position-sensitive PMT manufactured by Hamamatsu⁴⁸ and used by Kurz *et al* at KFA⁴⁷ (Fig. 11).

Figure 22 shows the charge-division method extended to a multiwire cathode, as would be found in 2-D detectors.

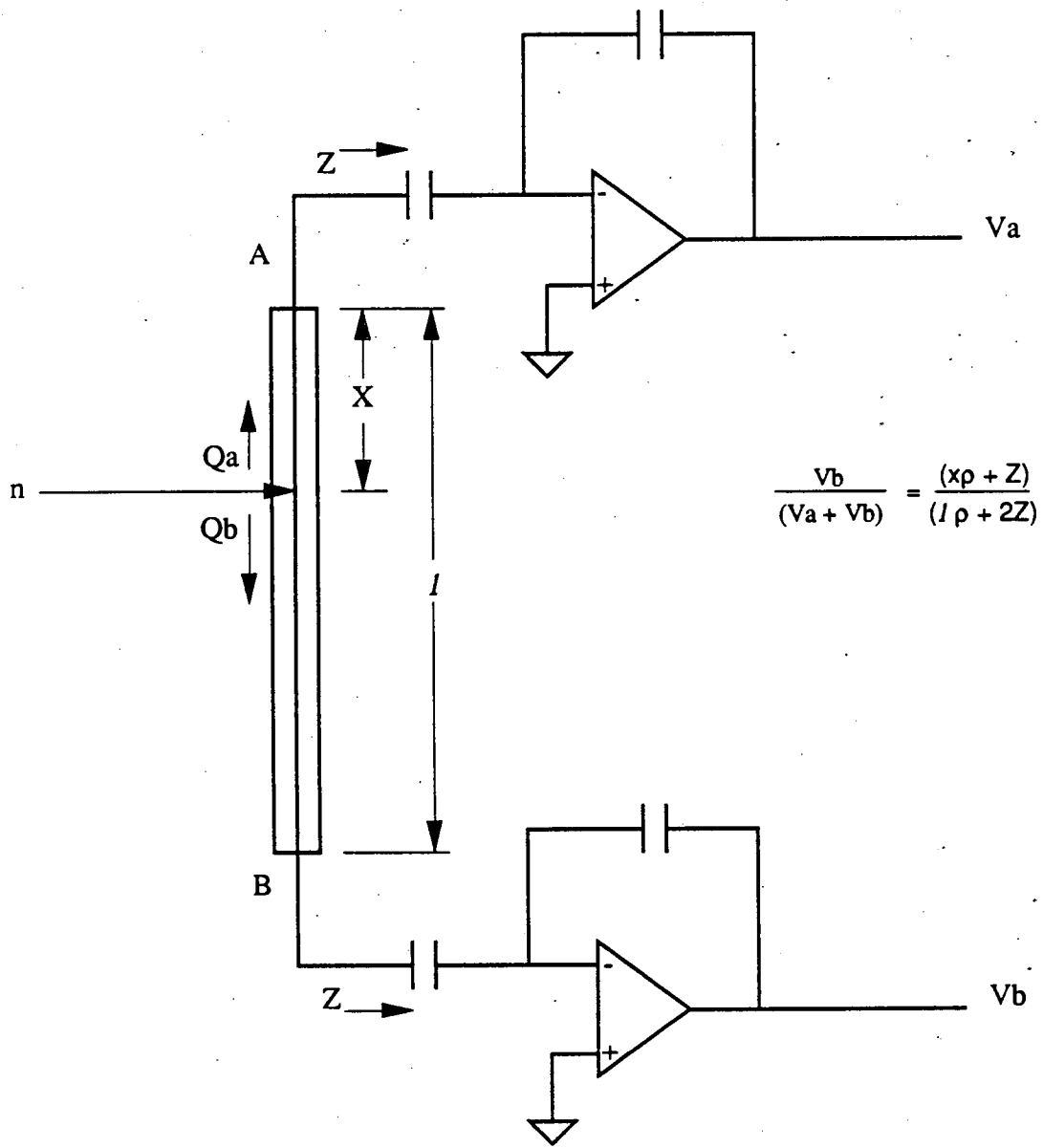


FIGURE 21: Basic charge-division decoder. The difference in amplitude between Va and Vb is related to the distance x.

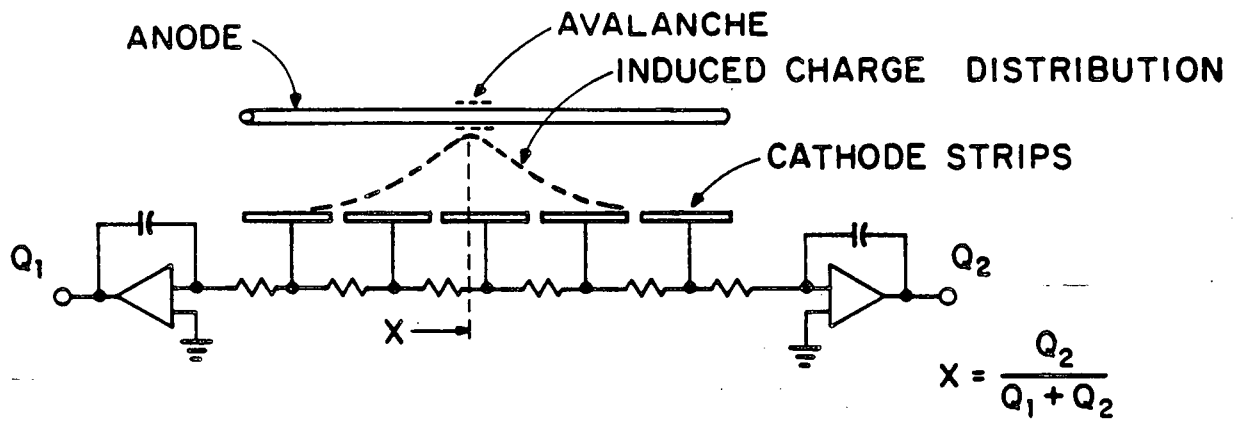


FIGURE 22: Charge-Division Encoding Applied to a Multiwire Cathode.

2. Time-Difference Decoding

Another method of coordinate determination using resistively encoded PSDs is through time-difference decoding, which was pioneered by Borkowski and Kopp¹¹. This method of decoding treats the detector cathodes as distributed RC networks, determining the position of neutron captures by the difference in rise times of the signals coming from each end of the cathode wires. Detectors using this method of decoding are being used at ORNL, Riso, and NIST.

Figure 23 shows a block diagram of the decoding circuitry being used at NIST¹². A similar electronic system is used at Riso¹⁵. Signals from the preamps are fed to Gaussian shaping amplifiers with 3 μ s shaping time constants. The bipolar outputs of the shaping amplifiers are sent to timing single channel analyzers (TSCA) which are used as crossover detectors, and the unipolar outputs are sent to a summing amplifier and TSCA. If the summed signal falls within a specified amplitude range, its TSCA generates an output pulse that enables the direct time digitizer (DTD), converting the time-difference interval from each cathode into digital x and y coordinates. The two 8-bit binary words are then converted into a 16-bit address, which is written into memory using DMA.

The useable count rate of this particular system is rather low, being about 2500 c/s. This rate is primarily due to the long ($\sim 18 \mu$ s) signal processing time, which is dominated by the duration of the bipolar outputs of the shaping amplifiers.

B. INDIVIDUAL COUNTER ARRAYS

Individual counter arrays (ICA) are characterized by a number (sometimes large) of individual detector elements, either gas, semiconductor, or scintillation, arranged in a closely-packed array. The positional resolution of the detector is dependent on the size of each element. Two ICAs will be covered here as examples: the MURR-SANS individual resistive wire multidetector, which is a gas ICA PSD; and the RAL fiber-optic coded PSD, which is a scintillator PSD.

1. Individual Resistive Wire Encoding

This detector is described by Berliner *et al* at MURR⁴. It is composed of 43 linear ³He PSPCs in a 50 cm X 64 cm array. Position encoding in the x-direction is performed via charge division as in a standard 1-D single-element gas PSPC, and y-direction encoding is accomplished by identifying the detector element in which the neutron event occurred.

A block diagram of the frontend electronics for a single element of the MURR array appears in Fig. 24. As usual, charge-sensitive preamps are used to amplify the output charge pulses from the two ends of the detector. These pulses are then further amplified and sent to a summer and to separate ADCs. The summed signals are detected by a low level discriminator, which triggers the two ADCs to convert the two signals into digital codes. From this point the data is fed to a microcomputer's address and data busses for further manipulation. The advantage of this system is that it uses readily-available commercial PSPCs, which, in addition to reducing the amount of precision design, also simplifies maintenance and reduces costs.

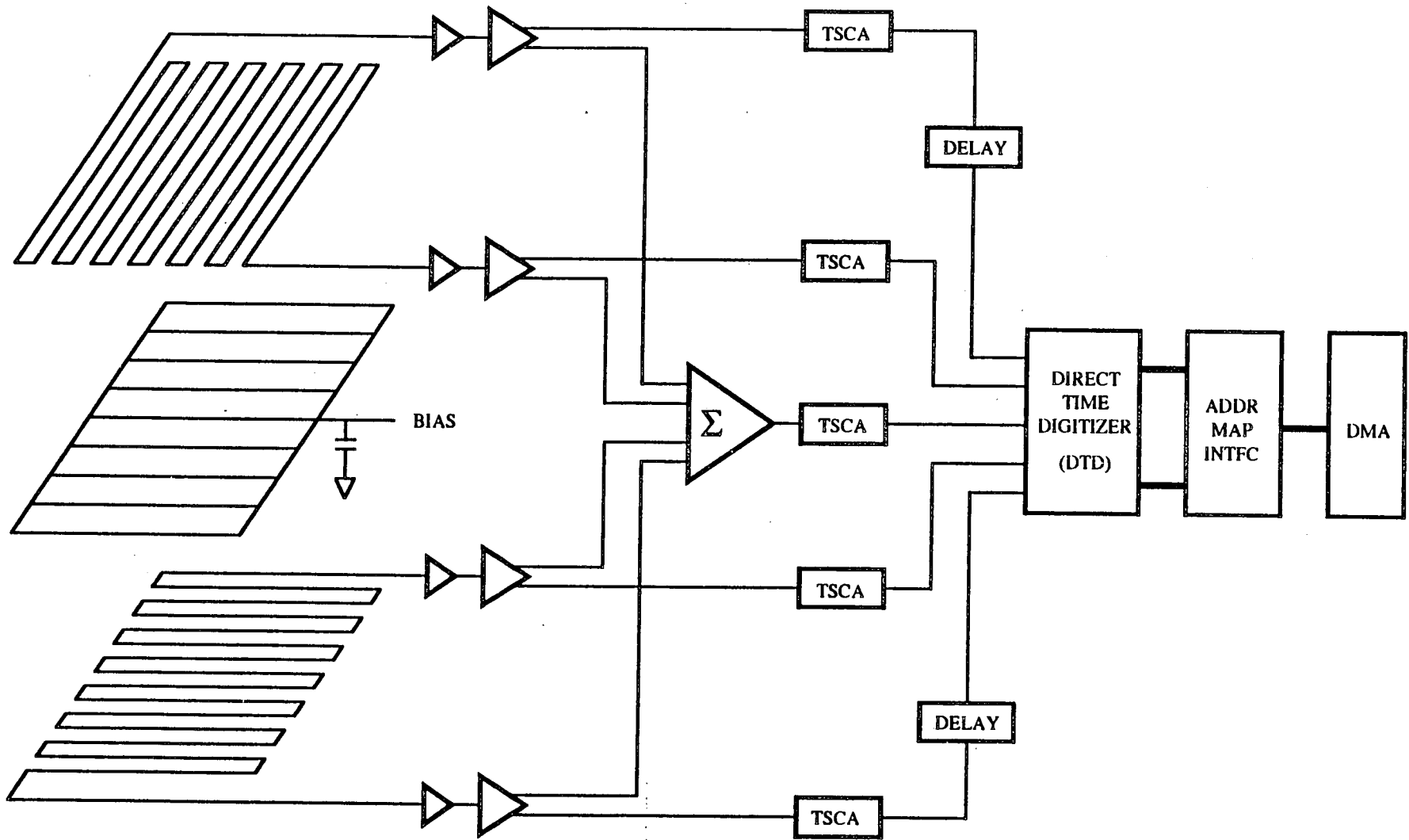


FIGURE 23: Decoding Circuitry for the NIST Detector.

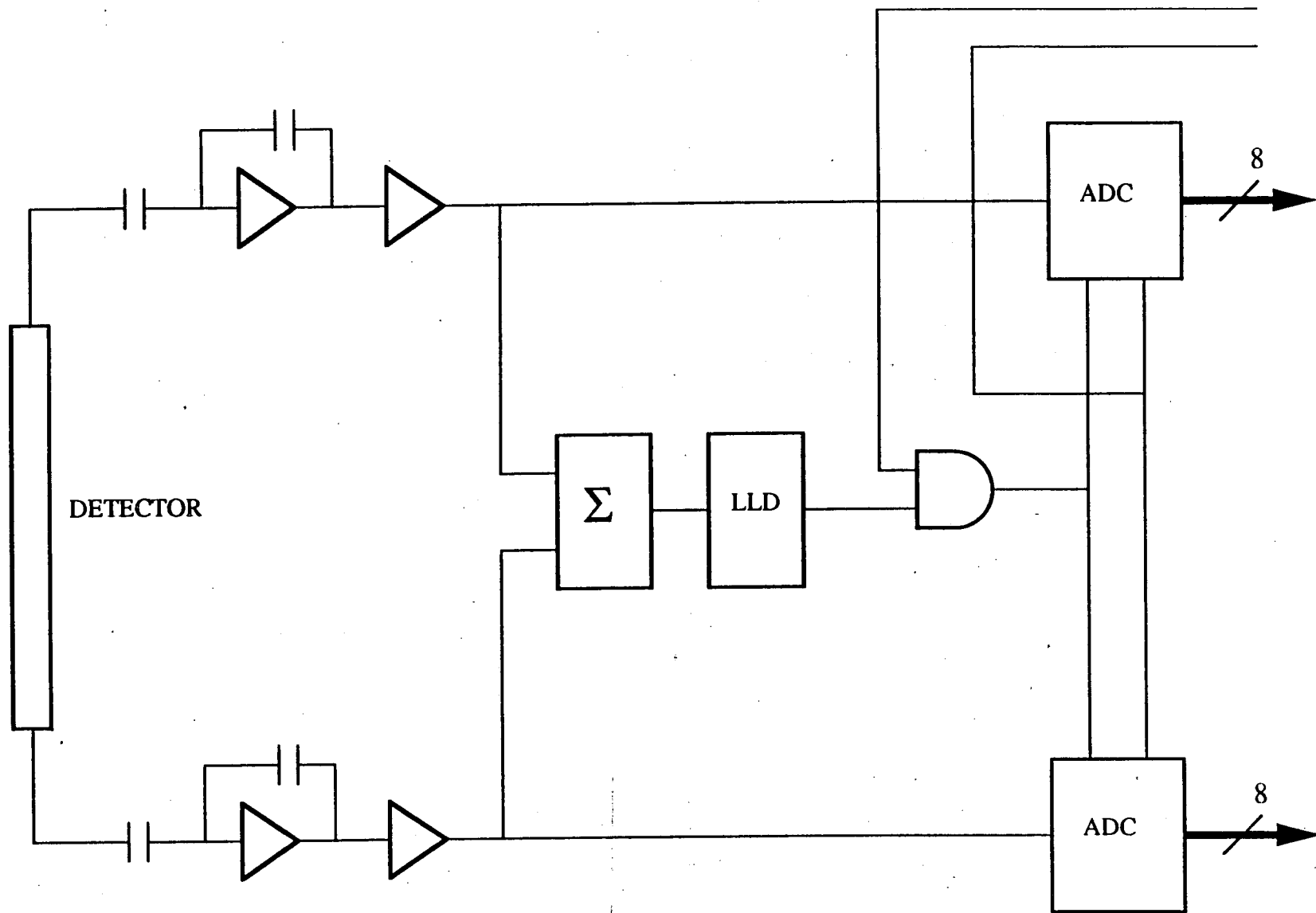


FIGURE 24: MURR-SANS Detector, Single Channel.

At this time, the count rate limitation of this type of detector is dictated primarily by the conversion time of the ADCs, which is about $10 \mu\text{s}$ ⁸⁰. Although some progress is being made by the electronics industry in this area, the A to D conversion process will likely be the critical link for some time.

2. Fiber-Optic Encoding

The fiber-optic encoding scheme developed by Davidson and Wroe of RAL⁵² reduces the number of PMTs needed for a given number of scintillation elements. A schematic illustration of this method appears in Fig. 12. The prototype system described in ref. 52 consisted of 200 scintillation elements, arranged in a two-layered "banana" array with three coding fibers per element. Each element in turn consisted of three scintillator pieces. The prototype system as implemented was a 1-d array; if, however, each of the pieces within the elements were encoded separately, a 2-d detector could be made. The number of elements is greatly expandable; a 1600-element detector was envisioned as a goal for this type of detector.

The encoding scheme for this type of detector is detailed in Fig. 25. Each scintillator element is connected to a unique combination of three of twelve PMTs. For this particular encoding algorithm, the x, y, and z values are simply the numbers of the PMTs that each element is connected. D is derived from the element number minus the z-value.

The electronics for this encoding scheme appears in block form in Fig. 26. Each PMT is followed by an amplifier/discriminator, and the logic pulses produced therein are routed to a coincidence circuit that produces a "validity signal" if 3 (and only 3) of the 12 PMTs register a neutron event within a 200 ns window. The validity signal initiates the sequence controller, and the three valid pulses are sent to a pattern register and a priority encoder. The output of the encoder is, in turn, the 4-bit binary numbers for x, y, and z. Since x, y, and z are 4 bits wide, up to 16 PMTs can be used with this circuit. The sequence controller latches the x, y, and z numbers into registers. The x and y values feed a ROM, which generates D, and this number is then combined with z to produce a 12-bit position descriptor. The position descriptor is then utilized by a computer.

Currently, the anticipated maximum count rate is 10^5 c/s for each detector element, and about 5×10^6 c/s for the full 1600 element array. The primary limitation is in the electronics, which has a 400 ns (eventually 100 ns) decoding time.

A second type of fiber-optic encoded PSD was recently unveiled by Davidson⁵⁸ (Fig. 27). This system uses a matrix-style encoding in which an event is localized to one of 135 elements by the coincidental signals on one of 15 "group" PMTs and one of 9 "element" PMTs. According to Davidson⁸¹ the maximum count rate of this detector is estimated to be about 2×10^6 c/s, with the limiting factor being in the digital logic. With improved logic design the count rate could be increased to 3 or 4 MHz. The current design is limited to 1-d detection, but the system is adaptable to 2-d.

A disadvantage of fiber-optic encoded designs is gamma sensitivity. This is due in part to poor optical coupling in the fibers, which makes gamma discrimination more difficult.

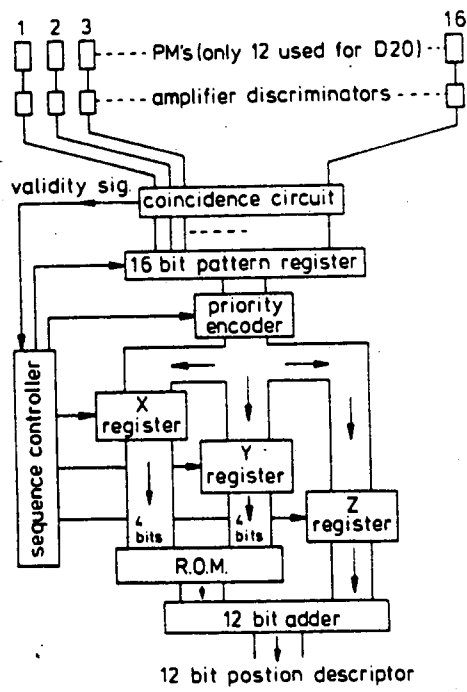


FIGURE 26: Electronics for the RAL Fiber-Optic Encoded PSD.

Element NO. A	Photomultiplier NO.																X	Y	Z	D= A-Z
	1	2	3	4	5	6	7	8	9	10	11	12	13	14	15	16				
1	X	X	X														1	2	3	-2
2	X	X	X														1	2	4	-2
3	X	X		X													1	2	5	-2
4	X	X			X												1	2	6	-2
5	X	X				X											1	2	7	-2
6	X	X					X										1	2	8	-2
7	X	X						X									1	2	9	-2
8	X	X							X								1	2	10	-2

15		X	X	X													2	3	4	+11
16		X	X		X												2	3	5	+11
17		X	X			X											2	3	6	+11
18		X	X				X										2	3	7	+11

FIGURE 25: Encoding Scheme for RAL PSD.

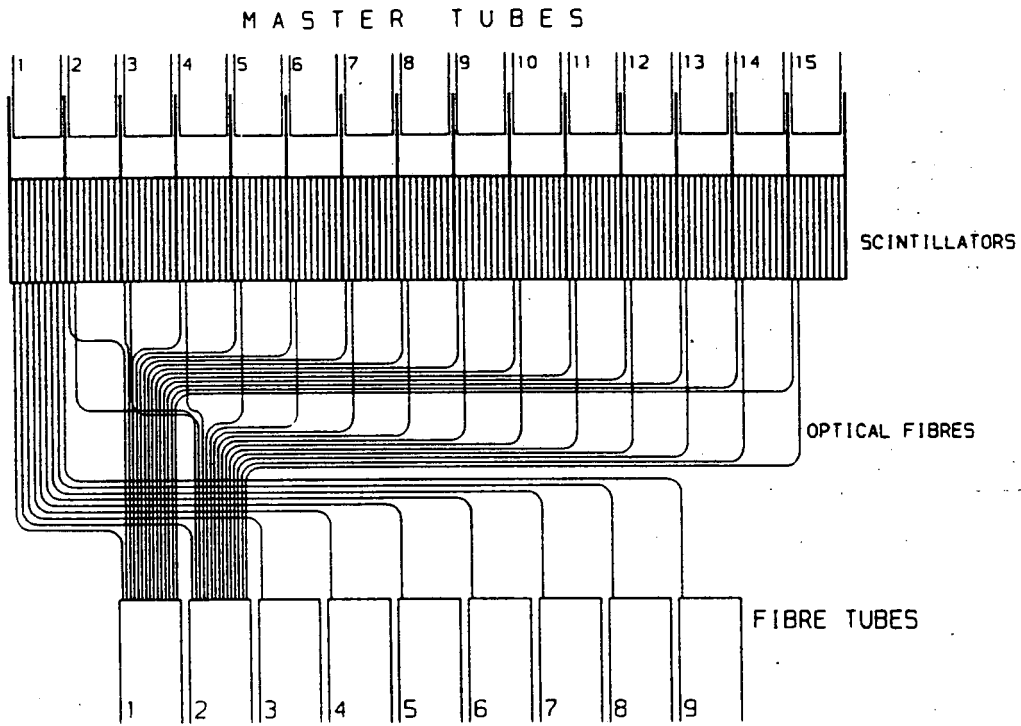


FIGURE 27: RAL Fiber-Optic Encoded PSD, Later version.

C. MULTIELECTRODE ENCODING

Multi-electrode encoding is an evolutionary step from the individual wire PSD. The detectors for this style of encoding can be visualized as a number of individual counter elements arranged in close proximity to each other and within the same detector housing. This type of encoding/decoding is usually used with gas detectors, but variations of this method can be used with scintillators.

1. Position Determination Through Coincidence

An example of the coincidence method of position determination is described by Allemand *et al*²⁵. This is perhaps the most straightforward of the multi-element encoding methods, deriving the position of the neutron event by the coincidence of output pulses from two orthogonal elements within a 2-d array. Figure 28 illustrates the principle of the coincidence method, using as an example the gas wire detector from ref. 25. A neutron capture will induce charges in a cluster of wires on each of the two cathode arrays, and the position of the event is essentially taken as the intersection of the two wires with the largest signals, although a higher precision can actually be realized through the interpolation of the amplitudes of the signals on consecutive wires (center-of-gravity method).

When used with multiwire detectors this method of readout usually has an amplifier and conditioning circuit on each element, so the detector is capable of higher count rates than is possible with other multiwire encoding methods such as RC and delay line. The current limiting factor on count rate is likely to be the electronics, most notably the ADC section as in the individual wire array at MURR, although the specifics of this area were not detailed in any of the available references.

2. Center-of-Gravity Method

The center-of-gravity method, also known as amplifier-per-wire, is shown schematically in Fig. 29. Ideally this method would process each amplifier/cathode output separately and in parallel to maximize count rate, as shown in Fig. 29b. However, for large detectors this method would be unmanageable and expensive. A more practical arrangement might be the circuit in Fig. 29c, where the outputs are read sequentially and digitized, then processed by a computer. An analog method of calculating the sums of the charges is seen in Fig. 29d, where centroid calculation is performed through resistive weighting.

A system using an amorphous silicon detector, under development by Mochiki⁶⁷, uses an approach similar to that shown in Fig. 29c. The detector, which is a charge-integrating type, is read out sequentially and digitized. A computer then takes the digitized samples and calculates the centroid. The primary drawback of this system is its speed of operation, which is about 1 μ s per scanned element.

3. Centroid Finding By Convolution

This method of centroid finding, developed by Redeka and Boie²¹ for a multiwire detector at BNL, subdivides the parallel readout of the wires (or strips) of a MWPC, as seen in

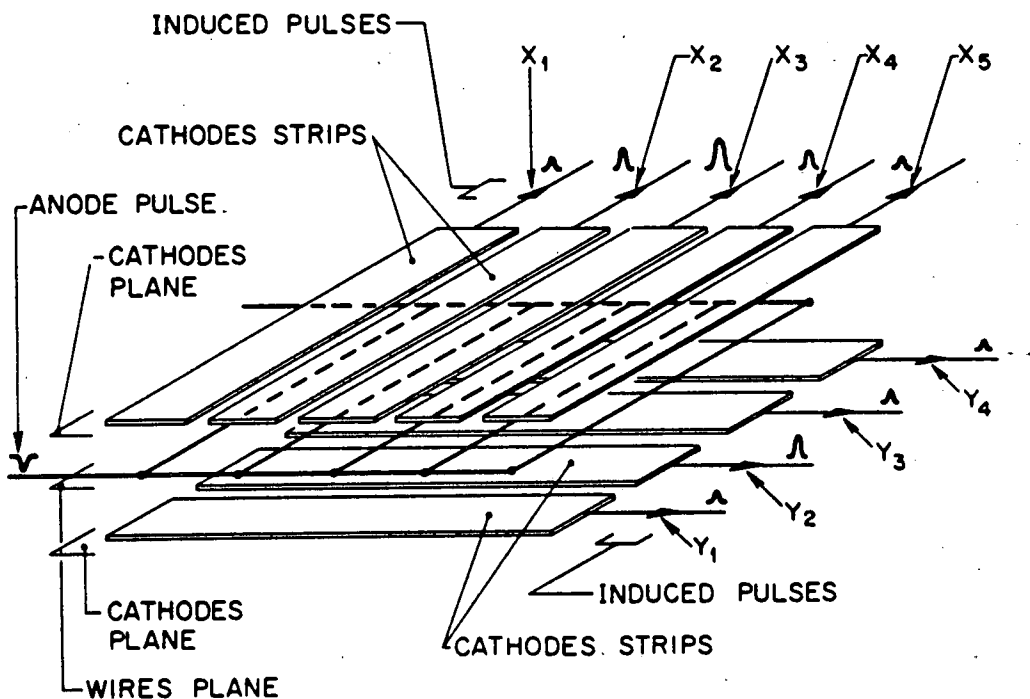


FIGURE 28: Coincidence Method Using Multicathode Area Detector. x,y position is determined by the coincidence of the two largest pulses, in this case X3 and Y2.

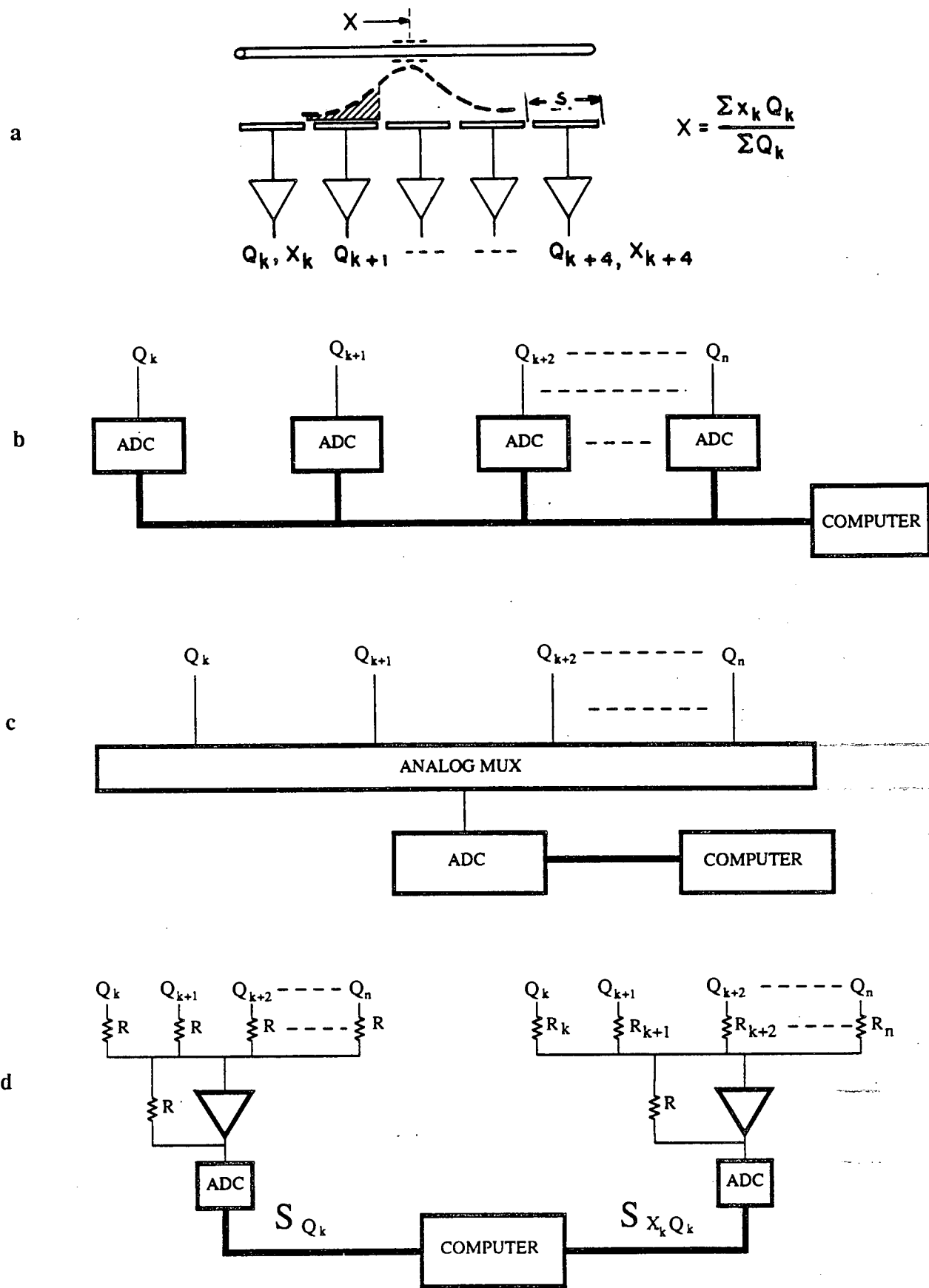


FIGURE 29: Center-of-Gravity Method.

Fig. 30. The number of amplifiers is related to the number of subdivisions, with the maximum being an amplifier per wire. The position resolution improves with the number of subdivisions.

The outputs of the amplifiers are sequentially switched, or sampled, at some high rate, producing a waveform that reflects the quantized charge distribution along one axis of the detector (Fig. 31). The sample rate and the time constant of the centroid finding filter are both related to the speed and accuracy of this method, and for high count rates both should be as fast as possible to minimize the time needed for centroid calculation. The waveform is then passed through the centroid finding filter, whose output will produce a zero-crossing that is delayed from the centroid by exactly one-half the width of the filter's impulse response. The time from the start of the sweep to the zero-crossing is thus related to the position of the centroid.

An interesting artifact of this method is that when the number of subdivisions is zero (i.e. two amplifiers, one at each end of the resistive electrode), the centroid finding circuit can be used as a substitute for the charge-division method.

An alternative method described in ref. 21 (Fig. 30b) is to simultaneously switch the outputs of the amplifiers onto a delay line, which then feeds the centroid finding filter. Due to variations in the delay increments, however, this method will exhibit limited accuracy.

Processing time (time to calculate the position of the centroid) is dependent primarily on the sample rate and the number of subdivisions: increasing the sample rate will improve the processing time, and increasing the number of subdivisions will improve the position resolution but will also increase the processing time for a given sample rate. Decreasing the number of subdivisions will increase the speed but will increase the noise as well. Thus a tradeoff must be made between position resolution, noise, and speed. A significant reduction in processing time could be realized by sampling only those subdivisions that contain charge samples.

A system that substitutes small pads for the cathode strips is now under development at BNL⁸³. The new system incorporates a large number of 1-D centroid finding detectors arranged in parallel.

4. Delay Line Encoding

Delay line encoding is another common method of 2-d resolution in multiwire detectors. The basic principle is outlined in Fig. 32. In delay line encoding, the induced charge on the cathode wires of the detector are coupled to a delay line. The difference in arrival times of the pulses from the anode and each cathode are used to determine the location of the neutron capture.

The pulses from the delay lines are fed to constant fraction discriminators (CFD), which produce accurate, amplitude-independent pulses. These pulses then go to the time-to-digital converters (TDC), which produce a digital equivalence of the time difference between the cathode pulses. The pulse from the anode circuit precedes the cathode pulses and is used to initiate the controlling sections of the electronics.

Delay line encoding is generally faster than the RC encoding methods because the delay lines are usually $<1 \mu\text{s}$ in length. However, there is a practical limit to the speed of this

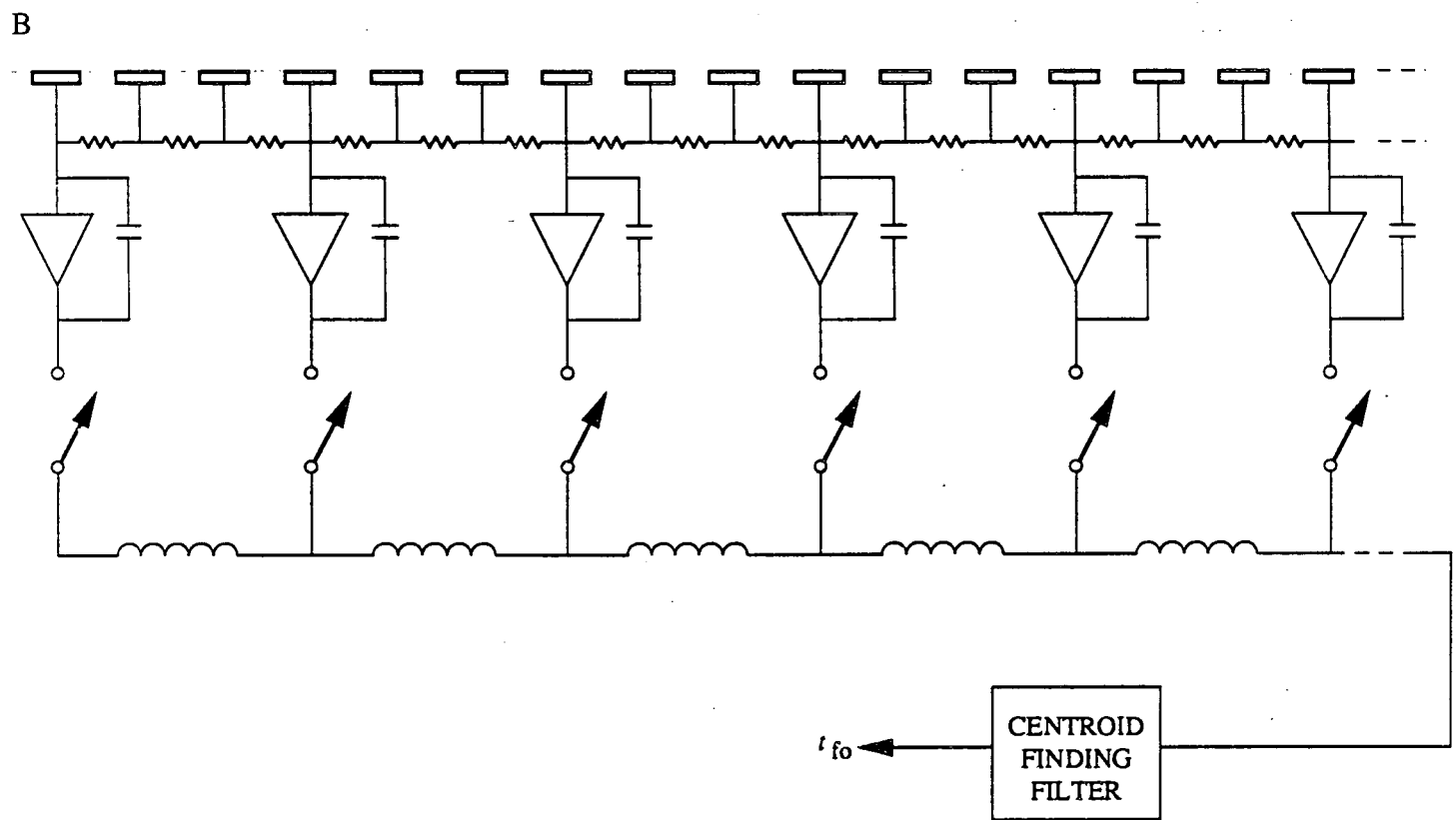
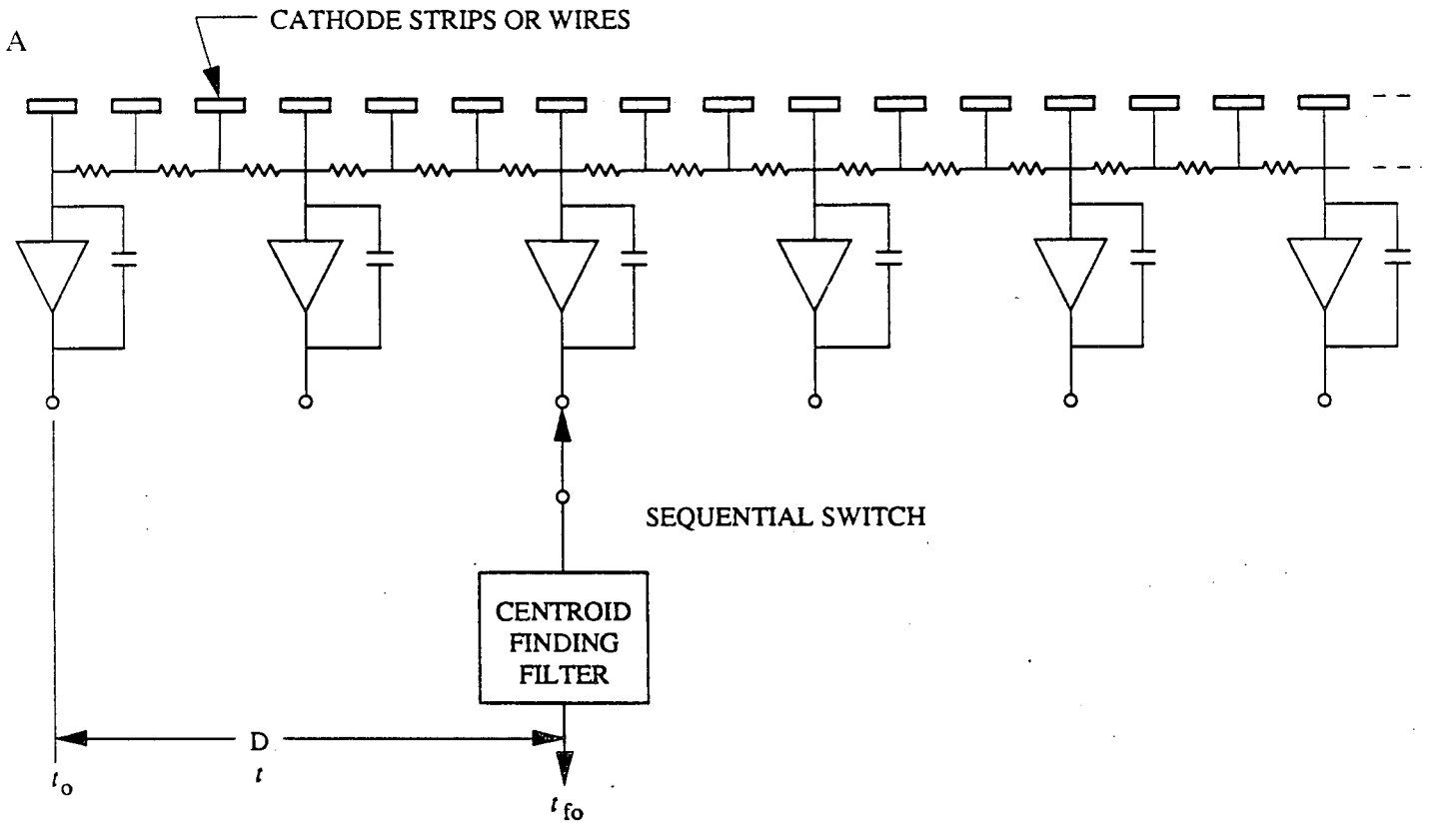


FIGURE 30:Centroid Finding By Convolution.

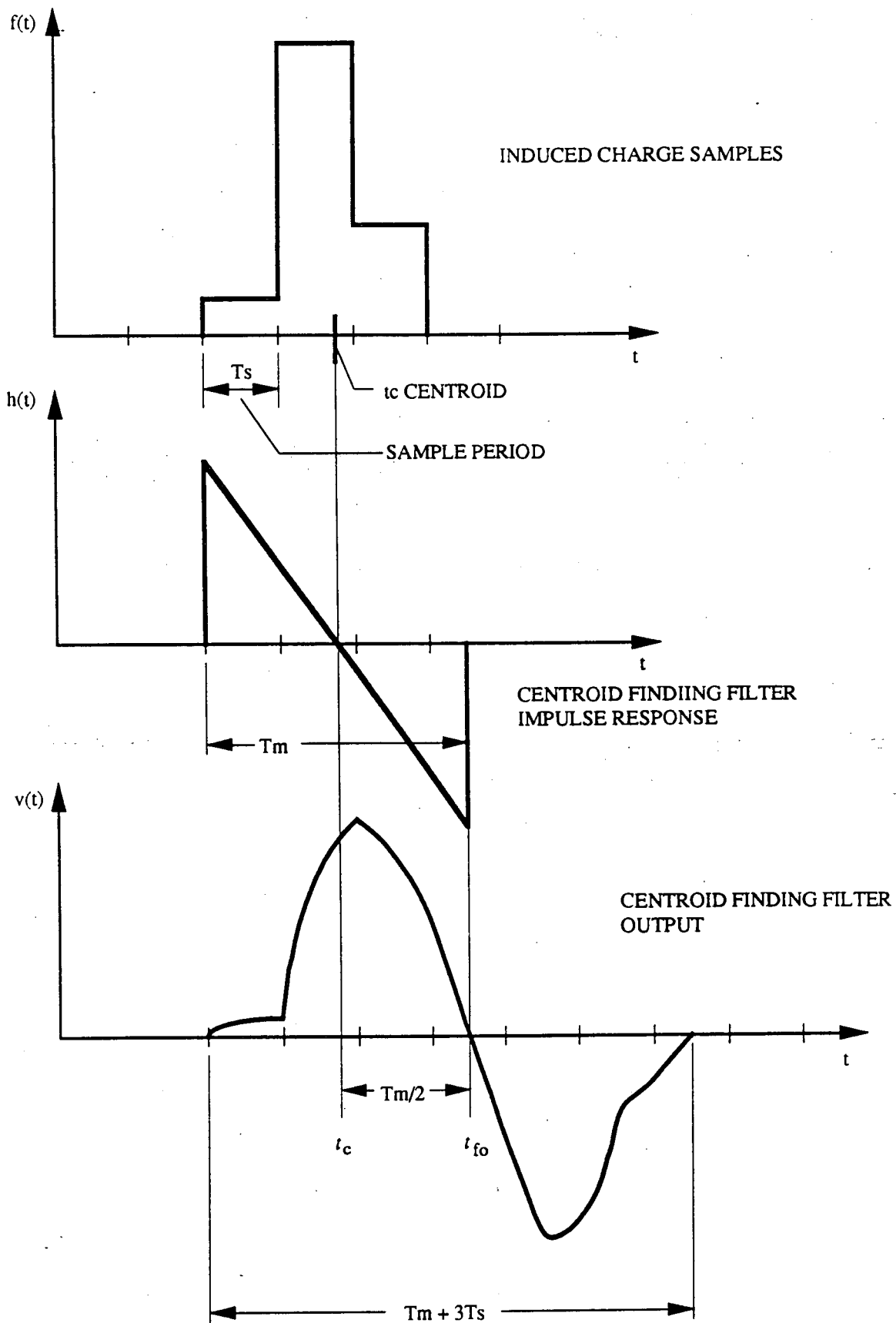


FIGURE 31: Centroid Finding By Convolution. The zero-crossing point of the CFF output is delayed by $T_m/2$ from the actual centroid position.

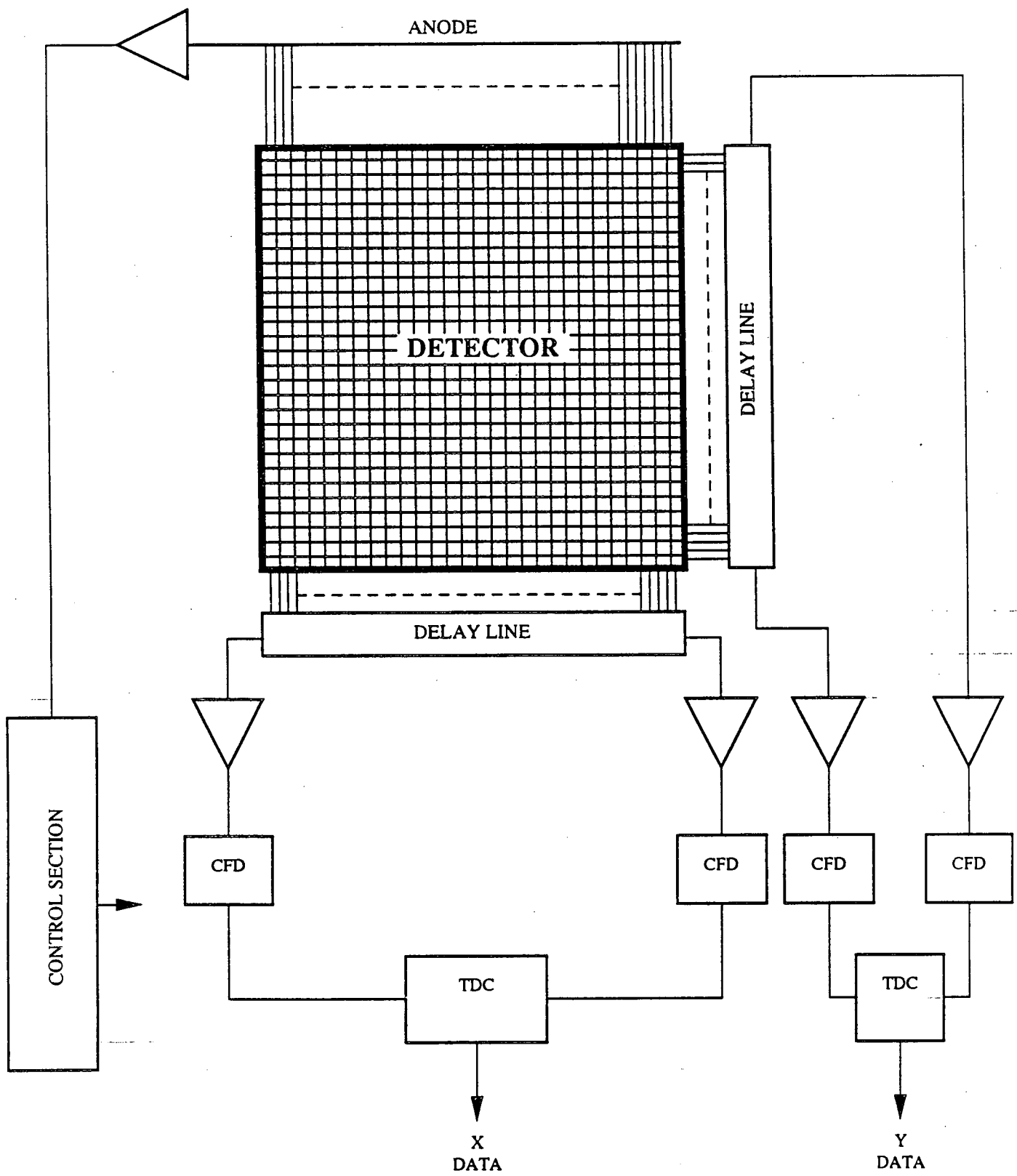


FIGURE 32: Delay Line Decoding.

method; the minimum length of the delay line, and thus its speed, will ultimately be determined by the ability of the processing electronics to accurately discriminate the time difference of the signals. This limit, of course, also applies to any other time-differencing method.

5. Center-of-Cluster

The center-of-cluster method of position encoding was developed by Jeavons *et al*⁸² for positron imaging, and was later adapted to x-ray detection by Hendrix and Lentfer³⁰. This method of encoding is in many respects similar to the linear scintillator encoding method by Davidson⁵⁸ and the multi-electrode banana detectors used in the ILL and other locations, in that encoding is accomplished in a group/element manner (Fig. 33). The center-of-cluster method was chosen for the application in ref. 30 because it uses fewer amplifier/discriminator channels and because the decoding circuits would ostensibly be faster than with interpolative methods.

The reported count rate for this method³⁰ was 2.5×10^5 c/s, with a conversion time of 60 ns attributed to the electronics.

D. ANGER CAMERAS

The Anger camera is currently used in two configurations, the "unifield" or "weighted" type, and the "multifield" or "parallel" type.

1. Unifield Anger Camera

The unifield Anger camera uses resistively-weighted encoding to determine the x and y coordinates of a neutron event. A block diagram of the basic unifield Anger camera is shown in Fig. 8. The output of each PMT is resistor-weighted according to its x and y coordinates, and each coordinate value (x, y) is then divided by the unweighted sum of all of the PMT signals (E). The result is a set of normalized coordinate signals that are then digitized by ADCs and processed by a computer. Because of the fast decay time of the ⁶Li scintillator (~ 60 ns), the count rate of an Anger camera is determined primarily by the processing time of the electronics. For the unifield approach the dead time is quite long (~ 10 μ s).

2. Multifield Anger Camera

The multifield approach, first proposed by Seeger⁴¹ at LANL, is considerably faster than the unifield approach. Its block diagram appears in Fig. 9. The multifield approach uses only the PMT directly under the point of scintillation plus the six PMTs surrounding it. The use of only 7 PMTs per scintillation means that more than one scintillation can be detected at once, provided that the scintillations are at different locations and thus do not interfere with each other. The current processing time of the RAL Anger camera using this design⁴¹ is about 400 ns, allowing a count rate in excess of 1 MHz.

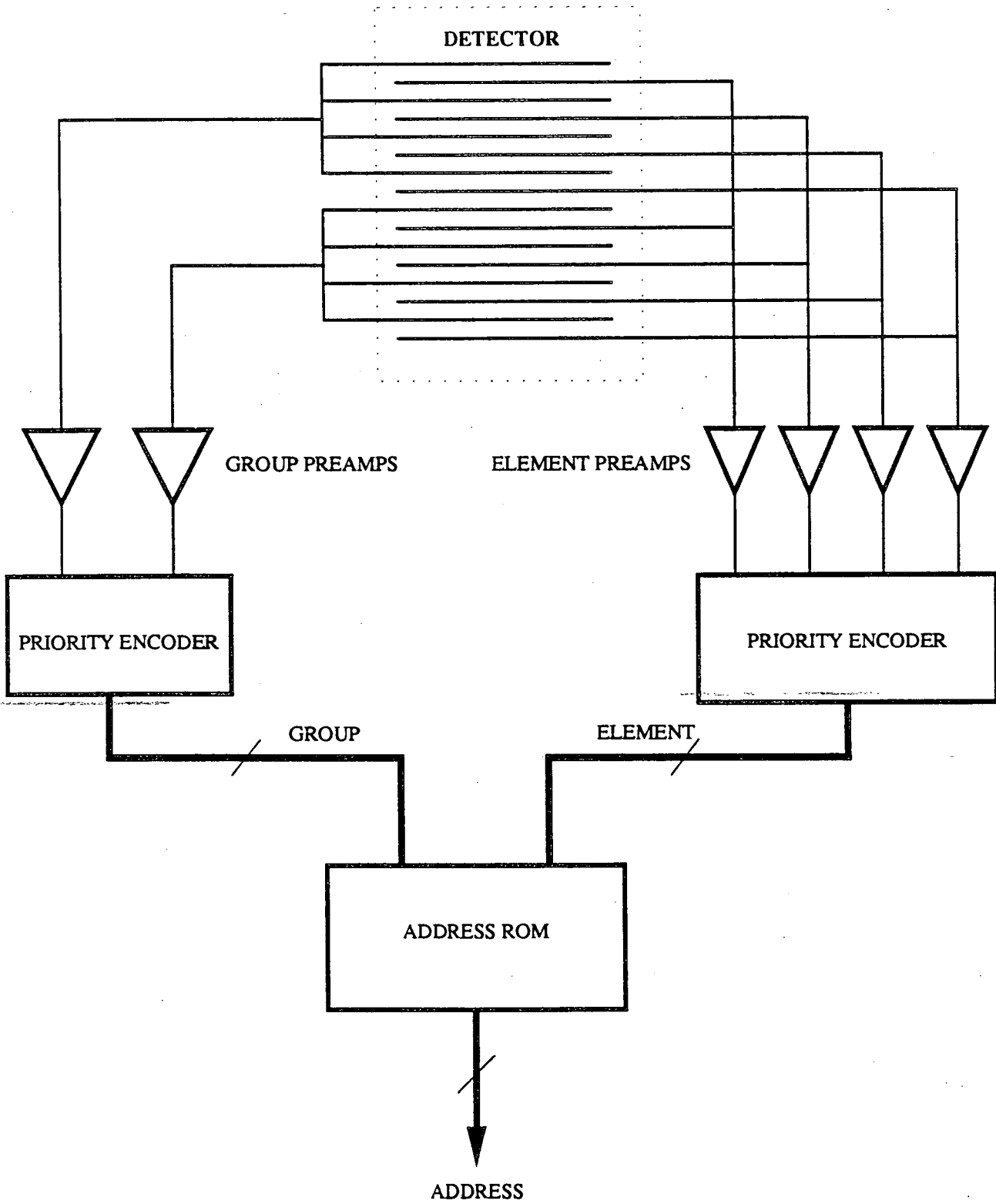


FIGURE 33: Center-of-Cluster Method. The position of the neutron capture is decoded in a group/element manner.

E. NEUTRON IMAGING SYSTEMS

There are two types of TV-based systems: Those that use TV camera tubes, such as the "Fly's Eye" camera by Davidson⁸⁴; and those that use charge-coupled devices (CCD), such as the system devised by Chernyshov *et al*⁷³.

Both types by necessity are integrating and use either the NTSC (525 lines, 30 frames/sec) or the CCIR (625 lines, 25 frames/sec, commonly referred to as PAL-M) TV formats. Since these types of detectors are integrating, TOF measurements are not possible.

1. TV Camera Tube

A representative system using a standard TV camera is the "Fly's Eye" system at ORNL, shown in Fig. 17. Neutrons detected on the ⁶LiF-ZnS phosphor are fiber-optically coupled to an image intensifier. The enhanced image is then fiber-optically coupled to a TV camera, where it is scanned, and the data thus read, in normal NTSC fashion. The data-pulses are then referenced to the vertical and horizontal sync pulses to yield their x and y coordinates.

Since the NTSC standard is used, the integrating time for this system is about 16.7 ms, and the vertical resolution can be up to 525 lines.

2. CCD

The CCD neutron imager is similar to the TV tube format, but uses a CCD instead of the TV tube. The system devised by Chernyshov *et al* operates on a PAL-M style format, so the integration time is about 20 ms, with a vertical resolution dependent upon the CCD device used. If the CCD device conforms to the PAL-M format the vertical resolution will be 625 lines.

XI. COMPUTER CONSIDERATIONS

Computers have become an integral, if not essential, part of neutron detection systems, owing mainly to the problems associated with the collection and storage of the large quantities of data that issue forth from the detector electronics. In many cases the data is of a raw and relatively cryptic nature that requires a good amount of manipulation to yield the finished data. Storage of the raw data can also be a critical issue because the count rate of the PSD can be limited by the rate at which the data is read out of the detector's electronics, and the read-out rate is usually dictated by the computer's ability to read and store the data quickly and efficiently.

Since the rate at which data is read from the detector is very critical to the detector's performance, the computer's ability to extract and store the data is of great importance. This is especially true for PSDs with high count rates and which depend upon the computer to read and store the data, as opposed to the PSDs in which small amounts of the data can be stored and accumulated on board, or in which the data can be transferred directly to memory without the direct indulgence of the computer. The latter situation, known as direct memory access (DMA), can be quite advantageous when data is created in large quantities and at high rates. In such a system, the DMA circuits within the detector electronics transfers the data directly to the computer's memory, essentially bypassing the computer's processor. The computer is then used in a supervisory capacity, arbitrating the transfer of data by deciding which DMA circuit will have permission to transfer data to memory. The use of DMA eliminates much of the "overhead" associated with using the computer's processor to collect and store the data. The 2-d PSD at NIST¹² uses DMA to transfer its data to the computer's memory, allowing the use of a relatively small computer for data acquisition and leaving the actual data reduction for a much larger computer.

There are a number of things to keep in mind when selecting the computer (or in general, the data acquisition system (DAS)) for a given system. Most of the criteria for selection fall into three categories⁸⁵: the requirements imposed by the PSD; the requirements imposed by the manner in which the neutron experiment is performed; and the requirements imposed by environmental factors, such as cost and maintenance.

The requirements of the PSD are probably the most fundamental to be imposed upon the computer system, at least in its role as a data acquisition system. The DAS has to be fast enough to read out the data faster than it can be created by the detector; a slower system will place limits on the detector's count rate. It must also read and store the data without introducing errors, and it must keep track of the data as it is accumulated. It is also possible that the format of the data from the PSD will influence the DAS system, in that the required size of the digital output could determine the type of computer that will most efficiently read the data.

The requirements of the experiment are mostly of a more general nature, in that it imposes conditions on the overall capabilities of the computer, especially in the areas of storage capacity and the form in which the data will be stored. In experiments where extremely large quantities of data will be generated the computer must have adequate storage capability, usually in the form of magnetic storage media. The form that the data takes when being archived will influence the memory needs. Storing (archiving) the raw unreduced data is preferable in terms of future analysis, for example if a whole new form of data reduction is devised later on and it is desired to reduce the data from previous experiments using the new method, but it will use more storage area. On the other hand, reduced or partially reduced data will take less storage room but may limit the use of future reduction strategies. The amount of available RAM will also be an important consideration,

especially if the PC-type or workstation computers are being considered. Most of the larger minicomputers and mainframes will not impose this consideration, since they generally have adequate memory resources to fit most experimental needs.

The environmental requirements of the computer are mostly of a practical nature. These include the availability of technical support, either contracted or in-house, the physical dimensions, the ease of operation, the user-friendliness, etc. Computers will generally not have to withstand harsh environments, so the physical environmental factors are probably not that important for most installations.

A factor that has appeared in recent years is the concept of having a complete data acquisition and reduction computer at each experimental station instead of just a DAS computer system. For the latter system, the computer is used strictly in a data acquisition function, with perhaps some small amount of data reduction for more efficient handling and storage of the data, and the real data reduction and analysis is done on a larger central computer with greater computational resources. With the advent of workstations and fairly powerful personal computers came the possibility of distributing the computing power to all of the experiment stations and therefore allowing all of the data reduction and analysis to proceed where the data was collected. Such a system offers significant advantages over the "central computer" approach, and it is conceivable that it could be implemented without an excessive investment of resources over the cost of a centralized system. With the networking of all of these computers will come improvements in communications and data handling.

XII. CONCLUSIONS

The ideal PSD for SANS should have a high efficiency ($> 80\%$), high count rate capability, (10^5 cps), good spatial resolution (< 5 mm), short dead time (< 1 μ s), low γ and detector background, and be stable, reliable, robust and inexpensive. From the detectors currently available, not one can meet all these requirements.

The gaseous electronic detectors provide high efficiency, good resolution, reliability, and excellent background rejection. They also have problems with timing, limited count rate capability, and expense. Currently, Kopp at ORDELA is working on a new encoding method which should increase the count rate capability to 10^7 n/s (10^5 n/s/pixel). Another effort showing promise is coupling of gaseous detectors and solid state devices, being developed at ILL. This design would combine the attributes of a gas with excellent timing and spatial resolution offered by solid state technology. In the future, continuous efforts by CERN and others to improve on existing MWPCs (such as avalanche chambers, etc.) may provide further advancements in position-sensitive neutron detectors.

The scintillation detectors are currently receiving the most development work around the world. They offer the possibility of higher spatial resolution, good efficiency, higher count rate capability, and shorter dead time. However, they have a serious problem with γ -sensitivity. Many institutes, including RAL, KFA, and ANL, are actively pursuing the development of scintillation detectors and addressing the γ -sensitivity problem. Developers at RAL have gone back to investigating the ${}^6\text{Li}/\text{ZnS}$ combination as a way to reduce γ contribution, while KFA is investigating other ${}^6\text{Li}$ scintillator possibilities, such as ${}^6\text{LiI}$, ${}^6\text{LiH}$, and ${}^6\text{LiD}$.

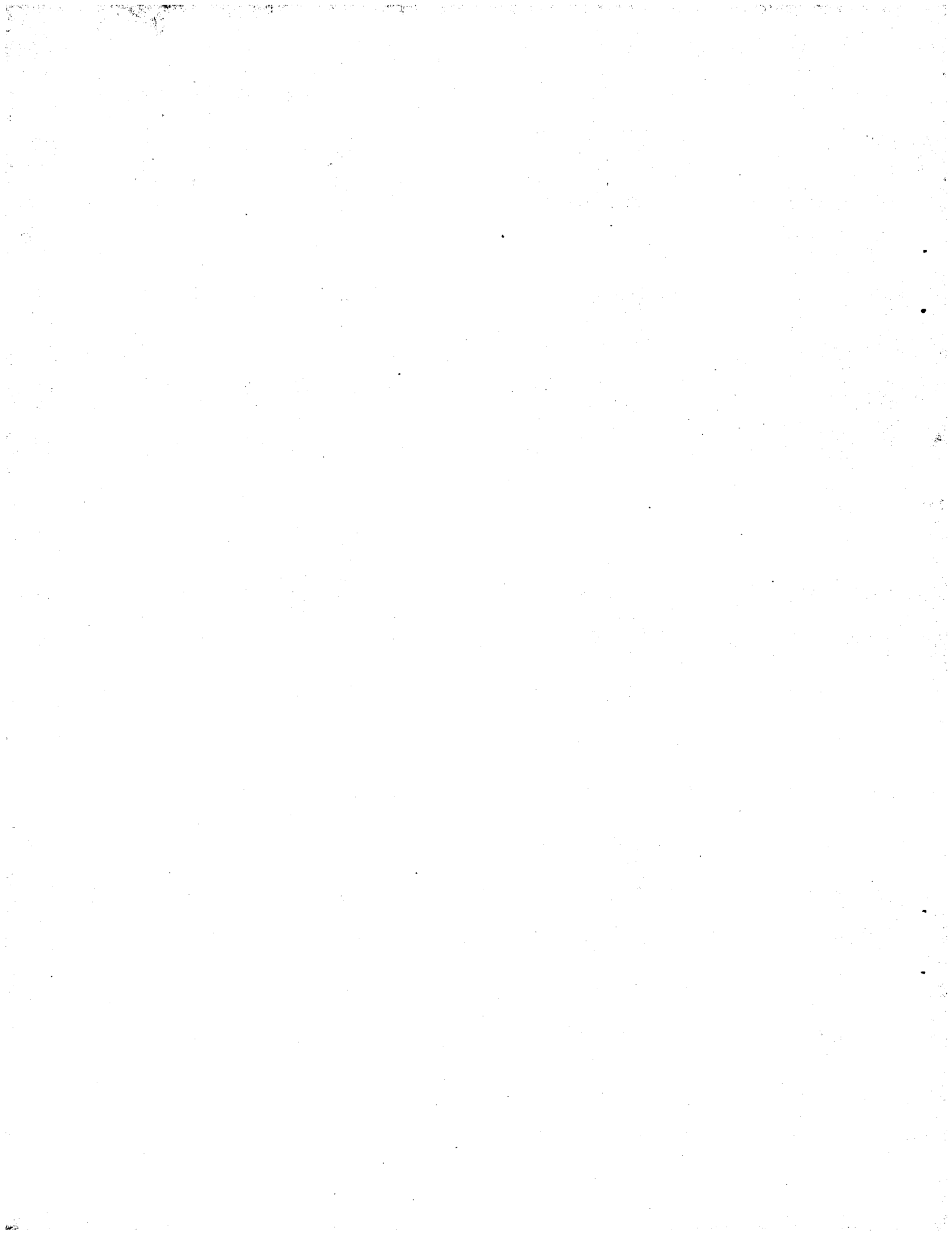
The semiconductor industry has grown and shows great promise for application to SANS. However, this field is still maturing and problems associated with γ -sensitivity and high cost must still be addressed. This is also true of neutron imaging systems and foil detectors. Their future application towards SANS will depend on developments to overcome limiting problems, such as low efficiency.

XIII. ACKNOWLEDGEMENTS

First of all, I would like to thank all the scientist who took the time from their busy schedules to respond to the questionnaire on SANS detectors and facilities. Their answers and assistance were most appreciated.

Secondly, I would like to thank those people at ORNL who assisted in this endeavor: J. B. Davidson, M. L. Bauer, and J. Hayter.

I am also grateful for the assistance of P. J. Tinnel, J. L. Kerley, S. E. Baity, and PAH.



XIV. REFERENCES

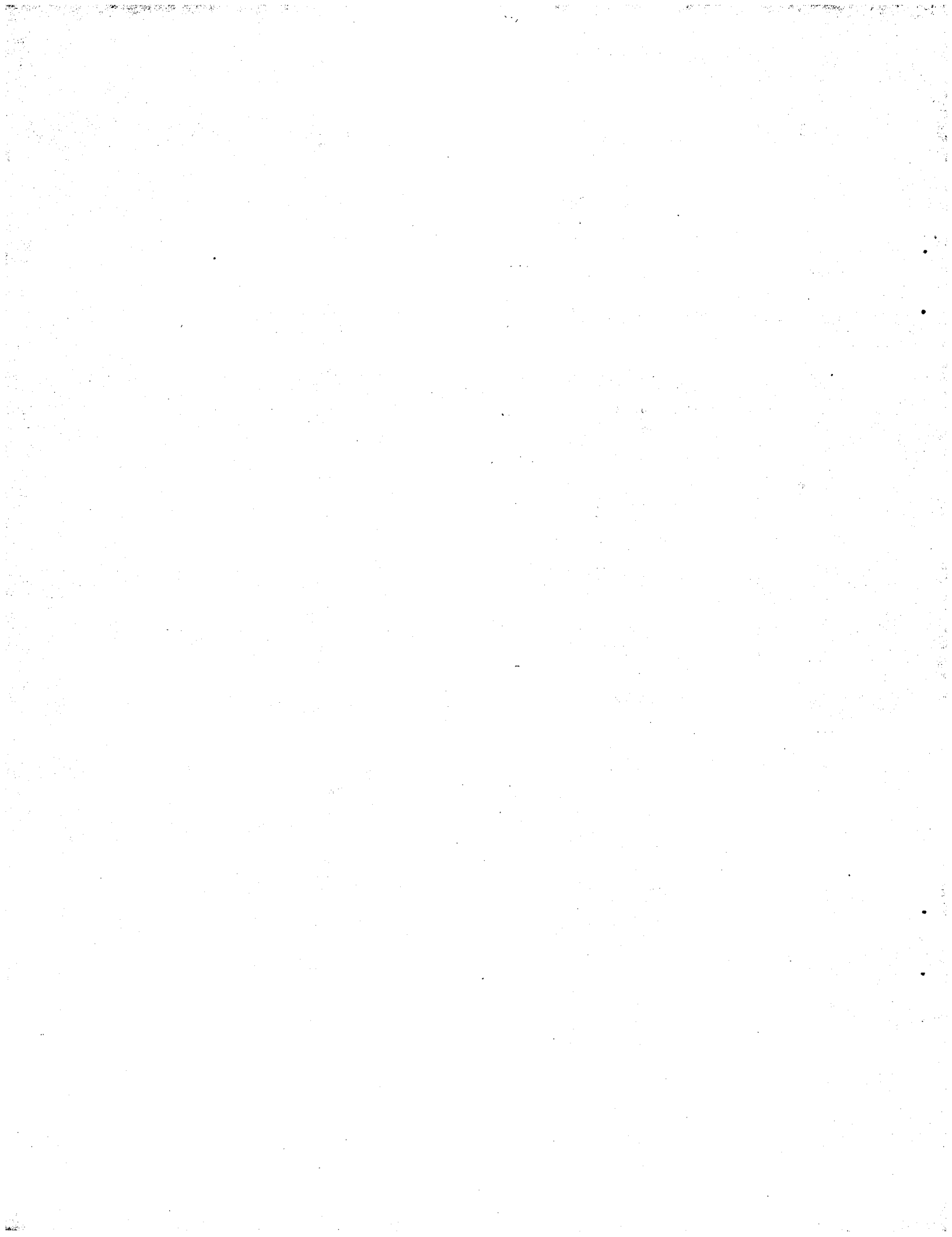
1. See, for example, "Proceeding of the London Conference on Position-Sensitive Detectors (1987)," Nuc. Instrum. Meth. A273, (1988) and "Proceedings of the Nuclear Science Symposium 1988," Trans. Nuc. Sci. NS-35, (1989).
2. See, for example, "International Workshop on Evaluation of Single-Crystal Diffraction Data From 2-D Position-Sensitive Detectors," J. Physique 47,(1986).
3. R. Berliner, D. F. R. Mildner, O. A. Pringle, and J. S. King, "A Large Area Position-Sensitive Neutron Detector," Nuc. Instrum. Meth. 185, 481(1981).
4. R. Berliner, D. F. R. Mildner, J. Sudol, and H. Taub, in Position-Sensitive Detection of Thermal Neutrons, edited by P. Convert and J. B. Forsyth (Academic Press, London, 1983) p. 120.
5. J. Alberi, in Neutron Scattering for the Analysis of Biological Structures: Brookhaven Symposium on Biology, edited by B. Schoenborn, BNL-50453, p. VIII-24.
6. M. M. Agamalyan, G. A. Panev, and A. A. Zavedia, "A Multichannel Detector System for Small-Angle Neutron Scattering Investigations," Nuc. Instrum. Meth. 213, 489(1983).
7. Y. Ishikawa, M. Furusaka, N. Nimura, M. Arai, K. Hasegawa, "The Time-of-Flight Small-Angle Scattering Spectrometer SAN at the KENS Pulsed Cold Neutron Source," J. Appl. Cryst. 19, 229(1986).
8. ORDELA, Inc., 139 Valley Court, Oak Ridge Tennessee 37830, USA.
9. R. K. Abele, G. W. Allin, W. T. Clay, C. E. Fowler, and M. K. Kopp, "Large-Area Proportional Counter Camera for the U. S. National Small-Angle Neutron Scattering Facility," IEEE Trans. Nuc. Sci. NS-28, 811(1981).
10. M. K. Kopp, K. H. Valentine, L. G. Christophorou, and J. C. Carter, Nuc. Instrum. Meth. 209, 395(1982).
11. C. J. Borkowski and M. K. Kopp, "Design and Properties of Position-Sensitive Proportional Counters Using Resistance-Capacitance Position Encoding," Rev. Sci. Instrum. 46(8), 951(1975).
12. C. J. Glinka and N. F. Berk, in Position-Sensitive Detection of Thermal Neutrons, edited by P. Convert and J. B. Forsyth (Academic Press, London, 1983) p. 141.
13. E. Epperson, ANL, private correspondence.
14. J. K. Kjems, R. Bauer, B. Breiting, and A. Thuesen, in Neutron Scattering in the Nineties, edited by J. K. Kjems (Vienna, IAEA, 1985) p. 489.
15. K. Mortensen, B. Breiting, and J. Kjems, "Area Sensitive Detector for the Small-Angle Neutron Scattering Facility at Riso National Laboratory," RNL (December 1988).
16. H. H. van der Kroonenberg, NERF, private correspondence.

17. S. Funahashi, JAERI, private correspondence.
18. P. Seeger, LANL, private correspondence.
19. J. Fischer, V. Radeka, and R. A. Boie, in Position-Sensitive Detection of Thermal Neutrons, edited by P. Convert and J. B. Forsyth (Academic Press, London, 1983) p. 129.
20. B. P. Schoenborn, J. Schefer, and K. K. Schneider, "The Use of Wire Chambers in Structural Biology," *Nuc. Instrum. Meth.* **A252**, 180(1986).
21. V. Radeka and R. A. Boie, *Nuc. Instrum. Meth.* **178**, 543(1980).
22. H. Nishikara, RRI, private correspondence.
23. B. P. Schoenborn, D. S. Wise, and D. K. Schneider, "Neutron and Synchrotron X-Ray Small-Angle Scattering Instruments for Applications in Biology at the Brookhaven National Laboratory," *Trans. Amer. Cryst. Assoc.* **19**, 67(1983).
24. J. Jacobe, D. Feltin, A. Rambaud, F. Ratel, M. Gamon, and J. B. Pernock, in Position-Sensitive Detection of Thermal Neutrons, edited by P. Convert and J. B. Forsyth (Academic Press, London, 1983) p. 106.
25. R. Allemand, J. Bourdel, E. Roudaut, P. Convert, K. Ibel, J. Jacobe, J. P. Cotten, and B. Farnoux, "Position-Sensitive Detectors (P.S.D.) For Neutron Diffraction," *Nuc. Instrum. Meth.* **126**, 29(1975).
26. A. Axmann, "Hardware Aspects of Neutron Position-Sensitive Detectors," in Position-Sensitive Detection of Thermal Neutrons, edited by P. Convert and J. B. Forsyth (Academic Press, London, 1983) p. 91.
27. K. Ibel, "The Neutron Small-Angle Camera D11 at the High Flux Reactor, Grenoble," *J. Appl. Cryst.* **9**, 296(1976).
28. R. Heeran, RAL, private correspondence.
29. R. Allemand and G. Thomas, "Nouveau Detecteur de Localisation: Le Dispositif a Jeu de Jacquet," *Nuc. Instrum. Meth.* **137**, 141(1976).
30. J. Hendrix and A. Lentfer, "A Parallel Electrode Position-Sensitive Detector System for High Counting Rates," *Nuc. Instrum. Meth.* **A252**, 246(1986).
31. E. Mathieson and G. C. Smith, "Charge Distribution in Parallel Plate Avalanche Chambers," *Nuc. Instrum. Meth.* **A273**, 518(1988).
32. P. Bhattacharya, P. Basu, and M. L. Chatterjee, "Performance of a Position-Sensitive Multistep Parallel-Plate Avalanche Chamber," *Nuc. Instrum. Meth.* **A276**, 585(1989).
33. W. Seidel, H. G. Ortlepp, F. Stary, and H. Sodan, "Double-Grid Avalanche Counter with Large Dynamic Range," *Nuc. Instrum. Meth.* **A273**, 536(1988).
34. G. Charpak, "Parallax-Free, High Accuracy Gaseous Detectors for X-Ray and VUV Localization," *Nuc. Instrum. Meth.* **201**, 181(1982).

35. M. K. Kopp, ORDELA, private correspondence.
36. R. Heeron, RAL, private correspondence.
37. M. G. Strauss, R. Brenner, F. J. Lynch, and C. B. Morgan, "2-D Position-Sensitive Scintillation Detector for Neutrons," IEEE Trans. Nuc. Sci. NS-28, 800(1981).
38. H. O. Anger, Rev. Sci. Instrum. 29, 27(1958).
39. M. G. Strauss, R. Brenner, H. P. Chou, A. J. Schultz, and C. T. Roche, in Position-Sensitive Detection of Thermal Neutrons, edited by P. Convert and J. B. Forsyth (Academic Press, London, 1983) p. 175.
40. J. B. Forsyth, R. T. Lawrence, and C. C. Wilson, "A PSD For Neutron Diffraction," Nuc. Instrum. Meth. A273, 741(1988).
41. P. A. Seeger, in Position-Sensitive Detection of Thermal Neutrons, edited by P. Convert and J. B. Forsyth (Academic Press, London, 1983) p. 188.
42. A. J. Leadbetter, in Neutron Scattering in the Nineties, edited by J. K. Kjems (Vienna, IAEA, 1985) p. 219.
43. T. Springer, KFA, private correspondence.
44. E. Jansen, W. Schafer, A. Szepesvary, G. Will, and R. Kurz, "The Solid State Scintillation PSD JULIOS: A Fast and High Resolution Detector System for Thermal Neutrons," Physica B 156 & 157, 584(1989).
45. R. Kurz and J. Schelten, in Position-Sensitive Detection of Thermal Neutrons, edited by P. Convert and J. B. Forsyth (Academic Press, London, 1983) p. 192.
46. R. Kurz, R. Reinartz, S. Widdau, J. Schelten, A. Scholz, and W. Schafer, submitted to Physica B for publication.
47. R. Kurz, R. Reinartz, S. Widdau, J. Schelten, and A. Scholz, "Two-Dimensional Neutron Detector Based on a Position-Sensitive Photomultiplier," Nuc. Instrum. Meth. A273, 273(1988).
48. S. Suzuki, T. Matsushita, T. Suzuki, S. Kimura, and H. Kume, "New Position-Sensitive Photomultiplier Tubes For High Energy Physics and Nuclear Medicine Applications," IEEE Tran. Nuc. Sci. NS-35, 382(1988).
49. J. Baruchel, S. Kuroda, P. Liaud, A. Michalowicz, and D. Sillou, "A Position-Sensitive Detector for Neutron Diffraction Topography," J. Appl. Cryst. 21, 28(1988).
50. P. L. Davidson and H. Wroe, Proc. ICANS IV, KENS Report II, (1981).
51. P. L. Davidson and H. Wroe, Proc. ICANS VI, ANL 82-80.(1982).
52. P. L. Davidson and H. Wroe, in Position-Sensitive Detection of Thermal Neutrons, edited by P. Convert and J. B. Forsyth (Academic Press, London, 1983) p. 166.

53. H. Nguyen Ngoc, J. Jeanjean, J. Jacobe, P. Mine, "Neutron Detection with $^3\text{He-Xe}$ Proportional Scintillation Detector," *Nuc. Instrum. Meth.* **188**, 677(1981).
54. J. R. M. Annand, G. I. Crawford, and R. O. Owens, "Large Position-Sensitive Plastic Scintillation Detectors," *Nuc. Instrum. Meth.* **A262**, 329(1987).
55. R. A. Schrack, "A Microchannel Plate Neutron Detector," *Nuc. Instrum. Meth.* **222**, 499(1984).
56. R. S. Gao, W. E. Robert, G. J. Smith, K. A. Smith, and R. F. Stebbings, "High-Resolution Position-Sensitive Detector," *Rev. Sci. Instrum.* **59**(9), 1954(1988).
57. ISIS Annual Report, RAL-88-050, p.69.
58. P. L. Davidson, "Linear Scintillator PSD for Thermal Neutrons," *Nuc. Instrum. Meth.* **A273**, 735(1988).
59. R. Kurz and J. Schelten, KFA, private correspondence.
60. M. LeBlanc, C. Raymond, H. Tricoire, and L. Valentin, "SOFI: A Scintillating Optical Fiber Imager," *Nuc. Instrum. Meth.* **A273**, 583(1988).
61. T. O. White, "Scintillating Fibers," *Nuc. Instrum. Meth.* **A273**, 820(1988).
62. C. Peng Cheng and H. Wei Zheng, "Parameters of Various Types of Light Guides for Large Area Scintillation Counters," *Nuc. Instrum. Meth.* **A252**, 67(1986).
63. P. A. Bagryanskii, V. S. Belkin, V. G. Dudnikov, and E. I. Shabalov, "Gas Electroluminescent Proportional Detector with Photocathode in Working Chamber," *Instrum. Exp. Tech.* **30**(1), 51(1987).
64. V. A. Polyakov, V. I. Rykalin, and E. G. Tskhadadze, "Use of Electroluminescence of Gas Mixtures for Optical Data Acquisition From Wire Chambers," *Instrum. Exp. Tech.* **31**(1), 33(1988).
65. A. Oed, "Position-Sensitive Detector With Microstrip Anode for Electron Multiplication With Gases," *Nuc. Instrum. Meth.* **A263**, 351(1988).
66. I. Debusschere, E. Bronckaers, C. Claeys, and G. Declerck, "Electron Detection by Means of Silicon Solid State Imagers," *Nuc. Instrum. Meth.* **A273**, 636(1988).
67. K. Mochiki, K. Hasegawa, and S. Namatame, "Amorphous Silicon Position-Sensitive Detector," *Nuc. Instrum. Meth.* **A273**, 640(1988).
68. C. J. Glinka, NIST, private correspondence.
69. J. W. T. Dabbs, Intraspec, Inc, Oak Ridge, TN, private correspondence.
70. U. W. Arndt and D. J. Gilmore, "A Neutron Television Camera Detector," in Neutron Scattering for the Analysis of Biological Structures: Brookhaven Symposium on Biology, edited by B. Schoenborn, BNL-50453, p. VIII-16.
71. U. W. Arndt and D. J. Thomas, "X-Ray Television Area Detectors," *Nuc. Instrum. Meth.* **201**, 13(1982).

72. J. B. Davidson, in Neutron Scattering for the Analysis of Biological Structures: Brookhaven Symposium on Biology, edited by B. Schoenborn, BNL-50453, p. VIII-3.
73. P. N. Chernyshov, A. A. Sumbatyan, V. Ya. Kezerashvili, S. P. Gaevoi, V. M. Gataulin, and V. A. Turner, "Position-Sensitive Neutron Detectors Based on a Device With Charge Coupling," *Instrum. Exp. Meth.* **29**, 1297(1986).
74. J. B. Davidson, ORNL, private correspondence.
75. A. P. Jeavons; N. L. Ford, B. Lindberg, and R. Sachot, "A New Position-Sensitive Detector for Thermal and Epithermal Neutrons," *CERN* 77-01(1977).
76. G. Charpak, A. P. Jeavons, F. Sauli, and R. J. Stubbs, *CERN* 73-11(1973).
77. G. Melchart, G. Charpak, F. Sauli, G. Petersen, and J. Jacobs, "The Multistep Avalanche Chamber As A Detector for Thermal Neutrons," *Nuc. Instrum. Meth.* **186**, 613(1981).
78. Y. S. Anisimov, S. P. Chernenko, A. B. Ivanov, V. D. Peshekhonov, L. P. Smykov, Y. V. Zanevsky, J. Knourek, L. Moucka, T. Netusil, and L. Pellar, "A Device for Neutron Radiography with a Low-Pressure Multistep Avalanche Chamber," *Nuc. Instrum. Meth.* **A252**, 261(1986).
79. Y. S. Anisimov, S. P. Chernenko, A. B. Ivanov, T. Netusil, V. D. Peshekhonov, L. P. Smykov, Y. V. Zanevsky, M. Cisár, J. Horacek, J. Knourek, L. Moucka, L. Nezmar, L. Pellar, J. Pochman, Z. Schneider, Z. Sidak, I. Vrba, V. Bizek, Z. Zavadil, P. Beran, and K. Cerny, "Development and Investigation of a Neutron Radiography Imaging System with a Low-Pressure Multistep Chamber," *Nuc. Instrum. Meth.* **A273**, 731(1988).
80. R. Berliner, MURR, private correspondence.
81. P. L. Davidson, RAL, private correspondence.
82. A. Jeavons, K. Kull, B. Lindberg, and G. Lee, "A Proportional Chamber Positron Camera for Medical Imaging," *Nuc. Instrum. Meth.* **176**, 89(1976).
83. G. Smith, BNL, private correspondence.
84. J. B. Davidson in "Proceedings of the Workshop on Instrumentation for the Advanced High-Flux Reactor," edited by R. M. Moon, CONF-8405192, p.22.
85. P. Convert and J. Forsyth, Position-Sensitive Detection of Thermal Neutrons (Academic Press, London, 1983).

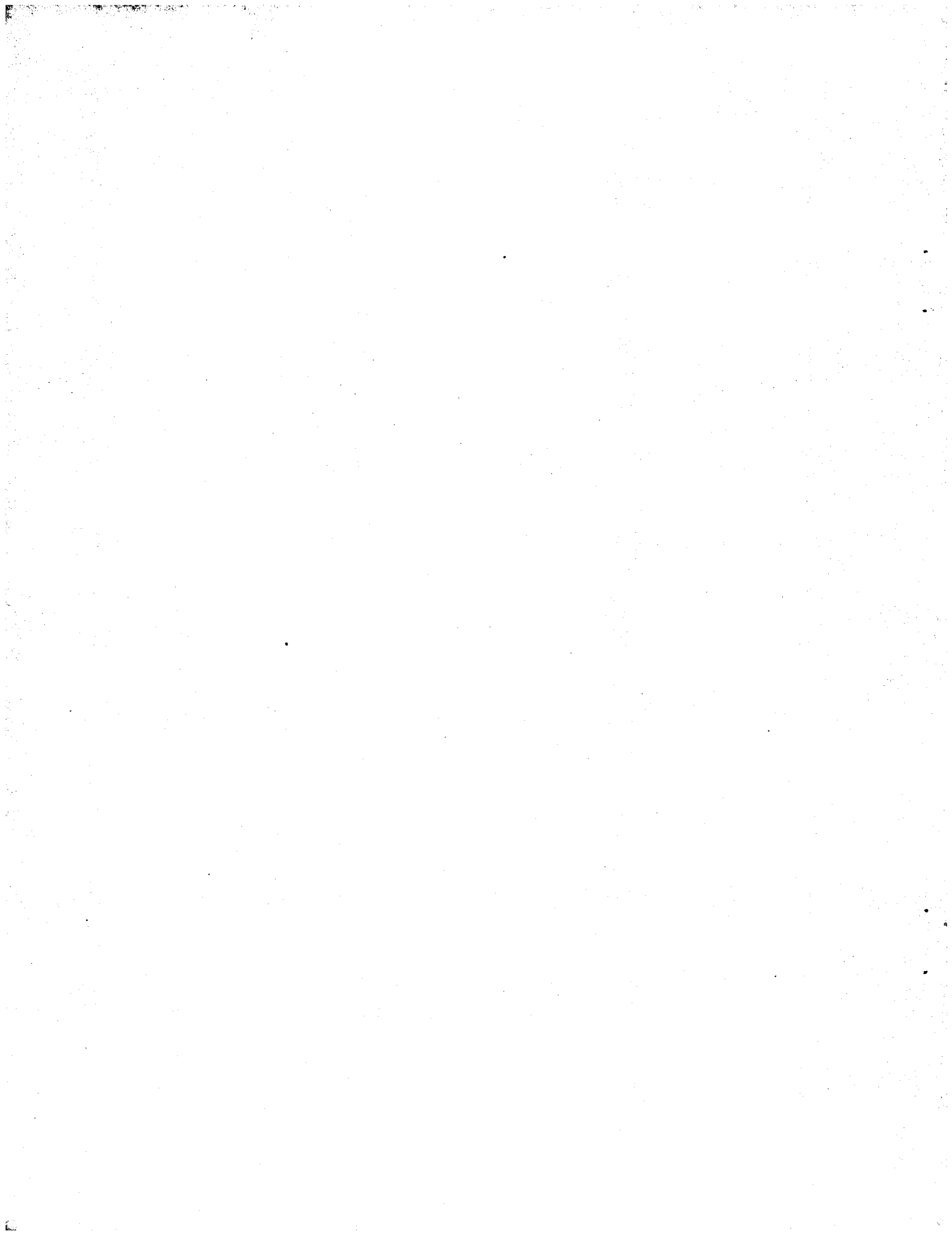


XV. ABBREVIATIONS

ADC	analog-to-digital converter
ANL	Argonne National Laboratory, USA
BNL	Brookhaven National Laboratory, USA
CCD	charge couples device
CCIR	International Radio Consultative Committee
CEA	Commissariat a l'Energie Atomique
CENG	Centre d'Etudes Nucleaires de Grenoble
CERN	Centre Europeene pour la Recherche Nucleaire, Geneva
CFD	constant fraction discriminator
CID	charge injection device
DAS	data acquisition system
DMA	direct memory access
DOE	Department of Energy, USA
DTD	direct time digitizer
ICA	individual counter arrays
ILL	Institut Laue Langevin, Grenoble
IPNS	Intense Pulsed Neutron Source (ANL)
ISIS	Spallation Neutron Source (RAL)
JAERI	Japan Atomic Energy Research Institute
JINR	Joint Institute of Nuclear Research, Dubna USSR
KEK	National Laboratory for High Energy Physics, Tsukuba, Japan
KENS	Pulsed Neutron Source, KEK Japan
KFA	Kernforschungsanlage, Julich
LANL	Los Alamos National Laboratory, USA
LETI	Laboratoire d'Electronique et de Technique de l'Informatique (CENG)
LNPI	Leningrad Nuclear Physics Institute, USSR
LPMSC	low-pressure multistep chamber
MCP	microchannel plate
MRC	Medical Research Council (Laboratory of Medical Biology), England
MS	microstrip
MURR	University of Missouri Research Reactor, USA
MWPC	multi-wire proportional chamber
NERF	National Energy Research Foundation, The Netherlands
NIST	National Institute of Standards and Technology, USA (Formerly the National Bureau of Standards)
NTSC	National Television System Committee
ORDELA	Oak Ridge Detector Laboratory, USA
ORNL	Oak Ridge National Laboratory, USA
PAL-M	Phase Alternative Line-Monochrome
PMT	photomultiplier tube
PSD	position-sensitive detector
PSPC	position-sensitive proportional counter
RAL	Rutherford Appleton Laboratory, England
RAM	random access memory
RC	resistance-capacitance
ROM	read-only memory
RRI	Research Reactor Institute, Japan

SANS	small angle neutron scattering
SBIR	Small Business Innovation Research
TDC	time-to-digital converter
TOF	time of flight
TSCA	timing single channel analyzer
TV	television
UV	ultra violet

APPENDIX



INSTITUTE Atomic Energy Research Establishment (AERE)

LOCATION Harwell Laboratories
OXON, OX11 0RA
England

CONTACT P. Iredale
Collin Windsor

SOURCE PLUTO reactor, 25 MW

FLUX E14

COLD SOURCE YES

NO

MATERIALS INVESTIGATED various

DETECTORS 2D flat BF3 (64 x 64 cm²), LETI detector

INSTITUTE Atominstitut der Osterreichischen Universitaeten (AOU)

LOCATION Schuttelstrasse 115
A-1020 Wien
Austria

CONTACT G. Eder
H. Rauch

SOURCE TRIGA Mark-II reactor, 250 kW

FLUX 1E13

COLD SOURCE YES

NO

MATERIALS INVESTIGATED metal-hydrogen systems [Ta-H(D), Nb-H(D), V-H(D), etc.],
magnetic materials (Fe-Nd, Fe-Co, Cu-Co, etc.)

DETECTORS BF3 detector (2 inch diameter)

FACILITY: ATOMIC ENERGY RESEARCH ESTABLISHMENT

Beam Tube: Tangential (7H)

Monochromator: Velocity selector

Incident Wavelength: 6 to 12 Å

Wavelength resolution: $\Delta\lambda/\lambda = 10\%$

Source-to-sample distances: 6 m

Beam size at specimen: 1 x 1 cm²

Angular resolution: NA

Sample-to-detector distance: 2.1 m

Q range covered: $0.03 \leq Q \leq 1 \text{ \AA}^{-1}$

Maximum flux at specimen: $3 \times 10^4 \text{ n/cm}^2/\text{s}$ at 6 Å

Detector: 2D BF₃ LETI detector (64 x 64 cm²), 128 x 128 cells

Background: NA

Auxiliary equipment: Furnace, cryostat, magnet

Other information: None

References: D. I. Page, AERE R-9878(1978).

FACILITY: ATOMINSTITUT DER OSTERREICHISCHEN UNIVERSITÄTEN

Beam Tube: No. C

Monochromator: Si-perfect crystal

Incident Wavelength: 1.76 Å

Wavelength resolution: $\Delta\lambda/\lambda = 2.5\%$

Source-to-sample distances: 3.5 m

Beam size at specimen: 25 x 35 mm

Angular resolution: 0.5 sec-of-arc

Sample-to-detector distance: 1 m

Q range covered: $0.00001 \leq Q \leq 0.001 \text{ \AA}^{-1}$

Maximum flux at specimen: 100 per second

Detector: 2 inch diameter BF₃

Background: 0.5 /s

Auxiliary equipment: cryostat, thermostat

Other information: Bonse-Hart perfect crystal system

References: D. Schwahn, A. Miksovsky, H. Rauch, E. Seidl, and G. Zugarek, Nuc. Instrum. Meth. A239, 229(1985).

INSTITUTE Australian Nuclear Science and Technology Organization

LOCATION Lucas Heights Research Labs
Sydney
NSW, Australia
2234

CONTACT David Cook

SOURCE HIFAR
DIDO Reactor, 10 MW

FLUX 1 E14

COLD SOURCE YES

NO

**MATERIALS
INVESTIGATED**

DETECTORS Not yet determined for SANS (1989).

INSTITUTE Bhabha Atomic Research Center

LOCATION Nuclear Physics Division
Bombay 400 085, India

CONTACT P. S. Goyal

SOURCE Cirus Reactor

FLUX 5.0E13

COLD SOURCE YES

NO

**MATERIALS
INVESTIGATED** Micellar solutions

DETECTORS BF3 proportional, viewing in end-on position
counter: 3.75 cm diameter and 20 cm active length

**FACILITY: AUSTRALIAN NUCLEAR SCIENCE AND TECHNOLOGY
ORANIZATION - Lucas Heights Research Laboratories**

Beam Tube: AUSANS Instrument (6" horizontal).

Monochromator: Pair of Multilayers.

Incident Wavelength: Not decided, within 2.5 - 8 Å.

Wavelength resolution: $\Delta\lambda/\lambda \sim 10\%$.

Source-to-sample distances: ~ 11 meters.

Beam size at specimen: 3 cm, maximum.

Angular resolution: 1.5 milliradians.

Sample-to-detector distance: 2 to 5 meters.

Q range covered: $0.005 \leq Q \leq 0.5 \text{ \AA}^{-1}$.

Maximum flux at specimen: NA.

Detector: Not yet decided.

Background: NA.

Auxiliary equipment: None.

Other information: Completion date ~ 1991.

References: None.

**FACILITY: BHABHA ATOMIC RESEARCH CENTER
CIRUS reactor**

Beam Tube: E13.

Monochromator: BeO filter.

Incident Wavelength: 5.2 Å.

Wavelength resolution: $\Delta\lambda/\lambda \sim 12\%$, not symmetric.

Source-to-sample distances: ~ 6.5 meters.

Beam size at specimen: 1 cm x 2 cm.

Angular resolution: $\Delta Q = 0.5^\circ$.

Sample-to-detector distance: 1.8 meters.

Q range covered: $0.02 \leq Q \leq 0.8 \text{ \AA}^{-1}$.

Maximum flux at specimen: 2.5×10^{-4} neutrons $\text{cm}^{-2}\text{s}^{-1}$.

Detector: BF_3 proportional counter.

Background: 20 counts/minute.

Auxiliary equipment: NA.

Other information: None.

References: NA.

INSTITUTE Bhabha Atomic Research Center

LOCATION Nuclear Physics Division
Bombay 400 085, India

CONTACT P. S. Goyal

SOURCE DHRUVA Reactor

FLUX 2E14

COLD SOURCE YES

NO

**MATERIALS
INVESTIGATED**

DETECTORS 2D flat PSPC (50 cm x 50 cm) under development.
A 15cm x 15 cm PSPC has been developed and tested.

INSTITUTE Brookhaven National Laboratory (BNL)

LOCATION Upton, NY 11973

CONTACT N. Samios

B. P. Schoenborn

SOURCE High Flux Beam Reactor (HFBR)
60 MW

FLUX 1 E15

COLD SOURCE YES

NO

**MATERIALS
INVESTIGATED** Polymers, model and biological membranes

DETECTORS 2D flat He3 (18 x 18 cm²), BNL detector
He3 detector with sollar collimator mounted on an auxiliary arm

**FACILITY: BHABHA ATOMIC RESEARCH CENTER
DHRUVA reactor**

Beam Tube: Guide 1.

Monochromator: Velocity selector.

Incident Wavelength: 4 Å to 6 Å, variable.

Wavelength resolution: $\Delta\lambda/\lambda \sim 10\%$.

Source-to-sample distances: ~ 31.5 meters.

Beam size at specimen: 0.5 or 1.0 cm diameter.

Angular resolution: NA.

Sample-to-detector distance: 5 meters.

Q range covered: $0.005 \leq Q \leq 0.4 \text{ \AA}^{-1}$.

Maximum flux at specimen: NA.

Detector: 2D flat PSPC (50 cm x 50 cm).

Background: NA.

Auxiliary equipment: None.

Other information: Instrument is not yet operational..

References: NA.

FACILITY: BROOKHAVEN NATIONAL LABORATORY

Beam Tube: H3B

Monochromator: Two parallel multilayer monochromators

Incident Wavelength: 1.5 to 4 Å

Wavelength resolution: $\Delta\lambda/\lambda = 3$ to 7% (adjustable)

Source-to-sample distances: 200 cm, monochromator to sample

Beam size at specimen: 1 x 1 cm², or less

Angular resolution: Limited by detector resolution. Horizontal - 1.5 mm and vertical - 3.0 mm

Sample-to-detector distance: 50 to 250 cm

Q range covered: $0.01 \leq Q \leq 3 \text{ \AA}^{-1}$

Maximum flux at specimen: $1 \times 10^6 \text{ n/cm}^2/\text{s}$

Detector: 18 cm x 18 cm ³He area detector

Background: $\sim 0.3 \text{ n/cm}^2/\text{s}$

Auxiliary equipment: Time slicing processor, linear sample changer, 8 Tesla magnet

Other information: None

References: B. P. Schoenborn et al, Aust. J. Phy. **38**, 337(1985).

INSTITUTE Institut Laue-Lagevin

LOCATION 156X
38042 Grenoble Cedex
France

CONTACT W. Glaser

SOURCE

FLUX 1.5E15 n/s

COLD SOURCE

YES

NO

MATERIALS INVESTIGATED Polymers, colloids, ceramics, metals, biological macromolecules

DETECTORS 2D BF3 PSPC (D11, D17)
2D 3He PSPC (D22)
Anger Camera (DB21)

INSTITUTE Institute for Nuclear Technology (IFE)

LOCATION POB 40, N-2007
Kjeller, Norway

CONTACT Tormod Riste
Department of Physics

SOURCE JEEP II reactor, 2 MW, D20 mod.

FLUX 3E13

COLD SOURCE

YES

NO

MATERIALS INVESTIGATED Microemulsions, biological structures, crystal structures

DETECTORS 2D flat He3 (40 cm), Riso detector

(This is the old SANS instrument at Riso National Laboratory, Denmark)

FACILITY: INSTITUT LAUE-LANGEVIN

Beam Tube: H15, cold guide (Instrument D11).

Monochromator: Helical Slot Velocity Selectors.

Incident Wavelength: 4.5 - 20 Å.

Wavelength resolution: 9 % or 50 %, FWHM.

Source-to-sample distances: Apparent source-sample 2.5 - 40 meters.

Beam size at specimen: 1 cm x 1 cm.

Angular resolution: NA.

Sample-to-detector distance: 1.2 - 3.7 meters.

Q range covered: $0.0005 \leq Q \leq 0.3 \text{ \AA}^{-1}$

Maximum flux at specimen: up to 10^7 n/cm²/s depending on λ and divergence.

Detector: LETI BF₃ PC, 64 x 64 pixels of 10 x 10 mm².

Background: ~ 1.4 c/s on whole detector.

Auxiliary equipment: Automatic sample changers (up to 20 positions), cryostat (1.3 - 300° K), electromagnet (1.7 Telsa), Oven, Couette type shear cell, stretching apparatus, and chopper for λ calibration.

Other information: None.

References: 1. Ibel, K. I., "The Neutron Small Angle Camera D11 at the High Flux Reactor, Grenoble," J. Appl. Crystal. 9 (1976), 269-309.
2. "Guide to Neutron Research Facilities at the ILL," available from SCAPRO, ILL, 156x, 38042 Grenoble Cedex, France.

FACILITY: INSTITUT LAUE-LANGEVIN

Beam Tube: H17, cold guide (Instrument D17).

Monochromator: Helical Slot Velocity Selectors.

Incident Wavelength: 8 - 20 Å.

Wavelength resolution: 5 % or 10 %, FWHM.

Source-to-sample distances: Collimated length: 2 meters.

Beam size at specimen: 1 cm x 1 cm.

Angular resolution: NA.

Sample-to-detector distance: 0.8 m, 1.4 m, 2.8 - 3.5 m.

Q range covered: $0.003 \leq Q \leq 0.1 \text{ \AA}^{-1}$

Maximum flux at specimen: $\sim 10^6 \text{ n/cm}^2/\text{s}$ depending on λ and divergence.

Detector: LETI BF₃ PC, 128 x 128 pixels of 5 x 5 mm².

Background: 1 -2 c/s on whole detector.

Auxiliary equipment: cryostat (1.3 - 300° K), automatic sample changer, Eulerian cradle, chopper.

Other information: Possibility of polarizing incident beam, capable of doing reflectometry.

References: 1. "Guide to Neutron Research Facilities at the ILL," available from SCAPRO, ILL, 156x, 38042 Grenoble Cedex, France.

FACILITY: INSTITUT LAUE-LANGEVIN

Beam Tube: H512, horizontal cold source (Instrument D22, under construction).

Monochromator: Velocity Selector.

Incident Wavelength: 4.0 - 20 Å (at sample).

Wavelength resolution: 10 %, FWHM (planned option: 5 %).

Source-to-sample distances: 1.4, 2, 2.8, 4, 5.6, 8, 11.2, 14.4, 17.6 meters.

Beam size at specimen: ~ 1 cm x 1 cm.

Angular resolution: NA.

Sample-to-detector distance: 1.2 - 18 meters.

Q range covered: $0.008 \leq Q \leq 1 \text{ \AA}^{-1}$

Maximum flux at specimen: ~ 10^7 n/cm² (planned).

Detector: ³He, 16K pixels of 0.75 x 0.75 cm² (planned).

Background: 1 - 2 c/s on whole detector.

Auxiliary equipment: Sample changer, cryostat, oven, Couette type shear apparatus.

Other information: None.

References: R. P. May and M. Thomas, "D22. A New Low-Q Scattering Instrument at the Second Cold Source of the ILL," ILL Technical Report 86MA07T (1987)..

FACILITY: INSTITUT LAUE-LANGEVIN

Beam Tube: H15, cold neutrons (Instrument DB21).

Monochromator: K intercalated HOPG.

Incident Wavelength: 7.6 Å.

Wavelength resolution: 2 - 3 %, FWHM.

Source-to-sample distances: 1 m.

Beam size at specimen: 0.5 mm x 0.5 mm.

Angular resolution: 2 - 3 x 10⁻² rad.

Sample-to-detector distance: 250 mm.

Q range covered: 0.01 ≤ Q ≤ 0.5 Å⁻¹ (resolution 12 - 500 Å).

Maximum flux at specimen: 10⁶ n/cm²/s.

Detector: Anger Camera with LiCe glass scintillator.

Background: background from the instrument (primary beam) is small compared to the background from the sample (protein).

Auxiliary equipment: Cooled dry air or Argon stream in the crystals (0 - 10° C).

Other information: Instrument designed for low angle neutron diffraction with contrast variation on biological macromolecules single crystals.

References: 1. Roche, Strauss, Brenner, IEEE Trans. Nuc. Sci. NS32 (1985), 373-379.
2. Roth in Position Sensitive Detection of Thermal Neutrons, Convert and Forsyth (Academic Press, 1983).

FACILITY: INSTITUTE FOR ENERGY TECHNOLOGY

Beam Tube: Tangential with reflecting sphere filled with liq. He as cold moderator

Monochromator: Multilayer crystal, NiTi, $d = 73 \text{ \AA}$ (or 100 \AA)

Incident Wavelength: 4.8 \AA (or 6.8 \AA)

Wavelength resolution: $\Delta\lambda/\lambda = 25\%$

Source-to-sample distances: 2.5 m, (monochromator to sample) and 5.06 m,
(monochromator to sample)

Beam size at specimen: 5 to 10 mm

Angular resolution: NA

Sample-to-detector distance: 1.5 to 4 m by exchanging flight tubes

Q range covered: $0.01 \leq Q \leq 0.15 \text{ \AA}^{-1}$

Maximum flux at specimen: $2.5 \times 10^5 \text{ n/cm}^2/\text{s}$

Detector: 2D ^3He Riso detector ($40 \times 40 \text{ cm}^2$)

Background: NA

Auxiliary equipment: Sample changer for 7 samples, peltier cell for setting the sample temperature ($-20^\circ \text{ C} < T < 100^\circ \text{ C}$)

Other information: Plans to have a pressure cell

References: T. Freltoft and J. Kjems, "Riso SANS Facility. User Guide," Riso M-2450 (1985).

INSTITUTE Institute of Atomic Energy

LOCATION P.O. Box 275
Beijing, China

CONTACT Sun Tsu-Xun

SOURCE HWRR reactor, 10 MW

FLUX 1.5E14

COLD SOURCE

YES

NO

MATERIALS INVESTIGATED Metals, alloys, etc.

DETECTORS 2D flat BF3 detector (64 x 64 cm²), LETI detector

INSTITUTE Intense Pulsed Neutron Source (IPNS)

LOCATION Argonne National Laboratory
9700 S. Cass Ave.
Argonne, IL 60439

CONTACT J. E. Epperson
Material Science Division

SOURCE Intense Pulsed Neutron Source

FLUX 3E14

COLD SOURCE

YES

NO

MATERIALS INVESTIGATED Metals, metallic alloys, polymers, biological structures, etc.

DETECTORS 2D flat He3 (18.9 x 18.9 cm²), ORDELA detector
2D flat He3 (40 x 40 cm²), ORDELA detector

FACILITY: INSTITUTE OF ATOMIC ENERGY, BEIJING

Beam Tube: Beam tube #4

Monochromator: Mechanical velocity selector

Incident Wavelength: 3 to 10 Å

Wavelength resolution: $\Delta\lambda/\lambda = 16\%$

Source-to-sample distances: 5 meters

Beam size at specimen: 0.5 to 2 cm diameter

Angular resolution: NA

Sample-to-detector distance: 2 to 4.2 meters

Q range covered: $0.01 \leq Q \leq 0.1 \text{ \AA}^{-1}$ (for $\lambda = 6 \text{ \AA}$)

Maximum flux at specimen: $10^5 \text{ n/cm}^2/\text{s}$

Detector: 2D flat BF₃ LETI detector (64 x 64 cm²)

Background: NA

Auxiliary equipment: NA

Other information: None

References: Not given.

FACILITY: INTENSE PULSED NEUTRON SOURCE (ANL)

Beam Tube: C1 beam line

Monochromator: None. This is a time-of-flight instrument

Incident Wavelength: 0.5 to 14 Å

Wavelength resolution: typically, $\Delta\lambda/\lambda$ is binned at 0.05, although actual resolution is much better.

Source-to-sample distances: 7.5 meters

Beam size at specimen: maximum, 12 mm

Angular resolution: NA

Sample-to-detector distance: 1.5 meters

Q range covered: $0.005 \leq Q \leq 0.35 \text{ \AA}^{-1}$

Maximum flux at specimen: 1 - 5×10^5 n/cm²/s, depending on whether MgO filter is in beam and aperture size.

Detector: 2D ³He ORDELA detector (18.9 x 18.9 cm²)

Background: NA

Auxiliary equipment: NA

Other information: 2D ³He ORDELA detector (40 x 40 cm²) purchased for second instrument, not completed

References: IPNS-PR-1986(1988).

INSTITUTE ISIS Spallation Neutron Source, RAL

LOCATION Chilton, Didcot
Oxon OX11 0QX
England

CONTACT RAL - P. R. Williams
ISIS - D. A. Gray

SOURCE Pulsed ISIS proton spallation
source

FLUX 7.5 E15

COLD SOURCE YES

NO

MATERIALS INVESTIGATED Collords, polymers, biomolecules, metal alloys, etc.

DETECTORS 2D BF3 detector (64 x 64 cm²), LETI detector
(originally used on HERALD reactor at Aldermaston)

INSTITUTE Japan Atomic Energy Research Institute (JAERI)

LOCATION Tokai-mura
Ibaraki - Ken 319-11
Japan

CONTACT Satoru Funahashi
Head of Solid State
Physics Laboratory III
Department of Physics

SOURCE New JRR-3 reactors
(to be completed in 1990)

FLUX 1.6E14

COLD SOURCE YES

NO

MATERIALS INVESTIGATED Metals and alloys, ceramics, polymers, biological materials, etc.

DETECTORS 2D flat He3 (58 cm), Riso detector

FACILITY: ISIS SPALLATION NEUTRON SOURCE (RAL)

Beam Tube: LOQ, N5

Monochromator: λ selection by supermirror bender (25 Hz chopper, frame overlap mirror)

Incident Wavelength: 2 to 10 Å pulses at 25 Hz

Wavelength resolution: $\Delta\lambda/\lambda \leq 2\%$

Source-to-sample distances: 11.1 m (4 - 6 m main collimation tube)

Beam size at specimen: normally 8 mm diameter, may use up to 25 mm

Angular resolution: NA

Sample-to-detector distance: 4.3 m

Q range covered: $0.006 \leq Q \leq 0.22 \text{ \AA}^{-1}$

Maximum flux at specimen: $1 \times 10^5 \text{ n/cm}^2/\text{s}$

Detector: 2D BF₃ LETI detector (64 x 64 cm²)

Background:

Auxiliary equipment: Sample changer (in air), water bath, numerous standard ISIS cryostats

Other information: None

References:

FACILITY: JAPAN ATOMIC ENERGY RESEARCH INSTITUTE

Beam Tube: C3 (New JRR-3)

Monochromator: Velocity selector

Incident Wavelength: 1.5 to 30 Å

Wavelength resolution: $\Delta\lambda/\lambda = 8.5$ to 30%

Source-to-sample distances: 10 m

Beam size at specimen: 0.35 to 2.0 cm diameter

Angular resolution: NA

Sample-to-detector distance: 1.5 to 10 m

Q range covered: $0.001 \leq Q \leq 1 \text{ \AA}^{-1}$

Maximum flux at specimen: $\sim 10^5 \text{ n/cm}^2/\text{s}$

Detector: 2D ^3He Riso detector (58 x 58 cm²)

Background: NA

Auxiliary equipment: NA

Other information: None

References: None

INSTITUTE Joint Institute for Nuclear Research

LOCATION Laboratory of Neutron Physics
Head Post Office, P.O. Box 79
101000 Moscow, USSR

CONTACT D. Kiss

SOURCE IBR-2 pulsed reactor

FLUX 1E16

COLD SOURCE YES

NO

MATERIALS INVESTIGATED Solutions, metals, membranes, bulk polymers, minerals, glasses

DETECTORS ^3He ; two units with 8 annular PCs in each.

INSTITUTE Kernforschungsanlage (KFA)

LOCATION IFF
Kernforschungsanlage
Postfach 1913
D-5170 Jülich, F.R.G.

CONTACT Dietmar Schwahn

SOURCE FRJ-2 DIDO reactor
23 MW

FLUX 2E14

COLD SOURCE YES

NO

MATERIALS INVESTIGATED Polymers, metals

DETECTORS 2D Li-glass scintillation, KFA detector
2D flat He^3 (55 cm), Riso detector

FACILITY: JOINT INSTITUTE FOR NUCLEAR RESEARCH

Beam Tube: Beam hole no. 5 (MURN).

Monochromator: Time of flight mode.

Incident Wavelength: 0 - 16 Å (useful 0.7 - 8 Å).

Wavelength resolution: 0.05 Å.

Source-to-sample distances: 18.5 meters.

Beam size at specimen: 1.4 - 2.8 cm diameter.

Angular resolution: $\Delta\theta/\theta = 0.1/0.01$

Sample-to-detector distance: 4.4 - 12.2 meters.

Q range covered: $0.005 \leq Q \leq 0.7 \text{ \AA}^{-1}$.

Maximum flux at specimen: $5 \times 10^6 - 3.2 \times 10^7 \text{ n cm}^{-2} \text{ s}^{-1}$ as determined by activation of gold foil, depends on size of first collimator.

Detector: 16 annular ^3He PCs, assembled in two separate units.

Background: Equivalent (without a sample in beam) to scattering cross section of $\sim 5 \times 10^{-3} \text{ cm}^{-1} \text{ sterad}^{-1}$; negligible with a closed beam, mainly comes from vacuum chamber windows.

Auxiliary equipment: Computerized sample changer (up to six samples in a single load), air cooling of samples down to -10° C , heating device (up to 90° C), slow (5 rev/sec) disc chopper for suppression of the reactor background between main power pulses.

Other information: None.

References: V. A. Vagov et al, JINR, P14-83-898, Dubna, 1983 (in Russian).

FACILITY: IFF KERNFORSCHUNGSANLAGE

Beam Tube: SV5 (KWS I)

Monochromator: Velocity selector

Incident Wavelength: 5 to 18 Å

Wavelength resolution: $\Delta\lambda/\lambda = 0.18$

Source-to-sample distances: 1 to 20 m

Beam size at specimen: (1 to 2 cm)²

Angular resolution: NA

Sample-to-detector distance: 1 to 20 m

Q range covered: $0.001 \leq Q \leq 0.3 \text{ \AA}^{-1}$

Maximum flux at specimen: $5 \times 10^6 \text{ n/cm}^2/\text{s}$

Detector: 2D ⁶Li glass scintillator (60 x 60 cm²)

Background: low

Auxiliary equipment: None

Other information: None

References: B. Alefeld et al, Nuc. Instrum. Meth. A274, 210(1989).

FACILITY: IFF KERNFORSCHUNGSANLAGE

Beam Tube: SV5 (KWS II)

Monochromator: Velocity selector

Incident Wavelength: 5 to 18 Å

Wavelength resolution: $\Delta\lambda/\lambda = 0.26$

Source-to-sample distances: 1 to 20 m

Beam size at specimen: (1 to 2 cm)²

Angular resolution: NA

Sample-to-detector distance: 1 to 20 m

Q range covered: $0.001 \leq Q \leq 0.13 \text{ \AA}^{-1}$

Maximum flux at specimen: $5 \times 10^6 \text{ n/cm}^2/\text{s}$

Detector: 2D ³He Riso detector (55 x 55 cm²)

Background: low

Auxiliary equipment: None

Other information: None

References: B. Alefeld et al, Nuc. Instrum. Meth. **A274**, 210(1989).

FACILITY: IFF KERNFORSCHUNGSANLAGE

Beam Tube: SV5 (Double Crystal SANS)

Monochromator: At the moment, Cu (future 311 Si)

Incident Wavelength: 2.52 Å

Wavelength resolution: $\Delta\lambda/\lambda = 2\%$

Source-to-sample distances: 1 to 2 m

Beam size at specimen: (3 cm)²

Angular resolution: $\Delta Q = 2.5 \times 10^{-5} \text{ \AA}^{-1}$

Sample-to-detector distance: 1 m

Q range covered: $0.00002 \leq Q \leq 0.001 \text{ \AA}^{-1}$

Maximum flux at specimen: 500 n/cm²/s

Detector: 1D ³He

Background: ~ 0.03 n/cm²/s

Auxiliary equipment: None

Other information: None

References: D. Schwahn et al, Nuc. Instrum. Meth. A239, 229(1985).

INSTITUTE Laboratoire Leon Brillouin

LOCATION CEN Saclay
91191 Gif-sur-Yvette
Cedex, France

CONTACT M. Lambert

SOURCE ORPHEE - Reactor, 14 MW

FLUX 3 E14

COLD SOURCE

YES

NO

MATERIALS INVESTIGATED Polymers, Alloys, Ceramics, microemulsions, High T superconductors, metals

DETECTORS 2D flat BF3 (64 x 64 cm²), 128 x 128 cells, LETI detector
2D flat BF3 (64 x 64 cm²), 64 x 64 cells, LETI detector
30 rings (1 cm ea.) 64 cm diam. BF3, LETI detector
2D He3 (19.2 x 19.2 cm²), 128 x 128 cells, ILL detector

INSTITUTE Manuel P. Lujan, Jr., Neutron Scattering Center (LANSCE)

LOCATION Los Alamos National Laboratory
P-LANSCE MS H805
Los Alamos, NM 87545

CONTACT R. Pynn

SOURCE WNR - Pulsed
LAMPF proton source

FLUX E14

COLD SOURCE

YES

NO

MATERIALS INVESTIGATED Biological structures, polymers, liquid crystals, ceramics, metals, etc.

DETECTORS 2D flat He3 (59 cm), Riso detector

FACILITY: LABORATOIRE LEON BRILLOUIN

Beam Tube: Neutron guide G1 (cold neutrons, characteristic $\lambda = 4\text{\AA}$)

Monochromator: Time-of-flight

Incident Wavelength: 3 to 30 \AA

Wavelength resolution: $\Delta\lambda/\lambda = 0.1 \text{\AA}$

Source-to-sample distances: 4 m

Beam size at specimen: variable (usually $0.5 \times 15 \text{ mm}^2$)

Angular resolution: 0.1°

Sample-to-detector distance: 3 m

Q range covered: typically, $0.009 \leq Q \leq 0.05 \text{ \AA}^{-1}$

Maximum flux at specimen: NA

Detector: 2D ^3He ILL detector ($19.2 \times 19.2 \text{ cm}^2$), 128 x 128 cells

Background: NA

Auxiliary equipment: NA

Other information: Data acquisition and data treatment with PC computer. Link to internal and external network/

References: Report on "Equipements Experimentaux," (1987) LLB.

FACILITY: LABORATOIRE LEON BRILLOUIN

Beam Tube: Neutron guide G1 (cold neutrons, characteristic $\lambda = 6\text{\AA}$)

Monochromator: Mechanical selector

Incident Wavelength: 2 to 25 \AA

Wavelength resolution: $\Delta\lambda/\lambda = 5$ to 20%

Source-to-sample distances: 1 to 5 m (variable)

Beam size at specimen: maximum 1 cm diameter

Angular resolution: NA

Sample-to-detector distance: 1 to 5 m (variable)

Q range covered: $0.002 \leq Q \leq 0.5 \text{\AA}^{-1}$

Maximum flux at specimen: $\sim 10^4 \text{ n/cm}^2/\text{s}$

Detector: Ring shaped detector (30 rings, 1 cm width) BF_3 PC, 64 cm diameter

Background: NA

Auxiliary equipment: Automatic sample changer 8 positions, sample holder with temperature regulator (1.5 to 800° K).

Other information: Data acquisition and data treatment with PC computer. Link to internal and external network/

References: Report on "Equipements Experimentaux," (1987) LLB.

FACILITY: LABORATOIRE LEON BRILLOUIN

Beam Tube: Neutron guide G2 (cold neutrons, characteristic $\lambda = 4\text{\AA}$)

Monochromator: Mechanical selector

Incident Wavelength: 2.5 to 20 \AA

Wavelength resolution: $\Delta\lambda/\lambda = 5$ to 20%

Source-to-sample distances: 2 to 7 m (variable)

Beam size at specimen: maximum 1 cm diameter, (possible 2.5 x 3 cm^2)

Angular resolution: NA

Sample-to-detector distance: 1 to 7 m (variable)

Q range covered: $0.003 \leq Q \leq 4 \text{\AA}^{-1}$

Maximum flux at specimen: $\sim 10^4$ n/cm²/s

Detector: 2D BF₃ LETI detector (64 x 64 cm^2), 128 x 128 cells

Background: 0.25 cph per cell

Auxiliary equipment: Automatic sample changer 8 positions, furnace (up to 200° C), low temperature (down to -50° C), cryostat for low temperature (down to 1.5° K), 1.5 Telsa magnet field.

Other information: Data acquisition and data treatment with PC computer. Link to internal and external network/

References: Report on "Equipements Experimentaux," (1987) LLB.

FACILITY: LABORATOIRE LEON BRILLOUIN

Beam Tube: Neutron guide G5 (cold neutrons, characteristic $\lambda = 2\text{\AA}$)

Monochromator: Mechanical selector

Incident Wavelength: 3 to 25 \AA

Wavelength resolution: $\Delta\lambda/\lambda = 5$ to 15%

Source-to-sample distances: 2 to 5 m (variable)

Beam size at specimen: maximum, 2.5 x 3 cm^2 (usually 1 cm diameter)

Angular resolution: NA

Sample-to-detector distance: 0.5 to 4.75 m (variable)

Q range covered: $0.002 \leq Q \leq 0.5 \text{\AA}^{-1}$

Maximum flux at specimen: $\sim 10^4 \text{ n/cm}^2/\text{s}$

Detector: 2D BF_3 LETI detector (64 x 64 cm^2), 64 x 64 cells

Background: NA

Auxiliary equipment: Sample changer 8 positions

Other information: Data acquisition and data treatment with PC computer. Link to internal and external network/

References: Report on "Equipements Experimentaux," (1987) LLB.

**FACILITY: MANUEL P. LUJAN, JR., NEUTRON SCATTERING CENTER
(LANL)**

Beam Tube: 10

Monochromator: Time-of-flight

Incident Wavelength: 0.2 to 15 Å

Wavelength resolution: $\Delta\lambda/\lambda = 1\%$

Source-to-sample distances: 8.65 m

Beam size at specimen: 1 cm or 2.5 cm

Angular resolution: $\Delta\theta = 0.001$

Sample-to-detector distance: 4 m

Q range covered: $0.003 \leq Q \leq 0.5 \text{ \AA}^{-1}$

Maximum flux at specimen: $\sim 10^5 \text{ n/cm}^2/\text{s}$

Detector: 2D ^3He Riso detector (59 x 59 cm²)

Background: NA

Auxiliary equipment: Under development

Other information: None

References: 1. J.K. Kjems, R. Bauer, B. Breiting, and A. Thuesen, in Neutron Scattering in the Nineties, IAEA-CN-46, 489(1985).
2. P. A. Seeger, R. P. Hjelm, Jr., and M. J. Nutter, in Neutron Scattering Studies of Polymers Workshop, LANL, Nov. 3-5, 1987, Mol. Cryst. Liq. Cryst. (in press).

INSTITUTE McMaster University Nuclear Reactor

LOCATION 1280 Main Street West
Hamilton, ONTARIO, Canada
L8S 4K1

CONTACT Malcolm Collins

SOURCE MU reactor, 2 MW

FLUX 3E13

COLD SOURCE YES

NO

MATERIALS INVESTIGATED Polymers, Colloids, Lipids, Microemulsions, Coal, Metals, H.T.
Superconductors, Organics

DETECTORS 2D flat He3 (65 x 65 cm²), ORDELA detector

INSTITUTE National Center for Small-Angle Scattering Research (NCSACR)

LOCATION Oak Ridge National Laboratory
P.O. Box 2008
Oak Ridge, Tennessee 37831

CONTACT George Wignall
Solid State Division

SOURCE High Flux Isotope Reactor
(HFIR), 100 MW

FLUX 1.2 E15

COLD SOURCE YES

NO

MATERIALS INVESTIGATED Polymers, biological structures, ceramics, etc.

DETECTORS 2D flat He3 (65 x 65 cm²), ORNL detector

**FACILITY: NATIONAL CENTER FOR SMALL-ANGLE NEUTRON SCATTERING
(ORNL)**

Beam Tube: HB-3A (Double Crystal Instrument)

Monochromator: Silicon in <111> Bragg reflection

Incident Wavelength: 2.6 Å

Wavelength resolution: $\Delta\lambda/\lambda = 2\%$

Source-to-sample distances: 2.5 m (monochromator to sample), 4.5 m (monochromator to source)

Beam size at specimen: maximum, 2 x 4 cm²

Angular resolution: $\Delta Q = 4 \times 10^{-5} \text{ \AA}^{-1}$

Sample-to-detector distance: 1 m, measured through Bragg reflection at analyzer crystal

Q range covered: $0.0005 \leq Q \leq 0.02 \text{ \AA}^{-1}$

Maximum flux at specimen: $10^4 \text{ n/cm}^2/\text{s}$

Detector: 1D BF₃ proportional counter

Background: Dependent on beam area and Q value (varies $\sim Q^{-1}$ for $0.001 < Q < 0.006$ and saturates at $0.03 \text{ c/cm}^2/\text{s}$ for $Q > 0.006 \text{ \AA}^{-1}$)

Auxiliary equipment: Cryostat and peripherals for $1.5^\circ \text{ K} < T < 300^\circ \text{ K}$, vertical magnetic field capability to $\sim 20 \text{ kGauss}$ and horizontal field capability $\sim 6 \text{ kGauss}$.

Other information: None

References: D. K. Christen, S. Spooner, P. Thorel, and H. R. Kerchner, "Determination of Low-Field Critical Parameters and Superconducting Niobium by Small-Angle Neutron Diffraction," J. Appl. Cryst. 11, 650(1978).

**FACILITY: NATIONAL CENTER FOR SMALL-ANGLE NEUTRON SCATTERING
(ORNL)**

Beam Tube: HB-4B

Monochromator: Six pairs of pyrolytic graphite crystals

Incident Wavelength: 2.38 or 4.75 Å

Wavelength resolution: $\Delta\lambda/\lambda = 6\%$

Source-to-sample distances: 7.5 m

Beam size at specimen: 0.5 to 3.0 cm diameter

Angular resolution: NA

Sample-to-detector distance: 1.3 to 19 m

Q range covered: $0.003 \leq Q \leq 0.6 \text{ \AA}^{-1}$

Maximum flux at specimen: 10^4 to 5×10^5 n/cm²/s depending on slit size and λ

Detector: 2D ³He ORDELA detector (64 x 64 cm²)

Background: NA

Auxiliary equipment: NA

Other information: None

References: R. K. Abele, G. W. Allin, W. T. Clay, C. E. Fowler, and M. K. Kopp, "Large Area Proportional Counter Camera for the U. S. Small-Angle Neutron Scattering Facility," IEEE Trans. Nuc. Sci. NS-28, 811(1981).

INSTITUTE National Institute of Standards and Technology (NIST)

LOCATION Reactor Radiation Division
Gaithersburg, MD 20899

CONTACT G. J. Glinka

SOURCE NBS Reactor, 20 MW

FLUX 2E14

COLD SOURCE

YES

NO

MATERIALS INVESTIGATED Polymers, ceramics, metals, biological macromolecules, etc.

DETECTORS 2D flat He3 (25 x 25 cm²), TEC (ORDELA) detector
2D flat He3 (65 x 65 cm²), TEC (ORDELA) detector
2D flat He3 (65 x 65 cm²), ORNL detector

INSTITUTE Netherlands Energy Research Foundation (NERF)

LOCATION P.O. Box 1
1755 ZG Petten
The Netherlands

CONTACT H. H. van den Kroonenberg

SOURCE Petten High Flux Reactor (HFR)
45 MW

FLUX E14

COLD SOURCE

YES

NO

MATERIALS INVESTIGATED Polymers, ceramics, alloys, colloidal solutions

DETECTORS 2D flat He3 (57 cm), Riso detector

FACILITY: NATIONAL INSTITUTE OF STANDARDS & TECHNOLOGY

Beam Tube: CT-E, 7 inch diameter tube which views 16 liter D₂O-ice cold source

Monochromator: Helical channel velocity selector, 80% transmission

Incident Wavelength: 5 to 20 Å

Wavelength resolution: $\Delta\lambda/\lambda = 25\%$ (FWHM)

Source-to-sample distances: 4.5 m

Beam size at specimen: 0.5 to 2.5 cm diameter

Angular resolution: 5 to 20 feet incident beam collimation

Sample-to-detector distance: 2 to 3.5 m

Q range covered: $0.003 \leq Q \leq 0.5 \text{ \AA}^{-1}$

Maximum flux at specimen: $8 \times 10^5 \text{ n/cm}^2/\text{s}$ at 5 Å

Detector: 2D ³He ORDELA detector (64 x 64 cm²)

Background: ~ 5 cps total detector counts

Auxiliary equipment: Thermostated multispecimen sample changers (-10 to 200° C),
electromagnet (18 kGauss), and various cryostats

Other information: Optional multibeam converging pinhole collimation

References: C. J. Glinka, J. M. Rowe, and J. G. LaRock, J. Appl. Cryst. **19**,
427(1986).

FACILITY: NETHERLANDS ENERGY RESEARCH FOUNDATION

Beam Tube: HB3b

Monochromator: 6 pairs of pyrolytic graphite crystals

Incident Wavelength: 4.75 Å

Wavelength resolution: $\Delta\lambda/\lambda = 2, 4, 6, 8, \text{ and } 10\%$

Source-to-sample distances: 8 m

Beam size at specimen: 5 - 20 cm²

Angular resolution: NA

Sample-to-detector distance: 95 - 425 cm

Q range covered: $0.005 \leq Q \leq 0.4 \text{ \AA}^{-1}$, $0.7 \leq Q \leq 1.4 \text{ \AA}^{-1}$

Maximum flux at specimen: $\sim 10^5 \text{ n/cm}^2/\text{s}$, depending on λ -resolution, etc.

Detector: 2D ³He Riso detector (57 x 57 cm²)

Background: $\sim 2 \text{ /ns}$ over whole detector

Auxiliary equipment: sample changer, cryostat, magnet, furnace

Other information: None

References: None

INSTITUTE Neutronenphysik (Dept. 7)

LOCATION Physikalisch-Technische
Bundesanstalt
POB 3345
3300 Braunschweig, FRG

CONTACT Dr. Jahr
Dept. 7

SOURCE Swimming pool reactor
1 MW

FLUX

COLD SOURCE YES

NO

MATERIALS INVESTIGATED Ferromagnetic single crystals (domain structure): Fe, Ni, Fe₃Si

DETECTORS BF₃ proportional counters (50 mm) - built by Twentieth Century, Limited

INSTITUTE Nuclear Physics Institute
Czechoslovakian Academy of Sciences

LOCATION 25068 REZ
Prague
Czechoslovakia

CONTACT J. Tucek

SOURCE VVR-S reactor

FLUX 1.2E14

COLD SOURCE YES

NO

MATERIALS INVESTIGATED Alloys, concrete, metals, polymers

DETECTORS BF₃
He₃
Linear PSD (4 x 250 cm²), being constructed by JINR, Dubna

FACILITY: NEUTRONENPHYSIK
Physikalisch-Technische Bundesanstalt

Beam Tube: S1 (Forschungs-und Mepreaktor Braunschweig).

Monochromator: Si lamellae in <111> Bragg reflection.

Incident Wavelength: 2.3 Å predominantly, variable.

Wavelength resolution: $\Delta\lambda/\lambda \sim 0.4\%$.

Source-to-sample distances: ~ 6.4 meters (1.3 meter monochromator to sample).

Beam size at specimen: 30 mm x 30 mm, maximum.

Angular resolution: $\Delta Q = 5 \times 10^{-5} \text{ \AA}^{-1}$ (determined by FWHM of double crystal Bragg peak).

Sample-to-detector distance: 1.8 meters.

Q range covered: $0.0002 \leq Q \leq 0.012 \text{ \AA}^{-1}$.

Maximum flux at specimen: $10^2 \text{ neutrons cm}^{-2}\text{s}^{-1}$.

Detector: BF₃ tube: 50 mm diameter and 400 mm active length.

Background: 2 min⁻¹

Auxiliary equipment: Furnace for crystals until 800° C, electromagnet, Kerr effect equipment.

Other information: At this facility the most preliminary experiments are made. Final experiments have been conducted at ILL Grenoble on D11.

References: 1. Seifert, R. et al, "Determination of Bloch Wall Thickness in Fe (4 at % Si) Single Crystals by Neutron Small Angle Scattering," Colloid and Polymer Sci. 259 (1981), 666-69.

2. Strothmann, H. et al, "Determination of Temperature Dependence of Bloch Wall Thickness in Fe (4 at % Si) Single Crystal By Means of Neutron Refraction," Conference Proc. of Soft Magnetic Materials 7 (1985), 102-4.

FACILITY: NEUTRONENPHYSIK
Physikalisch-Technische Bundesanstalt

Beam Tube: S1 (Forschungs-und Mepreaktor Braunschweig).

Monochromator: Si in <313> Bragg reflection.

Incident Wavelength: 1.73 Å fixed.

Wavelength resolution: $\Delta\lambda/\lambda \sim 0.15\%$.

Source-to-sample distances: ~ 6.1 meters (2 meter monochromator to sample).

Beam size at specimen: 40 mm x 40 mm, maximum.

Angular resolution: $\Delta Q = 4 \times 10^{-5} \text{ \AA}^{-1}$.

Sample-to-detector distance: 1 meters.

Q range covered: $0.0002 \leq Q \leq 0.012 \text{ \AA}^{-1}$.

Maximum flux at specimen: 50 neutrons $\text{cm}^{-2}\text{s}^{-1}$.

Detector: BF_3 tube: 50 mm diameter and 400 mm active length.

Background: 1 min^{-1}

Auxiliary equipment: Electromagnet, Kerr effect equipment.

Other information: In operation since January, 1989.

References: NA.

FACILITY: NEUTRONENPHYSIK
Physikalisch-Technische Bundesanstalt

Beam Tube: S7 (Forschungs-und Mepreaktor Braunschweig).

Monochromator: Pre-monochromator: 3 x graphite in <002> Bragg reflection.
Monochromator and analyzer: Multiple Si lamellae in <111> Bragg reflection.

Incident Wavelength: 4.6 Å to 4.86 Å simultaneously by all lamellae.

Wavelength resolution: $\Delta\lambda/\lambda \sim 1\%$.

Source-to-sample distances: ~ 10 meters (1 meter monochromator to sample).

Beam size at specimen: 40 mm x 40 mm, maximum.

Angular resolution: $\Delta Q = 3 \times 10^{-5} \text{ \AA}^{-1}$.

Sample-to-detector distance: 1.5 meters.

Q range covered: $0.00003 \leq Q \leq 0.001 \text{ \AA}^{-1}$.

Maximum flux at specimen: 7 neutrons $\text{cm}^{-2}\text{s}^{-1}$ per lamella.

Detector: 1-dimensional BF_3 .

Background: $0.05 \text{ cm}^{-2}\text{s}^{-1}$

Auxiliary equipment: None.

Other information: There are planned 60 lamellae as and 60 lamellae as analyzer.

References: Treimer, W., et al, "Development of a New Facility for Neutron Small Angle Scattering," Proceedings of the International Conference on Neutron Scattering, 1988 Grenoble (North Holland, 1989).

FACILITY: NUCLEAR PHYSICS INSTITUTE

Beam Tube: No. 8 (reactor channel)

Monochromator: Bent Si crystal. Double crystal arrangement

Incident Wavelength: 2 Å

Wavelength resolution: $\Delta\lambda/\lambda = 2\%$

Source-to-sample distances: NA

Beam size at specimen: 0.7 x 3 cm²

Angular resolution: 5 x 10⁻⁴ - 5 x 10⁻³ rad.

Sample-to-detector distance: NA

Q range covered: 0.0003 ≤ Q ≤ 0.012 Å⁻¹

Maximum flux at specimen: For minimum resolution, ~ 10³ n/cm²/s

Detector: Linear PSD. Spatial resolution ~ 2 mm.

Background: ~ 0.3 n/s per detector.

Auxiliary equipment: NA

Other information: The proposed new version of a double-crystal SANS equipment as well as the PSD is being constructed.

References: 1. P. Mikula, P. Lukas, and F. Eichhorn, "A New Version of a Medium-Resolution Double-Crystal Diffractometer for the Study of Small-Angle Neutron Scattering (SANS)," *J. Appl. Crystal.* **21**, 33(1988).
2. P. Mikula, P. Lukas, J. Kulda, and F. Eichhorn, "A Highly Efficient Multicrystal Camera for SANS Studies," *Physica B* **156 & 157**, 605(1989).

FACILITY: UNIVERSITY OF MISSOURI RESEARCH REACTOR

Beam Tube: Beam port B

Monochromator: Nine slightly misaligned pyrolytic graphite crystals

Incident Wavelength: 4.75 Å

Wavelength resolution: $\Delta\lambda/\lambda = 4.1\%$

Source-to-sample distances: 4.5 m

Beam size at specimen: 0.25 to 3 cm

Angular resolution: NA

Sample-to-detector distance: 3 or 4.5 m

Q range covered: $0.00675 \leq Q \leq 0.14 \text{ \AA}^{-1}$

Maximum flux at specimen: $2.4 \times 10^4 \text{ n/cm}^2/\text{s}$ in most used conformation (4.5 m matched paths, 2 cm and 1 cm source and sample apertures)

Detector: Array of 43 linear ^3He PSDs

Background: NA

Auxiliary equipment: NA

Other information: None

References: 1. R. Berliner, D. F. R. Mildner, O. A. Pringle, and J. S. King, "A Large Area Position-Sensitive Detector," *Nuc. Instrum. Meth.* 185, 481(1981).
2. D. F. R. Mildner, R. Berliner, O. A. Pringle, and J. S. King, "The Small-Angle Neutron Scattering Spectrometer at the University of Missouri Research Reactor," *J. Appl. Cryst.* 14, 370(1981).

FACILITY: NUCLEAR PHYSICS INSTITUTE

Beam Tube: No. 9 (reactor channel)

Monochromator: Silicon. Double crystal arrangement <111> Bragg reflection

Incident Wavelength: 1 to 2 Å

Wavelength resolution: $\Delta\lambda/\lambda = 2\%$

Source-to-sample distances: 70 cm

Beam size at specimen: 2 x 2 cm²

Angular resolution: $5 \times 10^{-4} - 5 \times 10^{-3}$ rad.

Sample-to-detector distance: 80 cm, measured through Bragg reflection at analyzer

Q range covered: $0.0003 \leq Q \leq 0.02 \text{ \AA}^{-1}$

Maximum flux at specimen: For minimum resolution, $\sim 10^3 \text{ n/cm}^2/\text{s}$

Detector: BF₃

Background: $\sim 0.5 \text{ n/s}$

Auxiliary equipment: Bent perfect Si crystals, bending devices

Other information: Step-by-step measurements in the curved angular range.

References: J. Kulda and P. Mikula, "A Medium-Resolution Double-Crystal Diffractometer for the Study of Small-Angle Neutron Scattering," *J. Appl. Crystal.* **16**, 498(1983).

INSTITUTE Paul Scherrer Institute
Eidgenossisches Institut für Reaktorforschung (Laboratory for Neutron Scattering)

LOCATION CH-5303 Würenlingen
Switzerland

CONTACT J. P. Blaser

SOURCE SINQ

FLUX E14 - expected

COLD SOURCE

YES

NO

**MATERIALS
INVESTIGATED**

DETECTORS SINQ is in construction, operational 1993
SANS instrument operational 1993

INSTITUTE Research Reactor Institute (RRI)

LOCATION Kyoto University
Kumatori-cho
Sennan-gun
Osaka, 590-04, Japan

CONTACT Kideaki Nishihara

SOURCE KUR reactor, 5 MW

FLUX 3E13

COLD SOURCE

YES

NO

**MATERIALS
INVESTIGATED** A new SANS will be built at a new cold guide tube for the studies of
biomolecules, polymers, and material sciences.

DETECTORS 2D flat He3 (51 x 51 cm²) 64 x 64 pixel, BNL type (RRI design)
2D flat He3 (21 x 21 cm²) 64 x 64 pixel, BNL type (RRI design)

FACILITY: RESEARCH REACTOR INSTITUTE

Beam Tube: Cold neutron guide tube

Monochromator: Mechanical velocity selector or multilayer monochrometer

Incident Wavelength: 4 to 15 Å

Wavelength resolution: $\Delta\lambda/\lambda = 10$ to 15%

Source-to-sample distances: 7 m

Beam size at specimen: 2 x 5 cm², standard 1 x 1 cm²

Angular resolution: NA

Sample-to-detector distance: 1 to 10 m

Q range covered: $0.001 \leq Q \leq 1 \text{ \AA}^{-1}$

Maximum flux at specimen: $\sim 10^6$ n/cm²/s, depending on λ

Detector: 2D ³He Riso detector (51 x 51 cm²), 64 x 64 pixel

Background: NA

Auxiliary equipment: NA

Other information: None

References: None

INSTITUTE Rhode Island Nuclear Science Center
& University of Rhode Island Physics Dept.

LOCATION Research Reactor
South Ferry Road
Narragansett, RI 02882

CONTACT Frank DiMeglio

SOURCE RIAECR reactor, 2MW

FLUX E12

COLD SOURCE YES

NO

MATERIALS INVESTIGATED Magnetic colloids, amorphous magnets, high Tc Superconductors

DETECTORS BF3, 1 atm

INSTITUTE Small-Angle Scattering Facility

LOCATION RISO National Laboratory
DK4000 Roskilde, Denmark

CONTACT Kell Mortensen

SOURCE

FLUX

COLD SOURCE YES

NO

MATERIALS INVESTIGATED Polymers, aggregates, biological structures, ceramics, etc.

DETECTORS 2D flat He3 detector (59 cm), RISO detector

FACILITY: RHODE ISLAND NUCLEAR SCIENCE CENTER

Beam Tube: R2 (10 inch diameter)

Monochromator: Hensler alloy (polymizer) or pyrolytic graphite

Incident Wavelength: $\sim 2.36 \text{ \AA}$

Wavelength resolution: $\Delta\lambda/\lambda = 3\%$

Source-to-sample distances: 15 feet - reactor core to monochrometer, 5 feet - monochrometer to sample

Beam size at specimen: 1 cm

Angular resolution: $\sim 0.1^\circ$, 2θ

Sample-to-detector distance: 2 m

Q range covered: $0.01 \leq Q \leq 0.6 \text{ \AA}^{-1}$

Maximum flux at specimen: $\sim 10^4 \text{ n/cm}^2/\text{s}$

Detector: 1D Harshaw ^3He detector (1 m x 2.5 cm)

Background: NA

Auxiliary equipment: 0.5 Tesla electromagnet, 0.15 Tesla electromagnet, liquid helium cryostat

Other information: Uses line-focussed beam

References: 1. A. C. Nunes, J. Appl. Cryst. **11**, 460(1978).
2. A. C. Nunes, Kerntechnik **S-44**, 811(1984).

FACILITY: THE SMALL-ANGLE SCATTERING FACILITY
Riso National Laboratory

Beam Tube: NA

Monochromator: Mechanical velocity selector

Incident Wavelength: 3 to 25 Å

Wavelength resolution: $\Delta\lambda/\lambda = 0.1$ to 0.2

Source-to-sample distances: 1 to 6 meters, variable in steps of 1 meter

Beam size at specimen: maximum, 2.4 cm diameter

Angular resolution: NA

Sample-to-detector distance: 1 to 6 meters continuous

Q range covered: $0.002 \leq Q \leq 0.5 \text{ \AA}^{-1}$

Maximum flux at specimen: $10^6 \text{ n/cm}^2/\text{s}$ at 3.5 Å

Detector: 2D flat ^3He Riso detector (59 cm)

Background: < 2 cps

Auxiliary equipment: Sample schanger for up to six samples, temperature controlled -5° C to 80° C, ^4He cryostat, displax, furnace to 250° C.

Other information: None

References: T. Freltoft and J. Kjems, "Riso SANS Facility. User Guide," Riso M-2450 (1985).

INSTITUTE Tun Ismail Atomic Research Center (PUSPATI)

LOCATION PUSPATI Complexes
Bangi, 43000 Kajang
Selangor, MALAYSIA

CONTACT Mohd. Ghazali Abd. Rahman

SOURCE TRIGA MARK II reactor
1 MW

FLUX 1.6E13

COLD SOURCE YES

NO

MATERIALS INVESTIGATED Ceramics and metals

DETECTORS 2D PSD (64 x 64 cm²), Riso design

INSTITUTE University of Missouri Research Reactor (MURR)

LOCATION University of Missouri
Research Park
Columbia, Missouri 65211

CONTACT J. Steve Morris

SOURCE Research Reactor, 10 MW

FLUX 1.0E14

COLD SOURCE YES

NO

MATERIALS INVESTIGATED Polymers, biological macromolecules, metal, porous edia, etc.

DETECTORS Array of 43 position-sensitive linear detectors (55 x 61 cm²)

**FACILITY: TUN ISMAIL ATOMIC RESEARCH CENTER
PUSPATI**

Beam Tube: Radial piercing beam port.

Monochromator: Three sets of ZYB highly oriented pyrolytic graphite (HOPG) crystals..

Incident Wavelength: 5 Å.

Wavelength resolution: 0.7.

Source-to-sample distances: 1, 2, and 4 m.

Beam size at specimen: 6, 12, 25 mm.

Angular resolution: NA.

Sample-to-detector distance: 1, 2, and 4 m (possibly 6 m in the future).

Q range covered: $0.008 \leq Q \leq 0.36 \text{ \AA}^{-1}$.

Maximum flux at specimen: $1.7 \times 10^4 \text{ n/cm}^2/\text{s}$.

Detector: 2D ^3He PSD (64 x 64 cm²), supplied by Riso.

Background: NA.

Auxiliary equipment: LN₂-cooled Be filter.

Other information: Instrument under construction and due to be completed in 1990.

- References:*
1. R. Caciuffo, M. Deraman, and A. G. Ramli, *J. Sains Nuklear Malaysia* **4** (1986), 15-26.
 2. A.G. Ramli, M. Deraman, and M. A. Sufi, "The Small-Angle Neutron Scattering Facility at PUSPATI," unpublished.
 3. A. G. Ramli and M. Deraman, "Malaysia's Entry Into a Neutron Scattering Program," 3rd AINSE Conf. on Neutron Scattering, Lucas Heights, Australia (1986).

Internal Distribution

- | | |
|------------------------|--------------------------------------|
| 1. C. W. Alexander | 69. B. H. Montgomery |
| 2. R. G. Alsmiller | 70. R. M. Moon |
| 3. J. L. Anderson | 71. F. R. Mynatt |
| 4. B. R. Appleton | 72. R. K. Nanstad |
| 5. H. R. Brashear | 73. R. E. Pawel |
| 6. J. R. Buchanan | 74. F. J. Peretz |
| 7. G. J. Bunick | 75. R. T. Primm, III |
| 8. N. C. J. Chen | 76. C. C. Queen |
| 9. H. R. Child | 77. S. Raman |
| 10. G. L. Copeland | 78. J. S. Rayside |
| 11. B. L. Corbett | 79. A. E. Ruggles |
| 12. J. B. Davidson | 80. T. L. Ryan |
| 13. F. C. Difilippo | 81. D. L. Selby |
| 14. J. R. Dixon | 82. H. B. Shapira |
| 15. S. R. Ervin | 83. R. P. Taleyarkhan |
| 16. F. F. Dyer | 84. P. B. Thompson |
| 17. R. E. Fenstermaker | 85. K. R. Thoms |
| 18. G. F. Flanagan | 86. D. B. Trauger |
| 19. W. R. Gambill | 87. C. D. West |
| 20. R. K. Genung | 88. J. Westbrook |
| 21. M. L. Gildner | 89. G. D. Wignall |
| 22. H. A. Glovier | 90. M. K. Wilkinson |
| 23. R. M. Harrington | 91. B. A. Worley |
| 24-33. J. B. Hayter | 92. G. T. Yahr |
| 34. D. T. Ingersoll | 93. G. L. Yoder |
| 35. J. A. Johnson | 94. A. Zucker |
| 36. L. M. Jordan | 95. ORNL Patent Section |
| 37. R. A. Lillie | 96. Central Research Library |
| 38. J. A. March-Leuba | 97. Y-12 Technical Library |
| 39. B. S. Maxon | 98-99. Laboratory Records Department |
| 40-44. M. R. McBee | 100. Laboratory Records (RC) |
| 45-68. S. A. McElhaney | |

External Distribution

101. Ronald R. Berliner, Research Reactor Facility, University of Missouri-Columbia, Research Park, Columbia, MO 65211
102. J. P. Blaser, Paul Scherrer Institute, Eidgenossisches Institut für Reaktorforschung, CH-5303 Würenlingen, Switzerland

103. Malcolm Collins, McMaster University Nuclear Reactor, 1280 Main Street, West, Hamilton, Ontario, Canada, L8S 4K1
104. David Cook, Australian Nuclear Science and Technology Organization, Lucas Heights Research Labs, Sydney NSW, Australia 2234
105. Frank DiMeglio, Rhode Island Nuclear Science Center, Research Reactor, South Ferry Road, Narragansett, RI 02882
106. G. Eder, Atominstitut der Osterreichischen Universitaten, Schuttelstrasse 115, A-1020 Wien, Austria
107. J. E. Epperson, Material Science Division, Intense Pulsed Neutron Source, Argonne National Laboratory, 9700 S. Cass Avenue, Argonne, Illinois 60439
108. B. Chalmers Frazer, Materials Sciences Division, U.S. Department of Energy, Germantown, ER-132, Washington, D.C. 20545
109. Ralph Fullwood, Brookhaven National Laboratory, Upton, NY 11973
110. Satoru Funahashi, Head of Solid State Physics Laboratory III, Department of Physics, Japan Atomic Energy Research Institute, Tokai-mura, Ibaraki-Ken 319-11, Japan
111. W. Glaser, Institut Laue-Langevin, 156X 38042 Grenoble Cedex, France
112. G. J. Glinka, National Institute of Standards and Technology, Reactor Radiation Division, Gaithersburg, MD 20899
113. P. S. Goyal, Bhabha Atomic Research Center, Nuclear Physics Division, Bombay 400 085, India
114. D. A. Gray, ISIS Spallation Neutron Source, RAL, Chilton, Didcot, Oxon OX11 0QX, England
115. P. Iredale, Atomic Energy Research Establishment, Harwell Laboratories, Oxon, OX11 0RA, England
116. Dr. Jahr, Neutronenphysik (Dept. 7), Physikalisch-Technische, Bundesanstalt, POB 3345, 3300 Braunschweig, Federal Republic of Germany
117. D. Kiss, Joint Institute for Nuclear Research, Laboratory of Neutron Physics, Head Post Office, P. O. Box 79, 101000 Moscow, USSR
118. Dr. Manfred Kopp, ORDELA, Inc., 139 Valley Court, Oak Ridge, TN 37830
119. J. A. Lake, Manager, Nuclear Engineering and Reactor Design, Idaho National Engineering Laboratory, P. O. Box 1625, Idaho Falls, ID 83415
120. M. Lambert, Laboratoire Leon Brillouin, CEN Saclay, 91191 Gif-sur-Yvette, Cedex, France
121. John Marks, Research and Test Reactor Fuel Elements, Babcock and Wilcox Co., P. O. Box 785, Lynchburg, VA 24505
122. M. H. McBride, U.S. Department of Energy, Oak Ridge Operations, Building 7900, MS-6387, P. O. Box 2008, Oak Ridge, TN 37831-6387
123. J. Steve Morris, University of Missouri Research Reactor, Research Park, Columbia, Missouri 65211
124. Kell Mortensen, Small-Angle Scattering Facility, RISO National Laboratory, DK4000 Roskilde, Denmark
125. Robert J. Neuhold, U.S. Department of Energy, Germantown, NE-472, Washington, DC 20545
126. Kideaki Nishihara, Research Reactor Institute, Kyoto University, Kumatori-cho, Sennan-gun, Osaka, 590-04, Japan
127. Les C. Oakes, Electric Power Research Institute (EPRI), Building 2, Room 252, P. O. Box 10412, Palo Alto, CA 94303
128. Roger Pynn, LANSCE, Los Alamos National Laboratory, P-LANSCE, MS-H805, Los Alamos, NM 87545

129. Mohd. Ghazali Abd. Rahman, Tun Ismail Atomic Research Center, PUSPATI Complexes, Bangi, 43000 Kajang, Selangor, Malaysia
130. Tormod Riste, Department of Physics, Institute for Nuclear Technology, POB 40, N-2007, Kjeller, Norway
131. John M. Ryskamp, Idaho National Engineering Laboratory, P. O. Box 1625, Idaho Falls, ID 83415
132. Dietmar Schwahn, Kernforschungsanlage IFF, Postfach 1913, D-5170 Jurlich, Federal Republic of Germany
133. Dr. Philip A. Seeger, LANSCE-H805, Los Alamos National Laboratory, Los Alamos, NM 87545
134. Dr. Graham Smith, Instrumentation Division, Building 535B, Brookhaven National Laboratory, Upton, NY 11973
135. J. L. Snelgrove, Coordinator, Engineering Applications, RERTR Program, Argonne National Laboratory, 9700 South Cass Avenue, Argonne, IL 60439
136. Iran Thomas, Director, Materials Science Division, Office of Energy Research, U.S. Department of Energy, Germantown, ER-13, Washington, D.C. 20545
137. Sun Tsu-Xun, Institute of Atomic Energy, P. O. Box 275, Beijing, China
138. J. Tucek, Nuclear Physics Institute, Czechoslovakian Academy of Sciences, 25068 REZ, Prague, Czechoslovakia
139. H. H. van den Kroonenberg, Netherlands Energy Research Foundation, P. O. Box 1, 1755 ZG Petten, The Netherlands
140. R. P. Wadkins, Idaho National Engineering Laboratory, P. O. Box 1625, Idaho Falls, ID 83415
141. D. K. Wilfert, Energy Programs, U.S. Department of Energy, Oak Ridge Operations, Building 7900, MS-6387, P. O. Box 2008, Oak Ridge, TN 37831-6387
142. R. J. Willard, U.S. Department of Energy, Oak Ridge Operations, P. O. Box 2001, Oak Ridge, TN 37831
143. P. R. Williams, ISIS Spallation Neutron Source, RAL, Chilton, Didcot, Oxon OX11 0QX, England
144. Office of Assistant Manager for Energy Research and Development, Department of Energy, Oak Ridge Operations, P. O. Box 2001, Oak Ridge, TN 37831
- 145-154. Office of Scientific and Technical Information, P. O. Box 62, Oak Ridge, TN 37831